Fall 12-16-2016

Polymeric Nanocarriers for Delivery of Small Molecules and miRNAs for the Treatment of Liver Fibrosis and Pancreatic Cancer

Virender Kumar
university of Nebraska medical center

POLYMERIC NANOCARRIERS FOR DELIVERY OF SMALL MOLECULES AND miRNAs FOR THE TREATMENT OF LIVER FIBROSIS AND PANCREATIC CANCER

by

Virender Kumar

A DISSERTATION

Presented to the Faculty of
the University of Nebraska Graduate College
in Partial Fulfillment of the Requirements
for the Degree of Doctor of Philosophy

Pharmaceutical Sciences Graduate Program
(Pharmaceutics)

Under the supervision of Professor Ram I. Mahato

University of Nebraska Medical Center
Omaha, Nebraska

August 2016

Supervisory Committee:

Surinder K. Batra, Ph.D.

Jered Garrison, Ph.D.

Carol Casey, Ph.D.

ACKNOWLEDGEMENTS

I could never have completed this daunting task without the help, support, guidance and efforts of a lot of people. My thanks and appreciation to Dr. Ram I Mahato for mentoring and supporting me as my academic supervisor throughout my research. I would also like to thank the members of my dissertation committee; Dr. Surinder Batra, Dr. Jered Garrison, and Dr. Carol Casey, who have generously given their time and suggestions to improve my work.

I would also like to thank Dr. Vaibhav Mundra, Dr. Saurabh Singh, Dr. Goutam Mondal, Dr. Krishna Kattel and Dr. Satyaprekash Rachanagi for their valuable guidance and help early on in my Ph.D. program. Special thanks to all my friends, colleagues and lab mates for their support and wonderful company over all these years.

Finally, I would like to dedicate this dissertation to my parents Mr. Bahadur Singh and Mrs. Sharda Rani; to my family members, Jitender, Jeetan, Ashish, my wife Bharti and my adorable loving son Kanishk for their endless love and continued support.

ABSTRACT

The aim of this thesis is to develop combination therapy of small molecules and miRNAs for treating liver fibrosis and pancreatic cancer. New amphiphilic biodegradable polymers capable of carrying small hydrophobic molecules and hydrophilic anionic nucleic acids were synthesized, characterized and evaluated in vitro and in vivo liver fibrosis and pancreatic cancer mouse models.

In **Chapter 1,** an overview of liver fibrosis, current treatments and the role of miRNAs in liver fibrosis as well as the design of their delivery systems is given. Further, a general introduction about pancreatic cancer and role of miRNAs in pancreatic cancer is given. In **Chapter 2,** small molecules GDC-0449 and rosiglitazone were encapsulated into nanoparticles prepared using a biodegradable copolymer mPEG-b-p(CB-co-LA) and used for the treatment of common bile duct ligation (CBDL) induced liver-fibrotic rats. GDC-0449 and rosiglitazone loaded nanoparticles could reverse early stage liver fibrosis by reducing ECM deposition in the liver and inhibiting Hh signaling pathway.

Chapter 3 reports the design of a cationic biodegradable copolymer methoxy poly(ethylene glycol)-block-poly(2-methyl-2-carboxyl-propylenecarbonate-graft-dodecanol-graft-tetraethylene-pentamine) (mPEG-b-PCC-g-DC-g-TEPA) for encapsulation of GDC-0449 into the micelle core and complexation of miR-let7b via electrostatic interaction with TEPA. These micelles were characterized for particle size, surface morphology, drug loading, and cytotoxicity and transfection efficiency in vitro. Micelles containing both these drugs were evaluated in a subcutaneous pancreatic tumor model. The combination therapy effectively inhibited tumor growth compared to micelles carrying either GDC-0449 or miR-let7b. Immunohistochemical analysis of tumor sections revealed decreased tumor cell proliferation and increased apoptosis of tumor cells of the animals treated with miR-let7b and GDC-0449 combination.

Chapter 4 describes the use of mPEG-b-PCC-g-DC-g-TEPA copolymer for delivery of miR-29b1 and GDC-0449 in CBDL mice. Systemic administration of these micelles into CBDL liver fibrotic mice resulted in high concentrations of GDC-0449 and miR-29b1 to the liver cells as determined by in situ liver perfusion. We observed a significant decrease in collagen deposition in the liver and serum injury markers, leading to improvement in liver morphology and disease condition. Combination therapy was effective in providing hepatoprotection, lowering liver injury related serum enzyme levels and reducing fibrotic protein markers such as collagen, α-SMA, FN-1 and p-AKT compared to monotherapy.

Finally, **Chapter 5** summarizes the results of this thesis and gives suggestions for future research.

TABLE OF CONTENTS

LIST OF FIGURES

LIST OF TABLES

LIST OF ABBREVIATIONS

BD	biodistribution
CMC	critical micelle concentration
CSCs	cancer stem cells
DOD	1-dodecanol
ECM	extracellular matrix
EPR	enhanced permeability and retention effect
GDC-0449	vismodegib
Hh	hedgehog
IFN-γ	interferon-γ
IL-1β	interleukin -1 beta
K-ras	Kirsten rat sarcoma viral oncogene homolog
MBC	2-Methyl-2-benzyloxycarbonyl-propylene carbonate
MDR	multidrug resistance
PEG	poly (ethylene glycol)
mPEG-b- P-(CB-co-LA)	methoxypoly (ethylene glycol)-b-poly(carbonate-co-lactide)
PEG-MBC	poly(ethylene glycol)-block-poly(2-methyl-2-benzoxycarbonyl-propylene carbonate)

PEG-PCC	poly(ethylene glycol)-block-poly(2-methyl-2-carboxylpropylene carbonate)
PPAR-γ	proxisome Proliferator activator receptor gama
RES	reticuloendothelial system
RISC	RNA-induced silencing complex
ROP	ring opening polymerization
ROSI	rosiglitazone
TGF-β1	transforming growth factor beta 1
TEM	transmission electron microscope
TEPA	tetraethylpentaamine
T_m	melting temperature
TNF-α	tumor necrosis factor alpha
TUNEL	terminal Deoxynucleotidyl Transferase nick end Labeling

CHAPTER 1. DELIVERY AND TARGETING OF MIRNAS FOR TREATING LIVER FIBROSIS

1.1. INTRODUCTION

Liver fibrosis is a histological change caused by liver inflammation. This pathological condition originates from liver damage and accompanied by excess accumulation of extracellular matrix (ECM) proteins. Causes of liver damage could be diverse including alcoholic abuse, hepatitis B virus (HBV) and hepatitis C virus (HCV) infection, metabolic disease, toxins, and ischemia-reperfusion (IR) injury [1]. Excess of ECM production in the perisinusoidal space (or space of Disse) results in a physical barrier between sinusoidal lumen and hepatocytes. Blood flow to hepatocytes is reduced, and liver function gets altered which can advance to cirrhosis. Currently, liver transplantation is the only option available to treat cirrhosis, which itself suffers from complications such as a complex procedure and limited organ donors. In the current situation, reversal of liver fibrosis before reaching the advanced stage of cirrhosis is the only possible approach [2].

Cessation of the causative agent is the most effective approach to fibrosis regression. Removal of excess alcohol consumption, treating viral infection, removing toxins and cholestasis are of major importance. Treatment approaches include the inhibition of collagen synthesis and abrogation of ECM deposition, stimulation of matrix degradation, modulation of hepatic stellate cell (HSC) activation, induction of HSC apoptosis and modulation of immune responses at the affected site. Interruption of fibrotic pathways and regulation of gene expression is an attractive approach to treat liver fibrosis. Various gene silencing methods used for treating liver fibrosis include antisense oligodeoxynucleotides (ODNs), triplex forming oligonucleotides (TFOs), small interfering RNA (siRNA), and miRNAs. The use of transgene modulating molecule is a highly specific and powerful technique to inhibit aberrant protein production, as it works at mRNA levels rather than at protein levels [3]. miRNAs are known to

alter gene expression at the post-transcriptional level in many developmental and physiological processes, especially in cell death and proliferation. Their expression profiles are different at normal and disease conditions and can also serve as diagnostic and prognostic purposes [4]. In this review, we will critically discuss the roles of miRNAs in liver fibrosis, current status and strategies for utilizing miRNAs as therapeutics to treat liver fibrosis.

1.2. PATHOGENESIS OF LIVER FIBROSIS

In normal injury healing mechanism, there is a balance between production and degradation of ECM, but this balance gets disturbed in liver fibrosis. The activation of tissue repair process following liver injury and complex cellular and molecular mechanisms of liver fibrosis have been well characterized. Local inflammatory responses and oxidative stresses are the major contributing factors to onset and progression of liver fibrosis [5]. Excessive production of ECM including collagen is the hallmark of fibrosis. ECM consists of collagen type I, II and V, laminin, proteoglycans and matricellular proteins. After the chronic liver injury, there is excess ECM production compared to its degradation, and there is net deposition of ECM due to the reduced activity of matrix metalloprotease (MMPs) in the presence of active forms of tissue inhibitors of metalloprotease (TIMPs) [6]. Hepatic fibrosis develops as a result of the progressive thickening of fibrotic septa and chemical cross-linking of collagen. Collagen is also known as an important mediator of cell survival and proliferation and promotes HSC proliferation in liver fibrosis [7]. The collapse of hepatic parenchyma and its substitution with a collagen-rich ECM reduces blood supply and associated with the onset of cirrhosis.

Cirrhosis is the advanced stage of liver fibrosis and is characterized by the replacement of liver tissue by unresolvable scar and regenerative nodules. Cirrhosis can lead to hepatocellular dysfunction and increased intrahepatic resistance to blood flow and results in portal hypertension. Ultimately, liver functions are lost, and there is fluid retention in the abdominal cavity called ascites or leads to visceral hemorrhage/encephalopathy [8]. Since

cirrhosis is irreversible end-stage disease, its treatment usually focuses on preventing progression or liver transplantation.

Various cell types such as activated HSCs, portal fibroblasts, bone marrow-derived myofibroblast precursors and hepatocytes after epithelial to mesenchymal transition (EMT) are considered as sources of ECM in liver fibrosis. However, among all these, HSCs are the main ECM-producing cells after liver injury. HSCs are present in the space of Disse in the liver and primarily store vitamin A in the quiescent or normal state. Damaged hepatocytes and Kupffer cells (KCs) release inflammatory cytokines and induce HSCs into the activated state **(Figure 1.1)**. After activation, HSCs become proliferative, increase α-smooth muscle actin (α-SMA) expression, lose their vitamin-A content, acquire a myofibroblast-like phenotype (MF-HSC)

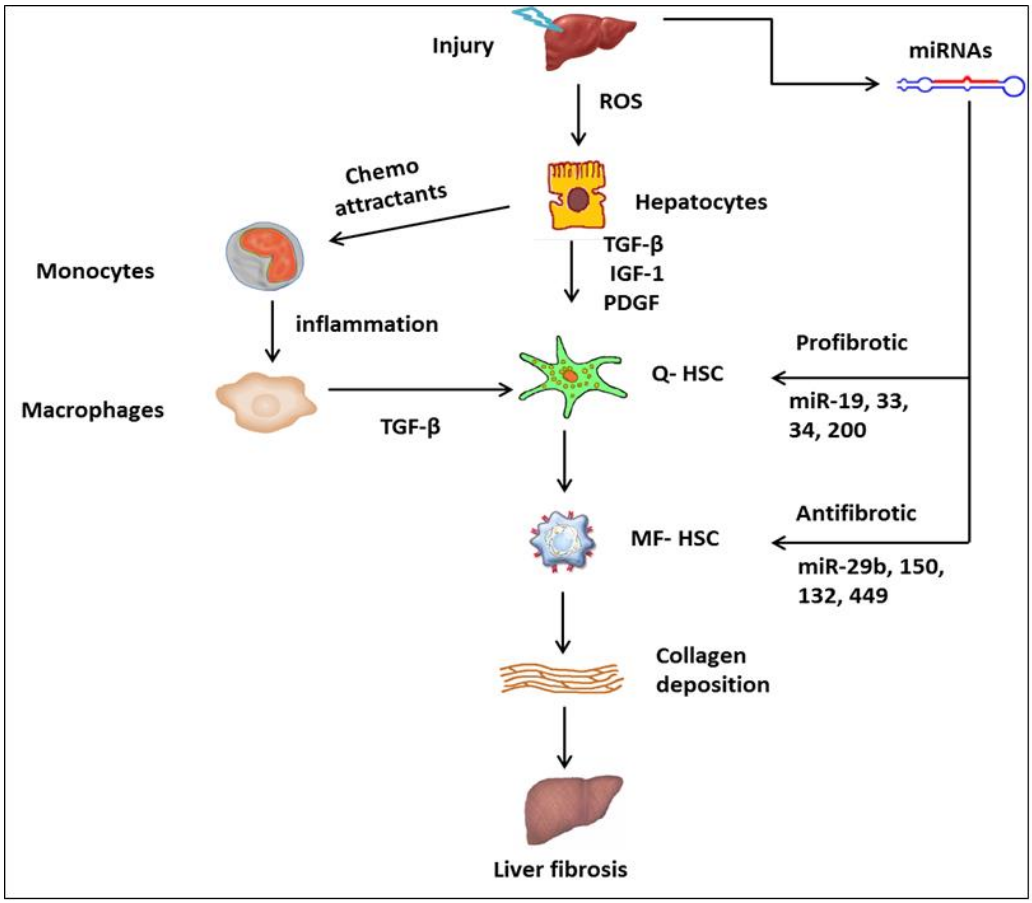

Figure 1-1. Pathology of liver fibrosis and role of miRNAs.

losing their typical star shape and start producing an excess of ECM [9]. Hepatocytes constitute the main tissue of the liver and are responsible for metabolism. Upon injury, hepatocytes experience high oxidative stress and endoplasmic reticulum stress resulting in lysosomal activation and mitochondrial damage leading to apoptosis or necrosis. Myofibroblasts phagocyte apoptotic hepatocytes and get activated themselves via NADPH oxidase 2 (NOX2) and the JAK/STAT and PI3K/Akt pathways [10].

Portal fibroblasts are essential for organ integrity, and their elimination promotes tissue necrosis and inflammation. In liver fibrosis, portal fibroblasts get converted into activated myofibroblast and contribute to fibrous scar tissue [11]. In portal fibrosis, biliary progenitors (also called activated cholangiocytes) proliferate and tend to form small clusters around the bile duct. Activation of Hh pathway promotes EMT in cholangiocytes and as a result, they acquired migratory phenotype and increased expression of various mesenchymal markers [12]. Upon activation, these cells secrete several chemoattractants that attract and activate HSCs/myofibroblasts to proliferate and deposit ECM [13,14]. CD4+ T cells with Th2 and Th17 polarization are the major driver of fibrogenesis. Th2 produce inflammatory cytokines such as IL-4 and IL-13, which stimulate macrophages in the liver [15]. Transforming growth factor beta (TGF-β1) and interleukin-6 (IL-6) induce Th17 cells, and they start secretion of IL-17A; which acts itself as profibrotic for myofibroblasts and further stimulates inflammatory cells for TGF-β1 secretion [16]. Regulatory T cells a have a dual function in fibrogenesis; subsets produce TGF-β1 and promote fibrosis, whereas other release immunosuppressive cytokines IL-10 [17].

KCs, which are resident macrophages of the liver, release inflammatory cytokines upon liver injury, which activate HSCs. After activation, HSCs starts producing cytokines, which stimulate macrophages. On the other hand, macrophages produce profibrotic mediators that directly activate fibroblasts, including TGF-β1 and platelet-derived growth factor (PDGF). They also propagate antigen-specific T cell responses; secrete MMPs, and TIMPs. As antifibrotic,

macrophages remove dead cells and debris by phagocytosis and dampen proinflammatory and profibrotic signals and thus play a significant role in the resolution of fibrosis [18]. Dendritic cells (DCs) are also implicated in inducing inflammation during fibrosis. DCs proliferate during liver fibrosis and start secreting several proinflammatory cytokines including tumor necrosis factor α (TNFα) and activate natural killer (NK) cells, cytotoxic T cells, and even HSCs [19].

Intra-hepatic inflammatory responses after liver injury play a critical role in the development of liver fibrosis. The process involves the recruitment of various cell populations in the liver microenvironment including sinusoidal endothelial cells, KCs, and even HSCs. Leukocytes are recruited at the site of hepatic injury. After reaching the affected site, they start adhering to blood vessels and transmigrate using various adhesion molecules of the integrin family, e.g. β2 integrins, and immunoglobulin gene superfamily, e.g. intercellular adhesion molecule-1 (ICAM-1). Infiltrated leukocytes and KCs secrete compounds and which can directly activate HSCs [20]. Monocytes and macrophages also produce nitric oxide (NO) and inflammatory cytokines such as TNFα, which is responsible for HSC activation and excess collagen synthesis [21]. KCs express TNF-related apoptosis-inducing ligand (TRAIL) with fas-ligand and mediate apoptosis in the liver, which further contribute to liver inflammation and fibrosis. KCs, as well as hepatocytes also secrete IL-8; which is a potent chemokine responsible for recruiting neutrophils, and T cells into inflammatory sites. IL-8 is secreted by cooperative interaction of nuclear factor κβ (NF-κβ), activator protein 1 (AP -1), and IL -6 [22,23].

A number of growth factors and cytokines are known to promote liver fibrosis. After liver injury, damaged hepatocytes and other surrounding cells in the liver secrete multiple signaling molecules and inflammatory cytokines including Hh ligands, TGF-β1, vascular endothelial growth factor (VEGF), PDGF-β, ILs, and TNF-α. Hh pathway plays an important role in the construction and remodeling of injured tissues and found to be active in liver fibrosis. In the presence of Hh, a cell surface transmembrane protein called Smoothened (SMO) gets

accumulated and inhibits the proteolytic cleavage of Gli proteins from microtubules. Decreased degradation of Gli enables them to accumulate in the cytoplasm and then translocate into the nucleus and allows transcription of growth factor family proteins. Activation of Hh pathway plays a key role in the transition of quiescent HSCs into myofibroblast and controls this mechanism via regulating their metabolism [24,25].

TGF-β plays a critical role in the progression of liver fibrosis. TGF-β is produced by KCs and HSCs, or establishes it's autocrine and paracrine loop production and upregulate collagen I and II protein expression. TGF-β mediates fibrosis via Smad3 and Smad4 proteins, while this signaling is intervened by Smad7. Some studies also conclude that TGF-β enhances collagen production via reactive oxygen intermediates in general, and H_2O_2 in particular. IL-6 is overexpressed by HSCs in the injured liver and implied to upregulate TGF-β expression and accordingly enhances its fibrogenic action [26-28].

VEGF is a well-characterized angiogenesis modulator, which is known to be upregulated during HSC activation and stimulates cell proliferation, migration, and collagen production [29]. Liver sinusoidal endothelial cells (LSECs) are known to secrete TGF-β and PDGF. Increased VEGF level in liver fibrosis promotes the growth of LSECs and thereby, increases hepatic levels of TGF-β1 [30]. PDGF is a dimeric protein that is one of the most potent mitogens for HSCs. PDGF signals via tyrosine kinase receptors PDGFR-α and PDGFR-β and sequentially activate Raf-1, MEK and extracellular-signal regulated kinase (ERK). Nuclear translocation of ERK phosphorylates transcription factors Elk-1, SAP, and triggers a proliferative response. Activated PDGF receptors also trigger phosphatidylinositol 3-kinase (PI3-K) which is involved in inflammation and fibrosis [31-33]. PDGF also induces liver fibrosis by expanding the population of collagen-producing cells and aid in TGF-β-stimulated ECM production.

MMPs are the family of endopeptidases, which are capable of tissue remodeling and degradation of all types of ECM proteins. MMPs are secreted by different cell types including

fibroblasts, osteoblasts, endothelial cells, macrophages, neutrophils, and lymphocytes in response to hormones and cytokines [34]. In the liver, HSCs are the key source of MMPs, and their level is regulated by a family of endogenous proteinase inhibitors known as TIMPs. In normal liver, the ratio between MMPs and TIMPs plays an important role in ECM turnover. In liver fibrosis, MMP level is down due to HSC activation and a net increase in TIMPs, resulting in higher ECM production but low degradation. Moreover, TIMP-1 also has an antiapoptotic effect on HSCs through BCl-2 pathway and promotes their survival [35]. TGF-β is also known to induce TIMP-1 expression, and results in reduced collagen degradation [36].

NF-κB is a heterodimer of p50 and p65 proteins and regulates inflammation, wound-healing response, and cell survival in various tissues [37]. NF-κB is an important mediator responsible for the activation and survival of HSCs in liver fibrosis. It maintains high Bcl-2 (pro-survival) expression and decrease BAX and PUMA (pro-apoptotic) expression in HSCs and prevents their apoptosis. Tissue transglutaminase (tTG) is an enzyme that catalyzes protein cross-linking in liver fibrosis. NF-kB increases tTG gene expression in liver fibrosis, and this enzyme stabilizes the fibrotic bands during hepatic fibrogenesis [38].

1.3. CURRENT TREATMENT OF LIVER FIBROSIS

Removing the primary cause is the most effective approach of treating liver fibrosis. Alcohol abstinence in patients with alcohol-induced liver fibrosis is recommended. In chronic hepatitis C virus (HCV) infection, treatment with antiviral drugs (i.e. ribavirin) to clear viral infection is recommended treatment. In obstructive cholestasis, removal of obstructive agent or surgery is the main option. This section will discuss various treatment strategies currently being explored including the inhibition of HSC activation, induction of HSC apoptosis, reduction of collagen production and deposition, a decrease in inflammation, and liver transplantation (**Table. 1**). These treatments are based on small drug molecules, antibodies, oligonucleotides (ODNs), siRNA and miRNAs.

Table 1-1. Current anti-fibrotic treatments

Small Drug molecules	**Mechanism**	**Limitations**	**Ref.**
Cyclopamine, GDC-0449	Hh inhibitor/inhibits HSC activation	Short half-life	[39]
Colchicine	Anti-inflammatory	Highly toxic	[40,41]
Silymarin	Decrease NF-kβ activity, inhibit HSC activation/ proliferation	Short half-life, low bio availability	[42,43]
Rosiglitazone	PPAR-γ agonist, anti-inflammatory	Poor water solubility, Short half life	[44]
Pentoxyfyline	Phosphodiesterase (PDE) inhibitor, antioxidant, anti-inflammatory	Poor bio-availability	[45,46]
Pirfenidone	Decrease TGF-β1	Short half-life	[47]
Amiloride	Na^+/H^+ pump inhibitor, PDGFR inhibitor, decrease oxidative stress		[48,49]
Imatinib	PDGFR inhibitor	Poor water solubility	[50,51]
Ursodeoxycholic acid	Reduce cytotoxicity bile acids, and reduce inflammatory cytokine	Not consistent in treating fibrosis	[52-54]
Farnesylthiosalicylic acid	RAS inhibitor		[55]
Cytokines			
Cardiotrophin-1	Reduced hepatocellular injury and oxidative stress		[56]
Antibodies	Neutralize TIMP-1	Poor in vivo delivery	[57]
	Neutralize TGF-β1	Stability, poor in vivo delivery	[58]
	Neutralize PDGF- β		[59]
Peptides and hormones			
P11 and P12	Decrease TGF-β1 activity	Poor in vivo delivery	[60]
Relaxin	Decrease TIMP-1	Poor in vivo delivery	[61]

1.3.1. Small Drug Molecules

Drugs currently being investigated for treating liver fibrosis are Hh inhibitors, TGF-β inhibitors, angiotensin inhibitors, endothelin inhibitors, PDGFR inhibitors, anti-inflammatory, and peroxisome proliferator-activated receptor (PPAR) agonists. Hh signaling plays a critical role in cellular proliferation, migration, differentiation, and the growth of HSCs. In the liver, Hh ligands such as Sonic Hh (SHh) and Indian Hh (IHh) are expressed by hepatocytes, bile ductular cells,

and HSCs. Quiescent HSCs respond to these ligands and transform into myofibroblasts and start producing excess ECM [62]. Hh inhibitors such as cyclopamine and vismodegib (GDC-0449) have been found effective in treating early stage liver fibrosis **(Figure 1.2)** in common bile duct ligated (CBDL) rats [39]. Realizing the role of activated HSCs in ECM production and liver fibrosis, various strategies to inhibit their activation or promote apoptosis are being explored. Small molecules such as silymarin, phosphatidylcholine, Vitamin-E, and S-adenosyl-L-methionine inhibit HSC activation/ proliferation. Inhibiting key signal transduction pathways involved in liver fibrogenesis can also be used to treat liver fibrosis. Disrupting TGF-β pathway using gene therapy results in decreased collagen production and retard the fibrosis progression. Other treatments such as the phosphodiesterase inhibitor (pentoxifylline), Na^+/H^+ pump inhibitor (amiloride), and Ras antagonist (S-farnesylthiosalicylic acid) have also been proven to be effective in a rodent model. PPAR-γ agonist keeps HSCs in a quiescent state by blocking the profibrotic effects in the liver.

Loss of these receptors is reported and leads to transdifferentiation of HSCs from the retinoid storing state to the ECM-producing myofibroblasts. Thiazolidinediones are PPAR-γ agonist that exerts beneficial effects on experimental liver fibrosis. Angiotensin-II mediates and exacerbates liver fibrosis through HSC activation and by stimulating TGF-β1 *via* angiotensin type-1 (AT_1) receptors. Inhibition of the renin-angiotensin system can also be used as a strategy to treat liver fibrosis. Blockade of endothelin-1 type A receptors and administration of vasodilators (prostaglandin E2 and nitric oxide donors) have also been reported to exert antifibrotic activity in rodents [63,64].

Inflammation has a major contribution in the progression of liver fibrosis; therefore, various anti-inflammatory drugs are being explored to retard the progression of liver fibrosis. Mainly, corticosteroids, colchicine, and vitamin D are shown to be effective in treating hepatic fibrosis in animal models [40]. Due to excess deposition of ECM, antifibrotic drugs are unable to

efficiently taken up by the liver and activated HSCs and may produce unwanted side effects. 5-methyl-1-phenylpyridine-2-one (commonly known as pirfenidone) is a small molecule that has well-established antifibrotic and anti- inflammatory properties. Pirfenidone has shown to reduce the production of fibrogenic mediators such as TGF-β and inflammatory cytokines such as TNF-α and IL-1β in a variety of fibrotic animal models [47]. Ursodeoxycholic acid (UDCA), also known as ursodiol, is one of the secondary bile acids which lower the progression rate of liver fibrosis in an early stage. UDCA binds to hepatocytes and exerts cytoprotective effect and

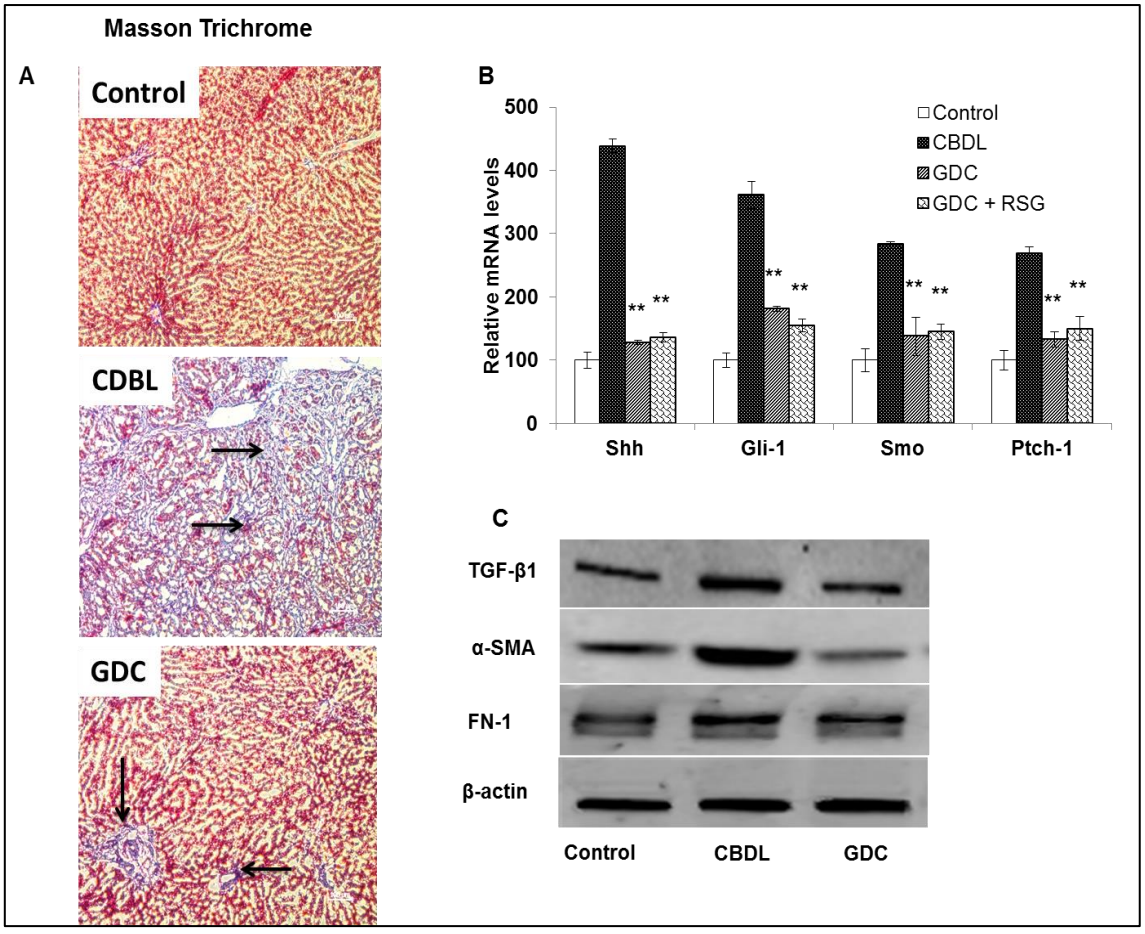

Figure 1-2. Effect of treatment with nanoparticles containing GDC-0449 on liver fibrosis in experimental animals. (A) Masson's trichrome staining shows increased collagen deposition in CBDL rats which is reduced after systemic treatment with GDC nanoparticles. (B and C) reduction in expression levels of Hh ligands after GDC nanoparticle treatment.

reduces local inflammation. It is not an anti-fibrotic agent in the liver; rather it may impede the progression of fibrosis in primary biliary cirrhosis via effects on biliary ductal inflammation. A peptide hormone relaxin is known to decrease TIMP-1 and TIMP-2 expression in HSCs [61]. Decreased expression of TIMP results in degradation of ECM and reduction in deposition of interstitial collagen. PDGF-β is a profibrotic stimulus and potential inducer of HSC transdifferentiation. PDGF-β overexpression causes liver fibrosis via the TGF-β1 independent mechanism. Small molecules imatinib and nilotinib block the tyrosine kinase activity of PDGF receptors [50,51]. These molecules also bind to the ATP-binding pocket of Abelson kinase (c-Abl) which is an important downstream signaling molecule of TGF-β signaling thus blocks two major pro-fibrotic pathways. A number of approaches and drug molecules have been applied to treat liver fibrosis. The main limitations of these drugs are either low uptake by activated HSCs or unwanted side effects. Targeted delivery to HSCs by different researchers has generated some encouraging results, but that has to be optimized to be an approved therapy.

1.3.2. Antibodies

Antibodies (Abs) against specific fibrosis causing disease have been studied by various researchers. Abs against TIMP-1, TGF-β1, and PDGF-β has been studied for reversing liver fibrosis in animal models [57-59]. Simtuzumab is a humanized monoclonal antifibrotic antibody. It binds to lysyl oxidase-like 2 (LOXL-2) enzyme, which promotes crosslinking of type-1 collagen. This Ab acts as an immunomodulator for treating liver fibrosis and is being currently tested in clinical trials [65].

1.3.3. Antisense Oligodeoxynucleotides

Antisense ODNs inhibit gene expression at post-transcriptional levels. ODN's bind to their target mRNA by the reverse complementarity and inhibit translation either by steric blocking of mRNA sequences important for translation or degrade mRNA by RNase H, which is

an endonuclease present in abundance in cytoplasm and cleaves only mRNA component of RNA: DNA hybrids. Therefore, each ODN can hybridize and degrade multiple RNA molecules [66]. The efficiency of ODNs to hybrid with mRNA depends on their physicochemical and thermodynamic properties. Minimum 12-15 bases are required to make stable duplex with mRNA, and for the practical purpose, ODNs are typically synthesized from 13 to 35 nucleotides (nt) in length. Chemical modification of ODNs can be used for enhancing their stability, efficiency, and target specificity. Phosphorothioate (PS) ODNs show enhanced stability without affecting RNase H activation efficiency. Modification with methyl phosphonate (MP) significantly reduces enzyme activation. These observations lead to synthesize ODNs containing nuclease-resistant MP modifications at the 3’ and 5’ ends while six to eight unmodified or PS-modified linkages in the middle portion [67,68].

1.3.4. Anti-gene Therapy

ODNs can form triple helices with genomic DNA and inhibit gene expression at the transcription level, which is advantageous as it blocks repopulation of mRNA. Furthermore, mRNA can have variant isoforms and inhibition of translation by ODNs may not be fully efficient. The triplex formation is sequence-specific and polypurine: polypyrimidine portion of DNA favors stable hybrid formation. Triplex-forming oligonucleotides (TFOs) are of typically 10–30 nt in length and bind to the major groove of duplex DNA. TFO can be both polypurine or polypyrimidine molecules, and they bind to the purine-rich strand of their target. Inhibition of gene transcription through TFO depends on its residence time on its target sequence and its stability against nuclease [69]. Some of the limitations of TFO are its inability to target gene sequence in condensed chromatin structure and the need of TFO translocation to the nucleus. TFO approach has been used and shown to treat liver fibrosis in our laboratory. Panakanti et al. used TFO against collagen type α1 (I) and demonstrated inhibition of liver fibrosis induced by CBDL in rats [70]. For site-specific delivery of TFOs to HSCs after systemic administration,

Yang et al. conjugated mannose 6-phosphate (M6P) to poly(*N*-(2-hydroxypropyl) methacrylamide (HPMA) polymer and then to TFO via GFLG linker. Compared with free TFOs, M6P conjugated TFO significantly accumulated in the liver and was mainly taken up by HSCs having upregulated M6P receptors in liver fibrotic animals [71].

RNA interference (RNAi) is a specific regulatory pathway that results in gene silencing at the post-transcriptional level [72]. Mechanistically, small double-stranded RNAs (siRNA) get incorporated into the RNA-induced silencing complex (RISC), where guide strand is used as a template to recognize the complementary or near-complementary region of target mRNA by RISC. When RISC finds its complementary strand, gene expression is suppressed either by degrading or blocking translation of target mRNA. Two proteins, Dicers and Argonaute (Ago) have been identified as essential for RNAi or as components of the RISC. Dicers are ∼200 kDa proteins complex and contain ATPase/RNA helicase, and Piwi–Ago–Zwille (PAZ) domains, two catalytic RNase III domains, and a C-terminal dsRNA binding domain (dsRBD). Among the two Dcrs, Dcr-1 process precursor molecules into siRNAs and miRNAs, while Dcr-2 function in downstream steps of RNAi. Ago is a ∼100 kDa protein consistently found in all RISC and microRNA ribonucleoprotein complex (miRNP) has characteristic PAZ and P-element induced wimpy testis (PIWI) domains. Among all Ago proteins, only Ago2 is believed to be responsible for mRNA degradation and gene silencing effect. Ago2 has three functional domains, PAZ, middle (MID) and PIWI. PIWI has an RNase H domain and performs the cleavage of the target mRNA substrates. Guide-strand 5′ monophosphate group tucks in between the MID and PIWI domains. Meanwhile, PAZ domain specifically recognizes the guide-strand 3′ dinucleotide overhang. This positioning exposes the guide strands “seed region” to complementary target mRNA for base pairing. Next base pairing at 10–11 nt correctly orients the scissile phosphate between them for cleavage by PIWI domain [73,74].

siRNA is a chemically synthesized short (usually 21bp), double-stranded RNA having a well-defined structure with a phosphorylated 5′ end and hydroxylated 3′ ends with two overhanging nt. siRNA get incorporated into RISC and its guide strand binds with perfect complementary to the target mRNA and degrade it. Within the RISC, mRNA cleavage ATP-independent and specific between residues base paired to nt 10 and 11 of the siRNA. After degradation, cleaved mRNA is released, and a new cycle of target mRNA degradation is started using the same guide strand in the RISC. Therefore, one siRNA molecule once associated with RISC can degrade several molecules of target mRNAs. Despite very attractive traits, there are some inherent problems associated with siRNA delivery: (1) being negatively charged macromolecules poor penetration into the cell membrane; (2) being a nucleotide, it's highly susceptible to degradation by RNases; (3) they can cause sequence dependent/independent off-target effects; (4) ineffective where target mRNA has mutated sequence, and (5) silencing effect is of short duration [75]. To improve stability and reduce off-targeting siRNAs can be covalently linked with functional or targeting molecules via either cleavable or non-cleavable bond. Zhu et al. conjugated 3′-sense strand of TGF-β1 siRNA to M6P and galactose via poly(ethylene glycol) (PEG) spacer to enhance cellular uptake by HSCs and hepatocytes, respectively [76].

Short hairpin RNA (shRNA) makes a tight hairpin turn and has been developed as an alternative RNAi molecule. An external expression vector bearing a short double-stranded DNA transcribes shRNA in the nucleus. Depending on the promoter driving their expression, shRNAs are transcribed by either RNA polymerase II or III. The shRNA transcript is then processed by Drosha, an RNase III endonuclease, which results in pre-shRNA and exported to the cytoplasm, wherein it is processed by Dicer (another RNase III enzyme) and forms siRNA, which is then incorporated into RISC. Depending on the type of expression vector shRNA can constantly be produced in the host cells leading to more durable gene silencing compared to siRNA [77].

Moreover, a shRNA technique is cost effective as an expression vector cost less than the bulk manufacturing of siRNA. Cheng et al. used two siRNAs targeting 769 and 1033 start sites of rat TGF-β1 mRNA and then converted into shRNA by cloning to enhance TGF-β1 gene silencing [78].

1.4. MICRORNAS

miRNAs are small regulatory non-coding RNA molecules of approximately 21-23 nt in length, which can modulate gene expression at post-transcriptional level. miRNAs are known to affect cell proliferation, apoptosis, inflammation, oxidative stress, and metabolism. Aberrant miRNA expression can be a key pathogenic factor in liver fibrosis. Therefore, there is an urgent need to understand the mechanisms involved in miRNA dysregulation to treat liver diseases [79]. Unlike siRNAs, miRNA do not require perfect base pairing of the seed region with mRNA for its degradation, and therefore, one miRNA can target several mRNAs. This is advantageous in term of efficiency especially when target mRNA has a mutation or alternative isoforms, but at the same time, it can induce off-target effects. This section will discuss the biogenesis, target prediction, possible chemical modification and some important deregulated miRNA in liver fibrosis [80].

1.4.1. Biogenesis and Mechanism of Action of miRNAs

More than 4000 miRNAs are known so far in the genomes of over 80 species. Multiple steps are involved in the process from 200 nt long primary transcripts translated from miRNA genes to form mature 19-25nt long miRNA. The majority of primary transcripts of miRNA originate from splicing of introns of other protein-coding genes, but miRNAs from the independent gene are also known. The primary transcript is in the form of hairpin conformation and called pri-miRNAs. This pri-miRNA contains a 5-cap structure and a poly-A tail similar to mRNA. These structures are recognized by RNAs III (Drosha) and cleaved into 70-100

nucleotide precursor miRNA called pre-miRNAs [81]. Pre-miRNA transcripts are recognized by Exportin-5 (Exp5) in the nucleus and transported to the cytoplasm. Exp5 is a nucleocytoplasmic factor and a member of karyopherin family that requires a GTP-bound form of Ran GTPase in RNA binding and nuclear export. Exp5 recognizes double-stranded RNA binding domain and double-stranded RNAs as well as RanGTP, which is present in high levels in the nucleus. This trimeric complex of RanGTP: Exp5: pre-miRNA then translocates in the cytoplasm, where RNA and Ran are released upon GTP hydrolysis. Exp5 is then recycled to the nucleus by diffusion through the nuclear pore complex for another round of transport. The expression level of Exp5 is a key factor and can affect the RNA-mediated gene silencing. In cytoplasmic Dicer enzyme recognizes pre-miRNA and cleaves the hairpin loop to produce mature miRNA duplex. Depending on the thermodynamic stability of the ends of the duplex, one strand functions as a mature miRNA and another strand is degraded. Within the original duplex, a strand with hydrogen bonding at its 5’ end is stabilized and selectively becomes the mature miRNA. Usually, miRNA strand having U residue at 5’ end forms less stable base pair (U: G or U: A) compared to G:C base pair and most likely the selection criterion for mature miRNA [82]. Despite various proposed modes of action, most studied and recognized mode of gene silencing by miRNAs is by inhibiting translation. Mature miRNA strand incorporates into RISC. RISC complex recognizes its target mRNA, based on the complementarity of different degrees as described. Perfect complementarity between a miRNA-target mRNA pair leads to mRNA degradation, whereas imperfection in pairing leads to several alternative mechanisms of repression including:

1. Promoting ribosome drop-off
2. Degradation of the nascent polypeptide
3. Sequestration of mRNAs in P-bodies or stress granules
4. Inhibition of translation initiation

5. Inhibition of translation at a step after translation initiation, and
6. Deadenylation of mRNA

In animals, miRNAs repress target protein expression by repressing mRNA translation either at the initiation stage or during the elongation phase [83].

1.4.2. Thermodynamic Properties of miRNAs

Thermodynamic stability of miRNAs correlates with their ability to induce RNA interference. In miRNA molecule, pair mismatches, gaps, and bulges generate low internal energy and important for duplex unwinding, strand selection, and RNAi pathway. When pre-miRNA is processed to mature miRNA, strand instability and sequence asymmetry play a major contribution in the selection of sense strand and entry into RISC. miRNA loading into Ago is divided into two different steps, physical association, and activation. Activation is the rate-limiting step of the unwinding process and facilitated by the thermodynamic instability rather than structure of the duplexes [84]. Normally, the first base pair of the 5’ antisense terminus is most destabilizing elements within the pre-miRNA precursors and is required for the RNAi processing. On average, the 5′ region of the antisense strand is less stable than the 5′ terminus of the sense strand. While unwinding step by RISC helicase, strand with 5’ low internal stability is selectively processed and retained by the RISC. Thus, selective modification of the guide strand utilized for loading into RISC for higher efficacy. Elmen et al. designed locked nucleic acid (LNA) at 5’ terminus of siRNA sense strand and increased loading of the antisense strand [85]. Nucleotides 2–8 from 5’ terminal (known as a seed region) overlap with the 5′-end. Gene silencing efficiency of miRNA-is mediated both by stability between seed and target pair and stability of 5’ end. Seed-target duplex stability is the function of the nucleotide sequence, whereas the stability in the 5′-terminal is a structural feature [86].

miRNA gene silencing can be correlated, with the correlation score 'miScore' and calculated as follows:

$$\mathrm{miScore} = \mathrm{T}_{\mathbf{m\ 2-8}} - 0.5 \times \mathrm{miT}_{\mathbf{m\ 1-5}} \quad (1.1)$$

Where,
$T_{m\ 2-8}$ is the melting temperature (T_m) of the seed-target duplex (positions 2–8),
$miT_{m\ 1-5}$ is T_m value of positions 1–5 of 5′-end of miRNA duplex, and 0.5 is a multiplier coefficient as the contribution of $miT_{m\ 1-5}$ might be half of $T_{m\ 2-8}$.

Thus for efficient gene silencing miRNA should have an unstable 5′-end 5-bp duplex and a stable 7-bp seed-target duplex.

Antisense strand thermodynamic stability in the position 9-14 from 5' terminal also affects the functional ability of miRNA. For efficient gene silencing, multiple turnovers of the target mRNA release from RISC is a necessary step. Antisense strand 9-14 positions bases have low internal stability compared to sense strand bases. Low internal stability of this region in the stands may facilitate cleavage of target mRNA for release, and allows the RISC to find the next target mRNA [87]. However, it is worth to mention that the thermodynamic stability of seed region and target mRNA also reduces the off-targeting effects [88]. G: U base pair in the seed region of miRNA are known to decrease miRNA silencing efficacy significantly, although they are thermodynamically similar to A: U base pair. G: U wobble base pairs within miRNA behave like a mismatch and reduce RISC loading and unwinding [89]. Sequence analyses of miRNAs from different species show that a U or an A at the 5' position of the antisense strand. The reason is simply that the mid-domain of Ago2 has a greater affinity for ATP or UTP than CMP or GMP. Therefore, A/U nucleotide 5' terminal influences the incorporation of the guide strand into RISC strongly [90].

1.4.3. Target Prediction of miRNA

Target gene identification of miRNAs is critical for functional analysis. Biological studies to predict targets are slow and complicated, because of multiple targeting capabilities. For fast prediction of miRNA functions/targets, numerous bioinformatic methods are being used. Some of these algorithms including miRanda, TargetScan, Pictar, TargetBoost, and PITA are the gold standard before starting any biological assay. Within the RISC, miRNAs form specific base pairing with mRNA, which forms the basis for in target recognition algorithms. Normally, 5' region base pairing of the miRNA is considered more important compared to 3' region. Bases of miRNA seed region form a perfect complement with 3' region of mRNA. Most of the miRNA target prediction programs use the same general principles in the development of their algorithm and search for targets in the 3'-UTR region of various mRNAs. Base pairing at 3′ region of miRNA is considered less important for target prediction [91,92]. The RNAfold program predicts the minimum energy of secondary structures and thus pairing probabilities, and the RNAduplex program predicts possible hybridization sites within the duplex. One another fact these algorithms apply in target predictions is the degree of sequence conservation. It is believed that if 3'-UTR sequences of miRNA is conserved in orthologous species, their targets are also conserved. This phenomenon provides a useful filter in target prediction [93,94].

To begin target scanning one of the most popular algorithms miRanda first retrieves the mRNA's 3'-UTR sequences and finds out maximum complementarity alignments with 5' UTR of mature miRNA. G: C and A: T are assigned +5 score, while G: U is given +2. The gap opening is considered unsuitable for complementarity and given a negative score (-8) and gap elongation if any is assigned -2. The complementarity scores up to certain regions depending on program and parameters from the miRNA 5' end is multiplied by a scaling factor of 2. No mismatching at positions 2 to 4 at the 5' end is tolerated, and less than five mismatches between positions 3-12; and in the last five positions less than two mismatches of the alignment

are considered as a potential target. Based on the alignment and matching scores, the algorithm creates a ranking of all non-overlapping hybridization down to some cut-off values. The key difference between most of the algorithms is the difference in weight score of certain positions in the alignment [95]. Another well-established algorithm TargetScan emphasizes on the seed pairing and scan for matching between 2 to 8 positions from the 5' end of the miRNA for perfect Watson-Crick complementarity (G: C or A: U) [96].

Thermodynamic properties of the miRNA: mRNA duplex in vivo is another important factor which estimates free energy of RNA secondary structure. The stability of base-pairing depends on the G:C content of the nucleic acid sequence. However, vertical stacking of bases in a sequence-dependent manner also contributes to helix stability and thermodynamic properties of the sequence and is the function of its structure [97]. Stability of the predicted miRNA: mRNA duplex, is estimated by calculating the free energy of the duplex and checked against a threshold value, usually Gibb's free energy (G)<-17 kcal/mol or G<0-14 kcal/mol depending on the type of algorithm being used in miRanda.

In TargetScan calculated Z score is used to rank the possible target for the miRNA:

$$\mathbf{Z} = \sum_{\mathbf{K=1}}^{\mathbf{n}} \mathbf{e}^{-\mathbf{G_k}-/\mathbf{T}} \qquad (1.2)$$

Where,

n is the number of seed matches in the UTR

G_K is the free energy of the duplex for the k^{th} target site

T is the relative weighting of UTRs binding affinity and the total number of sites.

Identification of orthologous 3′ UTR mRNA sequences and checking if the potential miRNA target site is conserved in other species is another criterion of target prediction. In this method, conserved target site between orthologous species is predicted and compared to the reference species. For example, if we want to predict target in the human genome, the alignment of the target sites is generated in UTR of a human with miRNA UTR of mouse or rat.

The complementary pair's position of target sites between species must fall within ±10 residues in the aligned 3' UTRs. Conserved target sites sequence between two species must also meet a certain threshold value (≥ 90% used for analysis in humans) **(Figure 1.3)**. Based on the alignment score, free energy secondarily and after passing the conservation filter, predicted target sites for each miRNA are sorted. If more than single miRNA shows targetability, miRNA with the highest complementary score and lowest free energy is considered appropriate. An important drawback of using this prediction is that miRNAs are present in different concentrations at different cell cycles. Many miRNAs may have single binding sites, but do not compete because they are never expressed at the same time, thus can result in false negative prediction. Algorithm PicTar considers co- direct relation with a number of binding miRNAs available at that time [98]. Seed region of miRNA is short and miRNA–mRNA duplexes may not

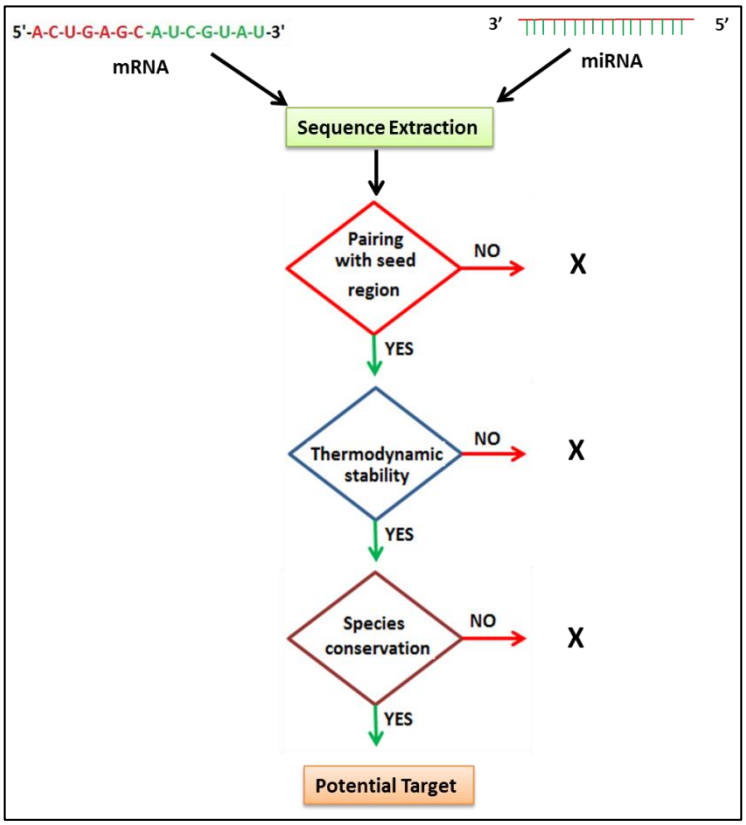

Figure 1-3. Representative steps used for miRNA target prediction by computational analysis.

be entirely complementary, which increases the complexity of gene regulation by miRNA and decrease the accuracy of target prediction. There are some reported cases where miRNAs regulate target gene independent of base pairing in the seed region. Algorithm program determines duplex stability by calculating the threshold free energy. The value of appropriate thresholds free energy is difficult to determine because it differs from organisms to organisms. At present, we have limited data sets of known free energy of miRNA–mRNA duplexes. Moreover, stable binding does not always represent the target genes.

1.5. DYSREGULATION OF miRNAs IN LIVER FIBROSIS

Aberrant expression of several miRNAs has recently been implicated in liver fibrosis and carcinogenesis. Various genes including CTGF, TGF-β1, PDGF-β, and TIMPs are markedly upregulated during hepatic fibrogenesis **(Table 1.2)**. All of these genes can be manipulated by different miRNAs, and therefore disease progression can be reversed. Two different approaches are being used for delivery and targeting of miRNAs to different cells and organs. First, is to increase the level of miRNAs in the target cells using miRNA mimic, and the second approach is to block upregulated miRNAs by using anti-miRNA, commonly known as antimiR.

1.5.1. Anti-Fibrotic miRNA

This approach uses synthetic ODNs that enhance the expression of a specific miRNA which possesses anti-fibrotic properties, but its expression is downregulated upon liver fibrosis. After entering the cells, one strand of this anti-fibrotic miRNA mimic is stabilized and get associated with the miRISC complex and inhibit the target mRNAs. Liver fibrosis leads to downregulation of several miRNAs which target several pro-fibrotic genes post-transcription level, and their overexpression decreases liver fibrosis **(Figure 1. 4)**.

1.5.1.1. miR-29b

Several recent studies have shown that miR-29 levels get significantly decreased by NF-kB in liver fibrosis, and its downregulation is inversely related to the activation of HSCs. There are three members in its family: miR-29a, b, and c. all of these target fibrosis associated key genes such as Akt, SP-1, laminin, collagen I and IV. Some studies have shown that replenishment of miR-29 family members leads to a significant decrease in collagen I and IV as well as phospho-FADD, cleaved caspase-8, 3, Bax, Bcl-2, PARP, and NF-κB expression. These results indicate that miR-29a can decrease cholestatic liver injury and fibrosis [99].

Table 1-2. Various Anti-fibrotic and pro-fibrotic miRNAs involved in liver fibrosis and their targets

Anti-fibrotic miRNA	**Target Gene**	**Reference**
miR-29b	Akt, SP-1, collagen	[100]
miR-150	C-myb, collagen, α-SMA	[101]
miR132	MeCP2	[102]
miR- 449	YKL40, NOTCH-1	[103]
miR-122	P4HA1	[104]
miR-335	TNC	[105]
miR-15b and miR-16	Bcl-2	[106]
miR-126	CRK	[107]
miR-19b, miR-101b	TGF-β	[108,109]
miR-449a,miR-107	IL-6R, JAK-1	[110]
miR-200a	Nrf2	[111]
miR-214	CCN2	[112]
miR-483	PDGF-β and TIMP2	[113]
miR-195	cyclin E1	[114]
Profibrotic miRNA		
miR-33a	PPAR-α	[115]
miR-200c	FAP-1	[116]
miR-34a	*ACSL1*	[117]
miR-27a, 27b	RXR gene	[118]
miR-21	PTEN/Akt signaling	[119]
miR-221/222	CDKN1B, PPP2R2A	[120,121]
miR-93 and miR-106b	c-Myc	[122]
miR-181b	p27	[123]
miR-615	IGF-II	[124]

1.5.1.2. miR-150

TGF-β1 suppresses miR-150, which target c-myb expression and inhibits the activation of HSCs and LX-2. c-myb is a proto-oncogene, and its activity level is increased in activated HSCs. In the influence of c-myb, HSCs gets activated and induces both collagen-I and α-SMA [125]. Overexpression of miR-150 in HSCs resulted in the inhibition of cell proliferation and reduction in ECM proteins and α-SMA. In another study, miR-150 was shown to target and downregulate ECM protein transcription factor Sp-1, without affecting Sp-1's upstream mediators, such as Smad2 and p-Smad2 [99].

1.5.1.3. miR-132

MeCP2 is a fibrosis promoting gene and regulates transdifferentiation of HSCs by inhibiting PPAR-γ transcription in hepatic fibrosis. miR-132 binds 3'-UTR of MeCP2 and inhibits its translation, and its expression is lost in HSCs upon activation. When miR-132 was incubated with myofibroblasts, it represses MeCP2 gene and hence activation [102].

1.5.1.4. miR-122

miR-122 is a liver-specific and most abundant miRNA found in the adult human liver and is downregulated in activated HSCs and fibrotic liver. miR-122 targets prolyl 4-hydroxylase (P4HA1) which is an enzyme that regulates the maturation of collagen. Overexpression of miR-122 inhibits the proliferation and activation of HSCs and collagen production [104].

1.5.1.5. miR- 449

miR-449a is an anti-fibrotic miRNA, and its level is downregulated in HCV infection mediated liver fibrosis. miR-449a plays as an anti-fibrotic role by targeting YKL40, which is upregulated in fibrosis. HCV infection upregulates TNF-α, which eventually increases NF-κB activity leading to increased inflammatory response and promote cell proliferation in the liver.

NOTCH-1 and YKL40 help TNF-α in the induction and nuclear retention of NF-κB. Increased NF-κB transcription factor leads to increased inflammatory response and promotes cell proliferation. Overexpression of miR-449a resulted in downregulation of NOTCH-1, and thus decreases overall progression of liver fibrosis [103].

1.5.1.6. miR-335

miR-335 is downregulated in activated HSCs compared to non-activated control. miR-335 targets Tenascin-C (TN-C), ECM glycoprotein, upregulated in liver fibrosis and promotes HSC migration and activation via integrin β1. Overexpression of miR-335 resulted in a decreased α-SMA and collagen Type-I level by decreasing the expression of TNC [105].

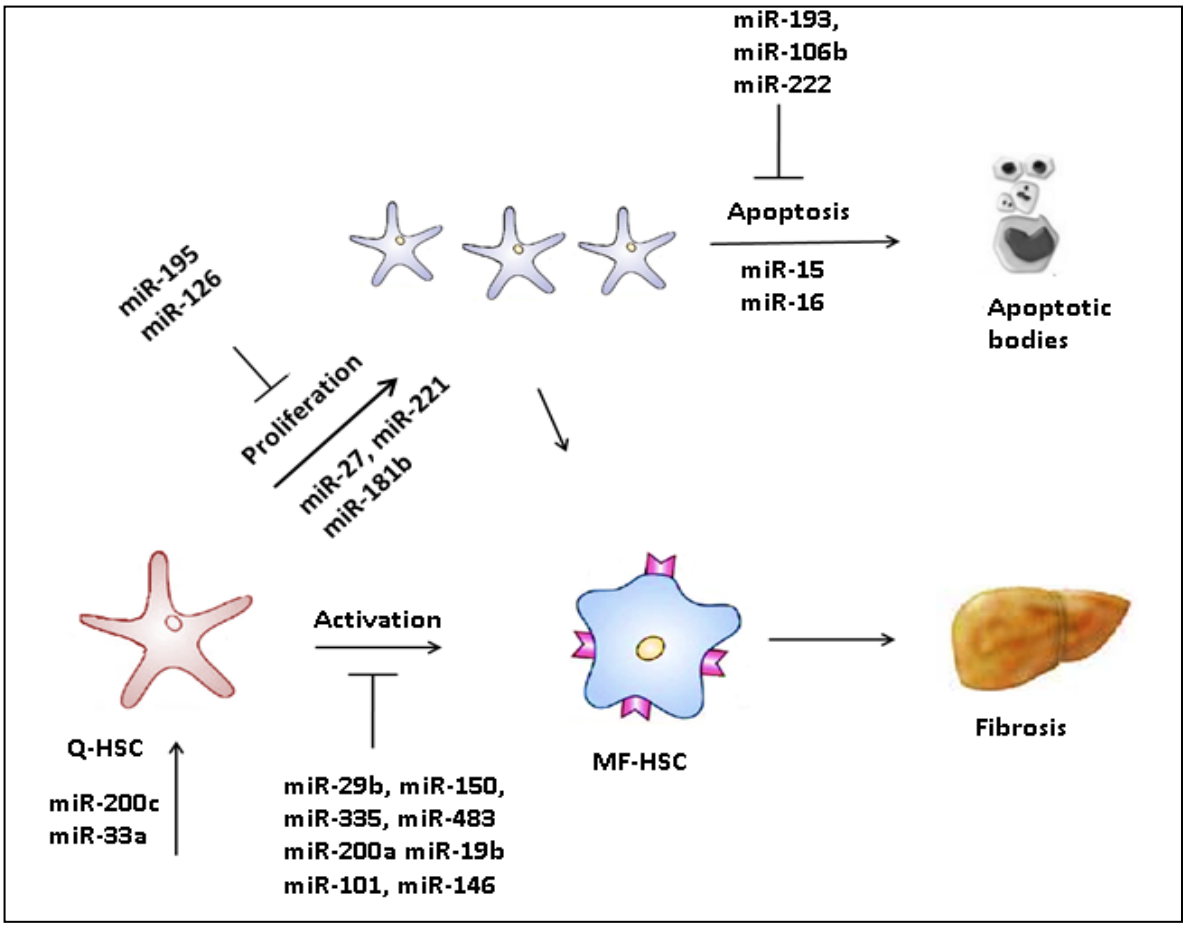

Figure 1-4. Role of various miRNA in progression as well as attenuation of liver fibrosis.

1.5.1.7. miR-126

v-crk avian sarcoma virus CT10 (CRK) expression increases during HSC's activation and has a key role in signaling pathways regulating cell adhesion, proliferation, and migration [126]. Gong et al. confirmed that due to overexpression of CRK, there was a low expression of miR-126 in activated HSCs. miR-126 directly targets 3'-UTR of CRK and controls the cell shape, cell to cell adhesion and locomotion of HSCs. Overexpression of miR-126 after transduction with lentiviral vector encoding miR-126 decreased α-SMA and collagen α (1) expression. Although miR-126 decreases HSC migration, it did not affect their proliferation [107].

1.5.1.8. miR-19b, miR-101, and miR-146a

Members of the miR-17-92 family and miR-106b-25 clusters play an important role in liver fibrosis. Ashley M. Lakner reported miR-17-92 cluster (19a, 19b, 92a) expression levels were significantly low in activated HSCs upon transfection with miR-19b, which also resulted in significant reduction in TGF-β receptor 2 (TGFBRII) expression. miR-19b also decreased SMAD3 expression post transfection and inhibited TGF-β signaling. The overall impact of miR-19b regulated HSC transdifferentiation and decreased myofibroblast marker α-SMA expression [108]. In a study by Tu et al., significant down-regulation of miR-101a and miR-101b was observed in the carbon tetrachloride (CCl_4)-induced fibrotic liver. Using computational analysis TGF-βRI mRNA, and Krueppel-like factor 6 (KLF6) mRNA were found two conserved targets of miR-101. miR-101 delivery through lentivirus suppressed liver fibrosis by reducing target genes along with collagen, vimentin, SMA , and snail [109]. He et al. investigated the antifibrotic role of miR-146a in HSCs and demonstrated that miR-146a targets SMAD4 and therefore, decreases profibrotic TGF-β pathway. miR-146a also reduces HSC proliferation and induces HSC apoptosis [127].

1.5.1.9. miR-107 and miR-449a

In a study, Sharma et al. reported down-regulation of miR-107 and miR-449a after HCV infection in patients. They demonstrated that miR-449a and miR-107 regulate IL-6-mediated chemokine (C-C motif) ligand 2 (CCL2) expression and STAT3 phosphorylation by targeting IL-6R and JAK1. CCL2 expression in HSCs. This regulates HSC chemotaxis to the site of injury and promotes HCV-induced liver fibrosis. When hepatocytes were transfected with a construct containing IL-6R UTR or JAK1 UTR along with the vector expressing miR-449a or miR-107, reduced expression of IL-6R and JAK1 was observed at RNA and protein levels [110].

1.5.1.10. miR-200a

Oxidative stress is known to involve in the activation of HSCs, ECM production, and induction of liver fibrosis. Nuclear factor-erythroid-2-related factor 2 (Nrf2) regulate transcripts of several antioxidant enzymes including NQO1 (NAD(P) H-quinone oxidoreductase, glutathione S-transferases (GSTs), and glucuronosyltransferases Kelch-like ECH-associated protein 1 (Keap1) negatively regulate (Nrf2) level and thus contribute to oxidative stress during liver fibrosis. In normal liver, miR-200 family target Keap-1 factor, and is often found down-regulated in liver fibrosis. Yang et al. demonstrated that miR-200a down-regulates Keap1 and ultimately results in Nrf2-dependent antioxidant pathways active in HSCs. miR-200a also decreased TGF-β induced α-SMA expression in HSCs [111].

1.5.1.11. miR-214

In fibrotic liver, connective tissue growth factor (CCN2) is activated by TGF-β1, and it stimulates connective tissue cell proliferation and ECM synthesis [128]. In HSCs, CCN2 levels are high during liver fibrosis, and in inverse relation with miR-214. miR-214 is transferred to neighboring HSCs or hepatocytes via exosomes to keep checking on CCN2, and its level is downregulated during fibrosis. Chen et al. when transfected pre-activated mouse HSCs with

pLmiR-214, decreased CCN2 mRNA and protein levels along with its downstream markers such as α-SMA or collagen α(I) were observed. Although collagen and SMA mRNA is not the direct target of miR-214, their levels decreased in a CCN2-dependent manner [112].

1.5.1.12. miR-483

miR-483 is down-regulated in HSCs during their activation in liver fibrosis. Fuyuan et al. determined the role of miR-483 in vivo using pre-miR-483 overexpressing transgenic mice. Compared to normal mice, pre-miR-483 overexpressing transgenic mice inhibited CCl_4-induced liver fibrosis and showed low expression of collagen and α-SMA. In LX-2 cells, miR-483 decreased TGF-β induced PDGF-β and TIMP2 expression in vitro and in CCl_4 induced fibrotic mouse model. Both PDGF-β and TIMP2 are the direct targets of miR-483. Interestingly, overexpression of miR-483 induced carcinogenesis in mouse liver by suppressing cytokine signaling 3 (Socs3) [113].

1.5.1.13. miR-195

IFNs are immunomodulatory cytokines with antiviral, and cell growth suppression effects. IFN-α is known to have antifibrotic properties in the liver [129]. Sekiya et al. reported that IFN-β induced miR-195 expression, and otherwise has low expression in normal mouse HSCs. miR-195 induction reduces cyclin E1 expression levels while increases p21 thereby inhibits cell proliferation by delaying their G1 to S phase. The direct interaction between miR-195 and cyclin E1 was studied by luciferase reporter activity by cloning two miR-195 target sites (497 bp) of the cyclin E1 3′-UTR from LX-2 cells. There was a significant decrease in luciferase activity after transfection of LX-2 cells with the miR-195 precursor. These results show the antifibrotic role of miR-195 and explain the antifibrotic mechanism of IFNs [114].

1.5.1.14. miR-15b and miR-16

Both of miR-15b and miR-16 are downregulated in HSCs upon activation. These miRNAs downregulate Bcl-2 gene expression and induce apoptosis of activated HSCs [106].

1.5.2. Pro-fibrotic miRNAs

Aberrantly up-regulated miRNA can cause a significant change in critical biological pathways. The inhibition of target miRNA is based on specific annealing with a synthetic complementary sequence known as antagomir or anti-miR. An ant-miR is usually complementary to the specific miRNA target with either mispairing at Ago2 cleavage site or some base modification to inhibit Ago2 cleavage. Studies by various groups have shown that modulating miRNA by anti-miR can effectively regulate biological process in liver fibrosis and can produce beneficial therapeutic effects.

1.5.2.1. miR-33a

miR-33a with its host gene sterol regulatory element-binding protein 2 (SREBP2) is overexpressed in activated Lx-2 cells than in quiescent cells. PPAR-α is one of the predicted targets of miR-33a using bioinformatics analysis. Anti-miR-33a significantly increases target gene PPAR-α at mRNA and protein levels, suggesting that miR-33a modulates HSC functions by targeting PPAR-α. Also, miR-33a activates PI3K/Akt pathway and induces expression of ECM through HSCs [115].

1.5.2.2. miR-200c

HCV infection results in the up-regulation of miR-200c, which is in direct correlation with increasing growth factors and hormones. HCV infection results in the inhibition of Fas-associated phosphatase 1 (FAP-1) that regulates the function of oncogenic SRC kinase and

upregulates different growth factors. Increased level of miR-200c decreases FAP-1 expression, and thus promotes fibrosis by modulating growth factor signaling Src activation [116].

1.5.2.3. miR-34a

miR-34a is upregulated in di-nitrosamine (DMN) induced liver fibrosis. It targets and decreases the levels of acyl-CoA synthetase long-chain member 1 (ACSL1*)* gene. ACSL1 regulates hepatocellular lipid metabolism and its low-level results in accumulation of high intracellular fat, which eventually leads to apoptosis, chronic liver injury and nonalcoholic liver fibrosis [117].

1.5.2.4. miR-27a, 27b

In one of the studies, miR-27a and 27b are found up-regulated in HSCs. miR-27a/b directly targets receptor retinoid X (RXR) gene and downregulate its expression in fibrosis. RXRα is involved in multiple signaling pathways related to cell proliferation and differentiation by forming a heterodimer with PPAR-γ. Transfection with anti-miR-27 partly reverses the phenotype of activated HSCs [118].

1.5.2.5. miR-21

miR-21 is upregulated in various organ fibrosis including liver fibrosis and plays an important role in PDGF-BB-induced liver fibrosis. In a recent study, miR-21 was found to regulate PTEN/Akt pathway and promote liver fibrosis [119]. miR-21 also targets Smad7, a negative regulator of TGF-β signaling. Overexpression of miR-21 enhances TGF-β signaling and leads to increased fibrogenesis [130].

1.5.2.6. miR-222

Ogawa et al. reported upregulation of miR-221/222 in human fibrotic patients and fibrotic rodent model. There was a direct correlation between miR-221/222 expression level with that of

collagen-1. miR-222 was found to target CDKN1B gene [121]. Wen-Jun et al. reported that high expression level of miR-222 in activated HSCs, with a direct correlation between miR-222 expression levels and biliary atresia (BA) disease. Pathology of early BA includes the absence of patent extrahepatic bile ducts (EHBD) with inflammation and fibrosis in the hepatic portal area and ultimately leading to cholestasis and liver fibrosis in infants. Increased miR-222 expression levels target PP2R2A gene and activate the Akt pathway. Phosphorylated Akt inhibits the release of mitochondrial cytochrome-c and active caspase-9, thus prevents apoptosis and stimulate proliferation of HSCs [120].

1.5.2.7. miR-93 and miR-106b

During chronic fibrosis, hepatocytes up-regulate c-Myc expression and consequently alters the levels of several miRNAs. Specifically, c-Myc up-regulate MCM7 gene, and miR-106b-25 cluster as this cluster is embedded in the intron of MCM7 gene. Pineau et al. reported up-regulation of miR-93 and miR-106b during the development of hepatic cirrhosis, which eventually leads to HCC. Target genes of this cluster induce cell proliferation or decreased apoptosis and metastasis in hepatocellular carcinoma [122].

1.5.2.8. miR-181

Wang et al. demonstrated significantly high levels of miR-181a and miR-181b in TGF-β1 treated HSC-T6 cells. miR-181b is a growth regulator and increases S phase of cell cycle, and thereby promotes HSC-T6 proliferation. Cyclin-dependent kinase inhibitor 1B (CDNK1B) gene encodes a p27 protein that binds to and controls the cell cycle progression at G1 phase by preventing cyclin E-CDK2 or cyclin D-CDK4 complex activation. 3'-UTR mRNA of p27 encompasses binding site for miR-181a and miR-181b. Experimentally, miR-181b, but not miR-181a, targets p27 and downregulates its endogenous expression in HSC-T6 cells. Moreover,

there is an elevated miR-181b expression in the serum of cirrhosis patients. Therefore, miR-181b can also serve as a biomarker for liver fibrosis and cirrhosis [123].

1.5.2.9. miR-615

Tayebi et al. investigated the role of miR-615 in hepatocellular carcinoma (HCC). The mir-615 level was undetectable in healthy liver tissues, but its expression was up-regulated significantly in HCC patient liver tissues. miR-615 represents a scenario where an anticancer miRNA only appears in cirrhotic and cancerous tissues. miR-615 showed a significant retardation in cellular proliferation and migration effect in HuH-7 and HepG2 cells. Using luciferase reporter assay 3'-UTR of IGF-II gene was found the direct target for miR-615-5p, which is a potent mitogen frequently overexpressed in HCC [124].

1.6. CHEMICAL MODIFICATION OF miRNAs

miRNAs are not stable molecules and tend to hydrolyze in the acidic or basic environment. Moreover, naked miRNAs are susceptible to degradation by various RNases present in the serum as well as in the intracellular environment and thus possess very short half-life in vivo. However, miRNA can be chemically modified to alter their properties such as nuclease resistance, binding affinity, increased cellular uptake and decreased off-target effects [131]. Resistance to degradation can be enhanced by chemical modifications in the backbone or in the sugar moiety. Type and site selection for modification can pose challenges while designing modified miRNAs. Some of the common modifications used for improving the stability and potency of miRNAs are:

1. PS modification includes replacement of non-bridging oxygen atom with sulfur atom.
2. 2'-O-methyl- (2′-OMe) or 2′-O-methoxyethyl oligonucleotides (2′-O-MEO)
3. Locked nucleic acid (LNA) oligonucleotides
4. Peptide nucleic acid (PNA)

5. Fluorine derivatives (FANA and 2′-F)

Most of these modifications are preferred in the passenger strand or at 3’ end of the guide strand to avoid any functionality issue of miRNA. There are certain rules which are followed while modifying RNA. The 5’-end of the guide strand is critical for activity, hence cannot be modified and should have free hydroxyl or phosphate group. Modification on 3’-end of both strands is less prone to efficacy loss and can be modified by various means. 5’-end of the passenger strand can be modified with protecting functional groups to reduce enzymatic degradation. Ribose sugars of both strands can be modified at 2’ position with halogens or small hydrocarbons. Large molecules such as 2’-OMe can only be acceptable in a passenger strand. O-methyl groups at 2’ position of the ribosyl ring in the guide strand alter the thermodynamic properties of the duplex and reduce off-target effects. With this modification, the binding affinity (melting temperature or Tm) of the duplex becomes higher than one without modification [132]. 3’-Exonucleases are the primary enzymes responsible for ODN degradation in the serum. 2’-OMe modified miRNA is less susceptible to degradation by these degrading enzymes. On the other hand, heavy 2’- OMe modification can abolish RNA potency completely. Pyrimidines in the guide strand can be halogenated for increasing the potency of miRNA. The 2’-F modification allow more favorable interactions of miRNA with the RISC and dramatically improve the efficacy. The combined use of 2′-F pyrimidines with 2′-OMe purines can result in enhanced stability of RNA duplexes and improved performance in-vivo [133].

Nucleic acid phosphate bonds between the nucleotides are cleaved by both endo- and exonucleases. The PS backbone modification is most common and can be used in either strand to stabilize the RNA structure. In this modification, a non-bridging oxygen atom in the phosphate backbone is replaced with a sulfur atom. This modification reduces the nuclease degradation of this bond. However, it has a significant impact on miRNA efficacy, as it reduces binding affinity, lower Tm and increases toxicity as the number of PS is increased. Therefore, it is critical to

place PS modification at selective locations only [134]. Combining 2'-OMe nt and PS modification at selective molecule can be a better strategy to protect from exonuclease attack and without additional negative effects [135]. An alternative backbone modification to PS is a boranophosphate linkage that not only increases serum stability but also substantially increases its potency. Mayumi et al. investigated the effect of the modification of anti-miR-21 and anti-miR-122 by 2′-OMe-4-thioribonucleoside in terms of potency and duration of activity in vitro. Moreover, after systemic administration modified miRNAs using a liposomal delivery system, there was an increase in the levels of target miRNA [136].

Locked nucleic acid (LNA) is a modified RNA nucleotide whose ribose moiety is modified with an extra bridge connecting the 2'-O of sugar is to the 4'-C via a methylene bridge and lock the structure into 3' conformation. This modification stabilizes the molecule against nucleases, but more importantly it increases binding affinity by increasing T_m from 1-6 °C per modification of miRNA duplex. Gunter et al. showed that 2'-OMe modified antimiR-21, but not 2'-DNA specifically inactivate target miRNA activity in HeLa cells [137]. LNA can be used alone or in combination with other modifications to get the desired properties of miRNA molecule. Modifications resulting in increased binding affinity make a miRNA nonspecific to its target. Joacim et al. used LNA and PS modified antimiR-122 to silence miR-122 function in non-human primates. Results show that highly substituted LNA modification enabled to reduce the dose in antagonizing miR-122 in vivo [138]. In morpholino modification, a six-membered morpholine ring replaces the sugar moiety to improve the physicochemical and binding affinity of oligomers. Morpholinos are non-toxic, charged neutral, stable against nucleases, and increase the binding affinity of oligomers to miRNAs. Wigard et al. used morpholino-modified oligo complementary to miR-206 and induced complete or near complete loss of target miRNA [139].

1.7. DELIVERY OF miRNAs

Despite their therapeutic potential, in vivo applications of miRNAs are limited due to their anionic charge, poor stability, and high molecular weight. These factors pose major obstacles to their therapeutic application. Several approaches have been explored for in vivo delivery and targeting of miRNAs to modulate gene expression. These include cationic polymers, nanoparticles, and bioconjugates. This section will discuss some of these approaches.

1.7.1. Non-Targeted Particulate Systems

Nanocarriers can overcome aforementioned challenges associated with the in vivo delivery of miRNAs. These miRNA carrying nanoparticles offer several advantages including increased stability and reduced dose frequency, tunable small nano-scale size facilitates passive targeting, possesses favorable biodistribution, they can neutralize the polyanionic charge of miRNAs and can facilitate its crossing through negatively charged cell membranes. Normally, these particles are non-immunogenic compared to viruses, allowing repeated treatment for chronic diseases, thus providing a platform for targeting and imaging. Several nano-delivery systems made of different materials with varying physicochemical properties have been pursued in vivo miRNA therapeutics **(Figure 1.5)**. They include polymer/lipid-based nanoparticles, lipid-based liposomes, and virus-like particles [140].

Ammar et al. designed nanoparticle complexes for the photo-activated miRNA delivery. miR-148b mimic was conjugated to the surface of silver nanoparticles via a photocleavable (PC) link. Upon discrete photo trigger, miRNA was released and upregulate its level in cell culture to modulate osteogenesis [141]. Shu-Hao et al. designed cationic lipid nanoparticles (LNP) for delivery of miR-122 for restoring deregulated gene expression in HCC cells. These LNP were safe upon systemic administration and did not cause an innate inflammatory response or systemic toxicity in immune competent mice. In miR-122 knockout (KO) mice LNP-DP1 loaded

with miR-122 when injected intravenously increased the expression level of miR-122 compared to the negative control and with a concomitant decrease in the protein levels of two of its validated targets namely, Adam10 and Mapre1. This delivery system was able to reduce angiogenesis in tumors and suppress tumor growth [142]. Similarly, Pasqualino et al. developed stable nucleic acid-lipid particles (SNALPs) that encapsulate miR-199b-5p and decreased medulloblastoma (MB) cancer stem cells (CSCs) through a decrease in CD133+/CD15+ cell population [143]. Dipankar et al. developed a systemic miRNA delivery to pancreatic cancer by liposomes prepared using cationic lipid DOTAP and co-lipids cholesterol and DSPE-PEG-OMe. They have evaluated these formulations for the systemic miRNA delivery and demonstrated the growth inhibition of subcutaneous pancreatic cancer xenografts [144].

miRNAs can degrade mRNA even without perfect base pairing of the seed region and may often lead to off-target effects. Therefore, it is important to track miRNA containing formulation into the transfected cells. For this purpose, Gomes et al. developed nanoparticles composed of poly(lactide-co-glycolide) (PLGA) carrying MRI detectable PFCE for cell tracking and simultaneous delivery of miR-132 [145]. Aramaki et al. developed a liposomal system that can encapsulate ultrasound contrast gas and miRNA. They utilized these bubble liposomes (BLs) for miR-126 delivery for an ischemia-induced angiogenic response. BLs contains perfluoro propane gas and can be tracked using ultrasound detection method in vivo [146].

Polyethylenimine (PEI) is protonated at acidic pH and can form complexes with negatively charged ODNs. These polyplexes internalized via caveolae- or clathrin-dependent mechanism into cells and followed “proton sponge effect” and thereby facilitate RNAi release from endosomes. For this property, PEI has been extensively studied to deliver RNAi in the past decades, but high toxicity limits its utilization as a carrier system. Low molecular weight PEI is less toxic and thus Ahmed et al. delivered miR-145 and miR-33a after complex formation with low molecular weight PEI for antitumor effects [147]. Pan et al. developed

miRNA delivery system based on bacteriophage MS2 virus-like particles (VLPs). These particles were loaded with a single plasmid expression system for the production of VLPs containing pre-miR-146a or negative control RNA. HIV Tat47–57 was conjugated to MS2 VLPs by reacting amino group of MS2 VLP capsids and the cysteine of Tat47–57 peptide with the help of sulfosuccinimidyl 4-(p-maleimidophenyl) butyrate (sulfur-SMPB). These MS2 VLPs had high transfection efficacy and suppressed its target gene IRAK-1 significantly in vivo [148]. Although transfection efficiency of virus-based systems is excellent, they are not considered safe for human use.

1.7.2. Targeted Particulate Systems

Transfection efficiency of chemically synthesized carriers can be enhanced by relatively optimizing particle size and surface properties and by attaching targeting moiety for a favorable biodistribution in vivo. Furthermore, targeted polymeric carrier system allows higher accumulation at the disease site and higher receptors based uptake in appropriate cells and minimize side effects. Normally, targeting ligands have high affinity to specific cell receptors and are attached to the exterior surface of carrier delivery system or directly to the miRNA. Various types of ligands including functional peptides, antibodies (Ab) and aptamers have been explored for targeting miRNA carriers. Huang et. al. developed a polycation-hyaluronic acid (LPH) based liposomal nanocarrier formulation conjugated with tumor targeting single-chain antibody fragment (scFv). These tumors targeted formulations were used for systemic delivery of miR-34a into experimental lung metastasis of murine B16F10 melanoma. Formulations containing miR-34a were more effective in inhibiting the tumor growth compared to non-targeted formulations [149]. Wang and coworkers have developed PEGylated cyclic RGD (cRGD) peptide modified LPH NP formulation delivery of anti-miR-296. These formulations were used to target αvβ3 integrin present on endothelial cells of the neo tumor vasculature. cRGD modified LPH NPs have shown the potential of delivering miRNA at target sites and produced significant

anti-angiogenic effect [150]. Hu et al. synthesized polyethylenimine-β-cyclodextrin (PEI-CD) by crosslinking β-CD with low molecular weight PEI (600Da), and conjugated a tumor homing and penetrating bifunctional peptide CC9 (CRGDKGPDC). Formulation complexed with miR-34a was able to accumulate significantly at the tumor site and downregulated target genes, such as E2F3, Bcl-2, c-Myc and cyclin D1 [151].

1.7.3. Non-particulate Systems

Esposito et al. used tyrosine kinase AXL receptor binding nucleic acid aptamer (GL21.T) as carriers for cell-targeted delivery of a miRNA. This aptamer itself antagonizes oncogenic receptors and also deliver tumor suppressor miRNA function in AXL-expressing tumors.

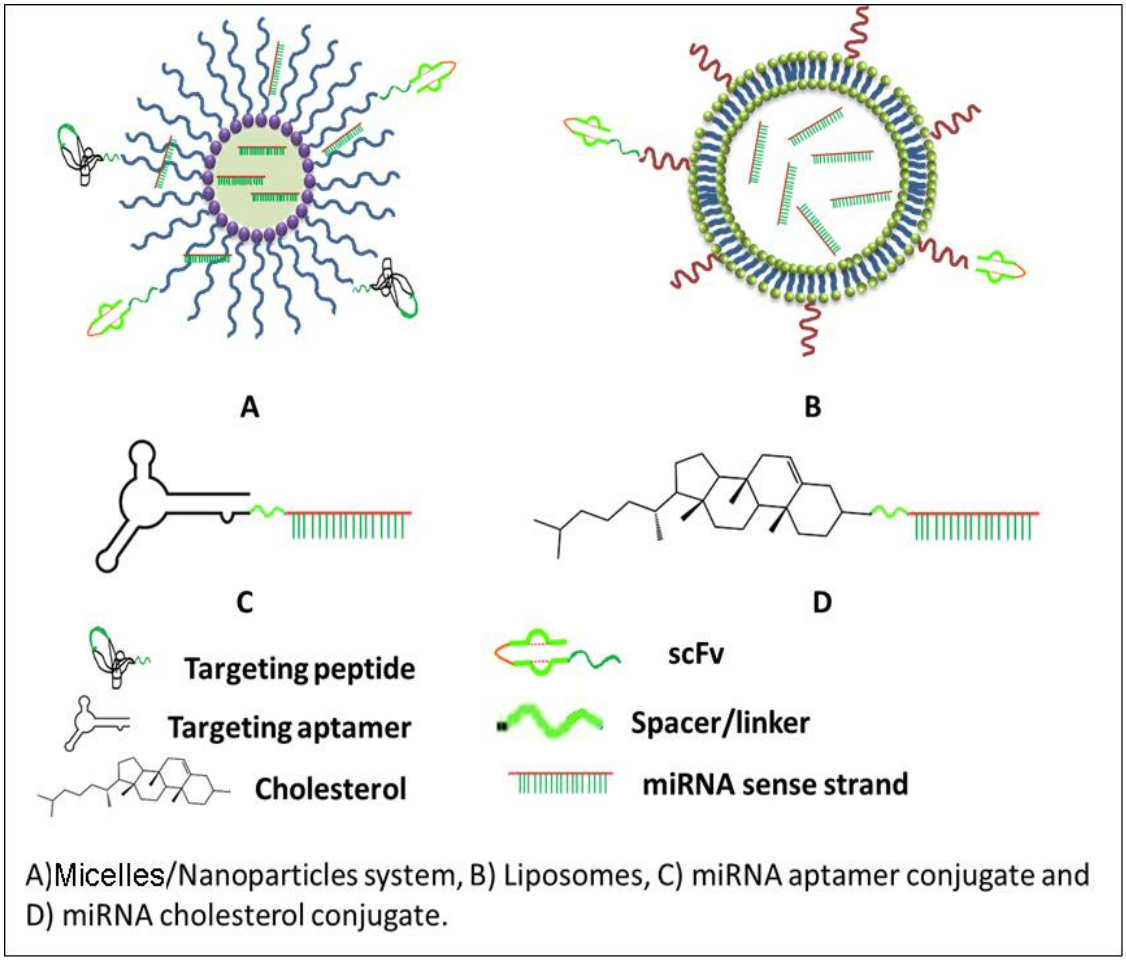

Figure 1-5. Strategies used for delivery and targeting of miRNA in vivo.

Conjugation of miR-let7g to GL21.T ensures its specific delivery to target cells and decreases the tumor growth **(Figure 1.5)** [152]. Krutzfeldt et al. developed 2′-OMe PS modified, 3′-end cholesterol-conjugated single-stranded RNA analogs complementary to miR-122. Whereas non-conjugated, but partially or fully PS modified backbone, and 2′-OMe sugar modifications led to only incomplete effect [153]. Neri et al. used similar modification for anti-miR-221/222 for treating a prostate tumor in mouse xenograft model [154]. Anti-tumor effect of cholesterol conjugated miR-199a/b-3p was determined by Jin et al. both in vitro and in vivo for treating hepatocellular carcinoma. After intratumoral injection of conjugated miR-199a/b-3p, its expression in the tumor was elevated while there was dramatic repression of HCC growth [155].

1.8. PANCREATIC DUCTAL ADENOCARCINOMA

Pancreatic ductal adenocarcinoma (PDAC) accounts for 90% of the pancreatic cancers with 5-year survival rate of only 6.7% [156]. PDAC is considered to be a fatal malignancy with estimated 53000 new cases and estimated 41000 deaths in 2016. Gemcitabine is the first line therapy of PDAC, and it has been tried in combination with several other chemotherapeutic drugs. However, improvement in overall survival failed in almost all up-to-date trials, which may be attributed to the emergence of chemoresistance and desmoplasia in PDAC [157].

1.8.1. Pathogenesis of Pancreatic Cancer

Advancement in the molecular analysis has revealed several molecular aberrations involve in the development and progression of PDAC. Wherein, a number of oncogenes are found activated, and several tumor-suppressor genes get inactivated leading to the clinical symptoms. In a study, averages of 63 genetic alterations affecting 12 cellular signaling pathways were found altered in 67–100% of the tumors [158]. Among various commonly found pathways, point mutations in K-RAS oncogene were observed in as high as 80–90% of pancreatic cancers. K-RAS is a GTP-binding protein, which is upstream of B-RAF, ERK, MEK proteins, and transmits signal from outside of the cell to the nucleus. In wild-type K-RAS

signaling, epidermal growth factor (EGF) receptor binding activates the cascade and results in increased cell growth and proliferation. The mutated K-RAS results in constitutive activation of signaling, leading to uncontrolled cell growth. The p16 gene is also found inactivated in most of the pancreatic cancer patients either by deletion, mutation or hypermethylation. p16 gene inactivates cyclin D1 and CDK4/6, which inhibits the cell cycle progression mediated by retinoblastoma (Rb) protein. Mutation in p16 results in uncontrolled cell growth and is directly correlated with larger tumor size and short survival of patients [159].

p53 gene arrests the cell cycle in G1 phase by activating p21WAF1 and controls cell cycle. Approximately 50% of pancreatic cancer patients have inactivated p53 gene either due to mutation or deletion [160]. Notch receptor is a single-pass transmembrane protein, its extracellular domain after binding to Notch ligands (D11-1, D11-3, D11-4, Jagged-1, and Jagged-2) translocate the intracellular notch into the nucleus and regulates target gene expression [159,161-163]. Further, Notch also induces nuclear factor-κB (NF-κB) and control the pancreatic cancer progression. Hh signaling is also found aberrantly activated in around 70% of pancreatic cancer patients [164]. Hh pathway components Shh, IHh, PTCH, and SMO levels are prominent during PDAC [165]. The Hh pathway is involved in epithelial to mesenchymal transition (EMT), desmoplasia, and cancer stem cell (CSCs) maintenance. Another gene DPC4 (SMAD4) plays a pivotal role in cellular growth and angiogenesis. It is found to be inactivated in approximately 50% of pancreatic cancer cases [166]. EGF receptors are a transmembrane protein. EGF ligand binding to its receptors activates several downstream pathways including PI3K, MAPK, Src, and STAT, which are involved in cell proliferation, invasion, metastasis and survival [167].

1.8.2. Chemoresistance

Chemoresistance is a major barrier to the treatment of PDAC. Resistance can be intrinsic due to the capability of cancer cells to bypass the drug effects, or acquired during

multiple treatment phases after which patients are irresponsive to therapy. Reduced uptake of chemotherapeutics is one of the mechanisms by which cells resist to therapy. For example, epigenetic changes in the tumor cells reduce nucleoside transporters and as a result gemcitabine uptake is reduced. ATP-binding cassette (ABC) efflux transporters like MDR1 or MRP1-6 upregulation can increase efflux of the drug by cancer cells, and result in resistance to chemotherapy [168]. Drug resistance by cancer cells could also be acquired by activating DNA-repair capacity and by a mutation in apoptosis-inducing pathways [169].

EMT in pancreatic cancer is well documented in acquiring chemoresistance. For example, EMT program is associated with gemcitabine drug resistance and poor patient survival. EMT process involves several cytokines and signaling pathways such as Wnt, TGF-β, Hh, Notch1, and NF-κB [170]. The mesenchymal cells morphology is characterized by decreased expression of CDH1 gene (up to 5-folds) which encodes for E-cadherin and increased expression of SNAI2 genes (up to 51-fold) which encodes for Slug. Moreover, drug-resistant CSCs are known to have decreased expression of E-cadherin and increased expression of vimentin a typical EMT feature [171,172]. Therefore, targeting EMT could be a promising strategy to eradicate SCCs and to chemosensitize cancer cells. `

1.8.3. Pancreatic Cancer Microenvironment

PDAC microenvironment is characterized by dysfunctional vasculature and intense desmoplastic reactions, resulting in high interstitial pressure. Therefore, delivery of chemotherapeutic drugs to the bulk of the pancreatic tumor is greatly impeded. Pancreatic stellate cells (PSCs) and activated fibroblasts are implied to secrete ECM proteins in PC. Secretion of ECM is regulated by several growth factors including FGF, EGF, TGF-β, and connective tissue growth factors (CTGF). TGF-β stimulates collagen 1 production in PCC increasing SNAIL through SMAD pathway and stimulates fibroblast induces through inducing

FGF [173]. Importantly, Hh signaling plays a crucial role in desmoplastic reactions in PC, and its pharmacological inhibition can overcome stroma. Further, inhibition of Hh has been reported to sensitize tumor cells to radiation therapy [174].

1.9. ROLE OF miRNAS IN PANCREATIC CANCER

Recent advances in cancer biology have revealed several miRNAs that take part in pancreatic cancer initiation and progression by regulating cell cycle, DNA repair, apoptosis, invasivity, and metastasis. Therefore, several miRNAs have been discovered and being investigated to overcome the inefficacy of chemotherapeutics [175]. miRNAs can be tumor suppressors (found down-regulated in cancer) or tumor initiators called “oncomiRs” (found upregulated). Dysregulated levels of various miRNAs correlate well with poor overall survival rate, drug resistance, EMT, and invasion and metastasis. Interestingly, a single miRNA can have multiple targets, and several of the cancer targets or phenotypes are interconnected. Therefore, the exact function of a particular miRNA can be overlapping. Some of the miRNAs which is directly related to PDAC are discussed blow.

1.9.1. Diagnostic

Detection of pancreatic cancer at the early stage is difficult and because mostly it’s asymptomatic, but if present any is non-specific. Early detection of the disease may increase chances of treatment. Therefore, early stage biomarkers of PDAC have high importance. The expression profiles of miRNAs could differentiate among normal pancreas, chronic pancreatitis, and pancreatic cancer, therefore, could be used as the diagnostic tools. For example, in pancreatic tumors miR-103 and miR-107 are up-regulated, and miR-155, and miR-200 are down-regulated in PDAC and could be used to discriminate tumor tissue from the normal pancreas [176].

1.9.2. Growth and Proliferation

Several miRNAs have been directly correlated with KRAS-EGFR pathway in PDAC. miR-146a is a tumor suppressor miRNA, which is reported to target EGFR directly and thereby decreases cell proliferation and invasion. miR-200c can target mitogen-inducible gene 6 which is a negative regulator of EGFR. AKT signaling pathway contributes to cancer cell survival and proliferation. miR-375 negatively regulates the expression of 3-phosphoinositide-dependent protein kinase 1 (PDK1) and reduces malignant behavior of PDAC cells through the AKT signaling pathway. MUC4 protein overexpression in PDAC up-regulates Her2 expression which is a key regulator of oncogenesis. The expression of miR-150 is downregulated in PDAC, and it targets MUC4 mRNA. Treatment with nanoparticles containing miR-150 showed decreased growth and clonogenicity of PDAC cells [177].

1.9.3. Chemoresistance

Various miRNAs play a pivotal role in the induction as well as suppression of chemoresistance in PDAC. For example, miR-21, miR-196a, miR-221, miR-200 family, and miR-214 can increase drug tolerance capacity of PC cells [178]. On the other hand, the miR-let7 family has demonstrated the potential chemosensitizer role in pancreatic cancer [179]. We delivered miRNA-205 with gemcitabine, in a pancreatic cancer ectopic tumor model developed using gemcitabine-resistant MIA PaCa-2R cells. We found miR-205 in combination with gemcitabine formulations effectively reversed chemoresistance. In pancreatic tumor model, the combination formulation treated group showed significant inhibition of tumor growth and decreased tumor cell proliferation [180]. TGF-β upregulation increases expression of membrane type-1 MMP and ERK1/2 and downregulates miR-let7 [181]. Thus, targeting TGF-β using RNAi could provide an attractive strategy to diminish desmoplasia mediated chemoresistance.

1.9.4. Stem Cells

miRNAs play an important role in CSCs maintenance and drug resistance capacity of CSCs [182]. miR-200 a/b/c is one such widely investigated miRNA family which suppresses stemness of cancer cells by inhibiting stem cell factors such as Sox2, SIP 1 and ZEB-1 [183]. Overexpression of miR-26a using metformin has been shown to decreased expression of EpCAM and EZH2 (CSC markers) in pancreatic cancer. Further, miR-200c works cooperatively with miR-203 and miR-183 to suppress the expression of stem cell factors. Moreover, decreased levels of Let-7a, miR-30c, miR-30b and miR-30a also helped stem cell to gain resistance. Activation of Notch has also been implicated in EMT and drug resistance. Notch activation is mediated through overexpression of miR-21 and downregulation of miR-200 family and let-7 family [184].

1.10. CONCLUSIONS

miRNA-based research is expanding because it gives the opportunity to control multiple targets simultaneously in various disease models. The role of miRNAs in liver fibrosis and as tumor suppressors, or oncogenic in cancer including PDAC, has been witnessing rapid progress. However, there is a significant vacuum regarding their in vivo delivery and product development at clinical scale. Further, their delivery aspect in diseases like liver fibrosis and PDAC is negatively affected by the stromal microenvironment. To overcome ECM barrier and drug resistance, we successfully co-delivered miRNA and small drug molecule using the micellar system in vivo. Apart from these delivery-related considerations, an investigation into the cellular and long-term effects of the delivered miRNA is crucial for the development of safe, effective and clinically relevant miRNA therapeutics. During the development of next generation delivery system some points should be considered, which are as follows: (i) simplicity of

the drug and its delivery system: the drug should be easy for manufacturing, quality control, handling and comparatively low-cost. (ii) Safety problems should be minimal. No extra chemical entities should be used which may affect structural stability. (iii) Oral delivery is still a challenge for therapeutic genes due to their resistance to proteolysis. Despite of these challenges, the ongoing miRNA-based human clinical trials including the use of miR-122 ODN (Miravirsen) in null responders to PEGylated IFN-α plus Ribavirin subjects with chronic HCV (Phase 2 clinical trial, NCT02031133), SPC3649 (Santaris Pharma, Horsholm, Denmark), a miR-122 antisense LNA, and MRX-34 (a liposomal miR-34 mimic) in primary HCC metastatic liver cancer (phase 1) have generated hope for better future of miRNA-based therapy [185].

CHAPTER 2. NANOMEDICINES OF HEDGEHOG INHIBITOR AND PPAR-γ AGONIST FOR TREATING LIVER FIBROSIS

2.1. INTRODUCTION

Hh pathway plays an important role in the construction and remodeling of injured tissues [186]. Hh ligand initiates smoothened (SMO) mediated signaling to activate Gli family transcription factors. Activation of Gli proteins results in the induction of epithelial to mesenchymal transition (EMT) which is a key event in the initiation and progression of fibrosis [187]. Upon activation, HSCs lose PPAR-γ, a nuclear family receptor, which maintain the quiescent state of HSCs through dimerization with liver X receptor-α and alters the transcription of numerous genes including PDGF-β, TNF-α, and TGF-β1 [188,189].

Although much is known about the molecular basis and pathophysiology of liver fibrosis, successful application of new therapeutic approaches is limited. Thus, there is an urgent need to develop an alternative and effective treatment for liver fibrosis. CBDL activates HSCs and increases the expression of patched homolog 1 (Ptch-1), sonic hedgehog (Shh) and Gli-1, but downregulates PPAR-γ expression [190,191]. We have recently shown that Hh inhibitor such as cyclopamine and GDC-0449 can significantly reduce the progression of liver fibrosis induced by CBDL in rats [39,192]. Treatment with PPAR-γ agonist rosiglitazone (RSG) inhibits HSC activation and inflammatory pathways such as nuclear factor κB (NFκB), IL-6, and TNF-α [193].

Since GDC-0449 has anticancer activity and RSG causes cardiac complications, the purpose of this study was to determine whether we can treat liver fibrosis by co-delivery of these two drugs at the half of their individual doses [194,195]. Since these two drugs are poorly soluble in water and RSG has a short half-life, we decided to encapsulate them into biodegradable nanoparticles. Since nanoparticles can improve their pharmacokinetic profiles and reduce their side effects, we first synthesized methoxy-polyethylene-glycol-b-poly(carbonate-co-lactide) [mPEG-b-P(CB-co-LA)] copolymer and characterized it by ^{1}H NMR.

Nanoparticles were characterized by particle size distribution, drug loading, and drug release. Anti-fibrotic properties of the formulations were determined by measuring the levels of Hh ligands, PPAR-γ and other fibrosis related markers in normal and CBDL rats after systemic administration of nanoparticles loaded with GDC-0449 and RSG as a single drug or both at half of their individual doses. Our main objective was to determine whether the combination treatment even at half dose can provide hepatoprotection and treat liver fibrosis.

2.2. MATERIALS AND METHODS

2.2.1. Materials

2, 2-Bis (hydroxymethyl) propionic acid, methoxy poly (ethylene glycol) (mPEG, Mn = 5000, PDI= 1.03), stannous 2-ethylhexanoate ($Sn(Oct)_2$), and benzyl bromide were purchased from Sigma-Aldrich (St. Louis, MO). Enzyme color endpoint assay kit for alanine aminotransferase (ALT) and aspartate aminotransferase (AST) was purchased from ID Labs™ Inc. (London, ON, Canada), and rat TNF-α ELISA, total bilirubin (BIL) detection kit from Bio-scientific (Austin, TX). Radioimmunoprecipitation assay (RIPA) buffer was purchased from (Roche, Indianapolis, IN). L-lactide (LA) was purchased from PURAC Biochem BV (Gorinchem, Netherlands) and recrystallized from ethyl acetate. All other reagents were obtained from Sigma-Aldrich and used without further purification.

2.2.2. Synthesis and characterization of mPEG-b-P(CB-co-LA)

mPEG-b-p(CB-co-LA) copolymer was synthesized by ring opening polymerization (ROP) as described previously [196]. Briefly, mPEG, 5-methyl-5-benzyloxycarbonyl-1, 3-dioxane-2-one (MBC) and L-lactide were taken at a ratio of 1:2.5:2.5, respectively to synthesize a copolymer of targeted average molecular weight of 30 kDa. $Sn(Oct)_2$ (10 mol% relative to mPEG) was used as a catalyst for the reaction. The mixture was stirred for 24 h at 130°C under vacuum. After cooling, the product was dissolved in chloroform and purified by precipitation in excess of diethyl

ether and hexane (1:2). The copolymer was characterized by ^{1}H NMR and spectra were recorded with a Varian (500 MHz, T =25) using deuterated dimethyl sulfoxide (DMSO-d6) as a solvent. Chemical shifts were calibrated using tetramethylsilane as an internal reference and given in parts per million.

2.2.3. Preparation of Nanoparticles

Nanoparticles were prepared using mPEG-b-p(CB-co-LA) copolymer by the emulsion/solvent evaporation technique [197]. Briefly, the 30mg copolymer was dissolved in dichloromethane and acetone mixture (50:50) containing 1.5mg GDC-0449 or 0.6mg RSG. For combination therapy, GDC-0449 and RSG nanoparticles were co-formulated by dissolving both the drugs with copolymer in dichloromethane and acetone mixture. The solution was then added to a vial containing 5ml of 1% aqueous poly (vinyl alcohol) solution and emulsified by a probe sonicator (50 W, 2 min) on an ice bath. Organic solvents were evaporated under vacuum. Nanoparticles were collected by ultracentrifugation at 25000 rpm for 35 min, (Du point, Sorvall Inc.), washed three times with distilled water and lyophilized.

2.2.4. Characterization of Nanoparticles

Mean particle size and size distribution of the nanoparticles were determined by dynamic light scattering using a Zeta Sizer^{TM} (Malvern 3800-ZLS, Boston, MA). Drug loading and encapsulation efficiency were determined using HPLC analysis. Briefly, GDC-0449 and RSG loaded nanoparticles with 0.5mg theoretical drug loading were dissolved in DCM for drug extraction using a bath sonicator for 30 min at 37°C. DCM was evaporated, and acetonitrile was added to dissolve residues. Drug content was determined by HPLC (Waters, MA) by using a reverse phase C-18 Inertsil ODS column (150 mm × 4.6 mm, 5 µm) (GL Sciences Inc.). Mobile phase composition was acetonitrile and 10 mM acetate buffer (pH 4.5) (60/40, v/v) at a flow rate of 1.0 ml/min. Detection wavelength of 330nm and 254nm were used for GDC-0449 and RSG,

respectively. Drug loading and encapsulation efficiency were calculated using the following equations:

$$\text{Encapsulation efficiency}\ (\%) = \frac{\textbf{weight of drug encapsulated}}{\textbf{initial weight of drug taken}} \times 100 \qquad (2.1)$$

$$\text{Drug loading}\ (\%\ \text{w/w}) = \frac{\textbf{weight of drug encapsulated}}{\textbf{total weight of formulation}} \times 100 \qquad (2.2)$$

2.2.5. In-vitro Drug Release

Drug-loaded nanoparticles containing 1mg of GDC-0449 and 0.5 mg of RSG were placed in a dialysis bag with a molecular weight cutoff of 1000 Da (Spectrum Labs Inc., Rancho Dominguez, CA). Dialysis bag was suspended in 50 mL of PBS (pH 7.4) containing 1.0% (w/w) Tween 80 to facilitate drug wetting and to maintain the sink conditions. The study was performed in a closed chamber orbital shaker at 37^{o}C, with a rotation speed of 100 rpm. Samples (1 mL) were taken at regular time intervals and replaced with the PBS (pH 7.4) containing 1.0% (w/w) Tween 80. The drug content in the samples was analyzed by HPLC-UV method as described above and cumulative drug release was plotted against time.

2.2.6. Animal Experiments

Animal experiments were performed in accordance with the NIH guidelines using a protocol approved by the Institutional Animal Care and Use Committee (IACUC) of the University of Tennessee Health Science Center. Male Sprague-Dawley (SD) rats weighing 230–250g were purchased from Charles River Laboratories, Inc. (Wilmington, MA), housed under the care of a licensed veterinarian and monitored daily for signs of sickness or pain after surgery. The animals were maintained on a 12h light-dark schedule and had free access to normal rat chow and water. To induce fibrosis in the liver, common bile duct of SD rats was ligated as described previously [70]. Animals were divided into the following five groups (5 per group): control (sham-operated), CBDL untreated, CBDL treated with GDC-0449 nanoparticles at a dose of 10mg/kg, CBDL treated with RSG nanoparticles at a dose of 4mg/kg, and CBDL treated

with GDC-0449 and RSG nanoparticles at a dose of 5mg/kg and 2mg/kg of GDC-0449 and RSG respectively. Nanoparticles containing GDC-0449, RSG, and both drugs were administered daily after three days of CBDL via intravenous tail vein injection for a week. Animals were euthanized under isoflurane anesthesia at the end of the study to collect serum and liver tissues. Serum was used for biochemical analysis, and the liver was fixed in 10% neutral buffered formalin or snap frozen in liquid nitrogen for further analysis.

2.2.7. Measurement of Serum Enzyme Levels and Liver Histology

Serum concentrations of liver injury markers such as ALT, AST, and BIL were measured using standard assay kits according to the manufacturer's instructions. For staining, liver specimens were fixed in 10% buffered formalin overnight, saturated in 30% sucrose solution and embedded in OCT (optimum cutting temperature) compound. For standard histology, 5µm thick sections were stained with Hematoxylin–Eosin (H&E) for detection of tissue architecture. Masson's trichrome staining was used to determine the levels of collagen deposition.

2.2.8. Immunofluorescent Staining

For immunofluorescent staining, snap frozen liver sections were fixed on glass slides in 95% cold ethanol for 10 min and blocked with 10% goat serum. This was followed by overnight incubation at 4°C with polyclonal antibodies for TGF-β1, Gli-1, (Santa Cruz, CA), and α-SMA (Abcam, Cambridge, MA). After washing with tris-buffered saline containing (0.05% w/w) Tween 20 (TBST), slides were incubated with anti-rabbit or anti-goat secondary antibodies (IgG - H&L DyLight® 488 (Abcam) for 2h at room temperature and visualized under a fluorescent microscope.

2.2.9. Quantitative Real Time RT-PCR

Total RNA was extracted from the liver tissues using RNeasy Mini Kit (Qiagen, MD) and reverse transcribed to cDNA using Taqman RT kit (Carlsbad, CA). Gene expression levels were determined by Light Cycler 480 (Roche, IA) using primer pairs **(Table 2-1)** and standard protocol as described previously [192]. All the real-time RT-PCR results were analyzed using comparative CT method and gene expression was normalized as compared to the control.

Table 2-1. Primers Sequences Used for Real Time RT-PCR Amplification

Gene	NCBI Accession #	Sequence
β- actin	NM_031144	CAACTGGGACGATATGGAGAAG (Sense) CTCGAAGTCTAGGGCAACATAG (AntiSense)
Shh	NM_017221	CTGGATTCGACTGGGTCTACTA (Sense) GCTTTCCCGGTTGCTTATCT (AntiSense)
Ptch-1	NM_053566	CAAAGCCAAGGTTGTGGTAATC (Sense) GCGGTCAGGTAGATGTAGAAAG (AntiSense)
Gli-1	NM_001191910.1	ACCTCCCTACCTCTGTCTATTC (Sense) GGCAGGATAGGAGACTGATTTG (AntiSense)
SMO	NM_012807	CCAGGACATGCACAGTTACA (Sense) GGAAGTAGCCTCCCACAATAAG (AntiSense)
α-SMA	NM_031004.2	CTGGCACCACTCCTTCTATAAC (Sense) CTCCAGAGTCCAGCACAATAC (AntiSense)
IL-6	NM_012589	CCGTTTCTACCTGGAGTTTGT (Sense) GTTTGCCGAGTAGACCTCATAG (AntiSense)
TGF-β1	NM_021578.2	CTGTGGAGCAACACGTAGAA (Sense) GGGTGCAGGTGTCCTTAAATA (AntiSense)
E-cadherin	NM_031334.1	AAGAGGGAGGTGGAGAAGAA (Sense) ACAGACAGACTGGTAGGTAGAG (AntiSense)
PPAR-γ	NM_013124.3	CTGGCCTCCCTGATGAATAAAG (Sense) GCGGTCTCCACTGAGAATAATG (AntiSense)
TNF-α	NM_012675	CAGCCGATTTGCCATTTCATAC (Sense) GGCTCTGAGGAGTAGACGATAA (AntiSense)
FN-1	NM_019143.2	GTGTCCTCCTTCCATCTTCTTAC (Sense) GTTCCCTCTGTTGTCCTTCTT (AntiSense)
COL1A1	NM_053304.1	CGGACTATTGAAGGAGCCTAAC (Sense) TGATGCAGGACAGAGAGAGA (AntiSense)

2.2.10. Western Blot Analysis

Snap frozen liver tissues were homogenized in RIPA buffer containing protease inhibitor cocktail to extract total protein. After resolving in sodium dodecyl sulfate-polyacrylamide gel electrophoresis (SDS-PAGE), proteins were transferred to Immobilon polyvinylidene fluoride membrane using iBlot^{TM} Dry Blotting System (Invitrogen, Carlsbad, CA). Transferred membranes were blocked in Odyssey blocking buffer and incubated with Shh, Gli-1, FN-1, NF-κB, α-SMA, TGF-β1, and PPAR-γ primary antibodies for 16h at 4°C. The membrane was then incubated with anti-goat or anti-rabbit IRDye 680RD secondary antibodies for 1h at room temperature. All the blots were re-probed with total β-actin antibody as a control. Target proteins were imaged using Odyssey IR imaging system (Li-Cor, Lincoln, NE).

2.2.11. ELISA for Tumor Necrosis Factor-α

TNF-α in rat serum was determined according to the manufacturer's instructions of ELISA kit. Briefly, ELISA plate provided in the kit was coated with capture antibody overnight at 4°C. The plate was washed and blocked with assay diluent and incubated at room temperature for 1h. Rat serum samples were added and incubated at 4°C overnight. After washing, detection antibody was added and incubated at room temperature for 1h. Avidin-HRP conjugated secondary antibody was added and incubated at room temperature for 30min. The plate was washed, and substrate solution was added to each well and read at 450nm.

2.2.12. Statistical Analysis

All values in the figures and text were expressed as the mean ± S.D. The results were analyzed, and individual group means were compared using Student's unpaired t-test. A p-value of at least 0.05 was considered statistically significant.

2.3. RESULTS

2.3.1. Preparation and Characterization of Drug-Loaded Nanoparticles

We synthesized $mPEG_{114}$-b-p(CB_{55}-co-LA_{160}) amphiphilic triblock copolymer and characterized by ^{1}H NMR. The polymer had an average molecular weight of 30,000 Da with carbonate and lactic acid contents of 55 ± 5 and 160 ± 5 moles, respectively, and mPEG content of 16.6 ± 2 % as determined by ^{1}H NMR **(Figure 2.1A)**. Using the above-synthesized copolymer, we were able to formulate nanoparticles with a mean particle size of 120-130nm and a polydispersity index of less than 0.2 **(Figure 2.1B)**. Drug loading was found to be 5.0% and 2.0% w/w for GDC-0449 and RSG, respectively, with little effect on the mean particle size and size distribution. The encapsulation efficiency was 98% and 95% for GDC-0449 and RSG, respectively. Nanoparticles carrying these two drugs were prepared using half of 5% & 2% theoretical drug loading with encapsulation efficiencies of 95% and 90% for GDC-0449 and RSG, respectively **(Figure 2.1C)**. In vitro release profile of drug-loaded nanoparticles was determined in PBS at 37°C. Nanoparticles carrying GDC-0449 and RSG followed Higuchi model with 80 ± 2.7% release in 10 days and 96 ± 3.1% in 4 days' cumulative release for GDC-0449 and RSG, respectively **(Figure 2.1D)**. At the end of the study, remaining unreleased drug was recovered from the dialysis bags. There was an initial burst release for about 5h possibly due to the dissolution and diffusion of surface adsorbed and poorly entrapped drug in the nanoparticles.

2.3.2. Effect of Drug Treatment on Liver Histology

For the treatment of CBDL-induced liver fibrosis in rats, drug-loaded nanoparticles were injected daily intravenously after three days of CBDL for a week. CBDL resulted in bile accumulation in the bile duct, resulted in proliferation and enlargement of the bile duct [198]. In untreated CBDL rats, maximum proliferation was observed but reduced after intravenous

injection of nanoparticles encapsulated with GDC-0449, RSG or in combination. These results suggest that treatment with GDC-0449 and RSG improved the overall condition of these liver fibrotic rats.

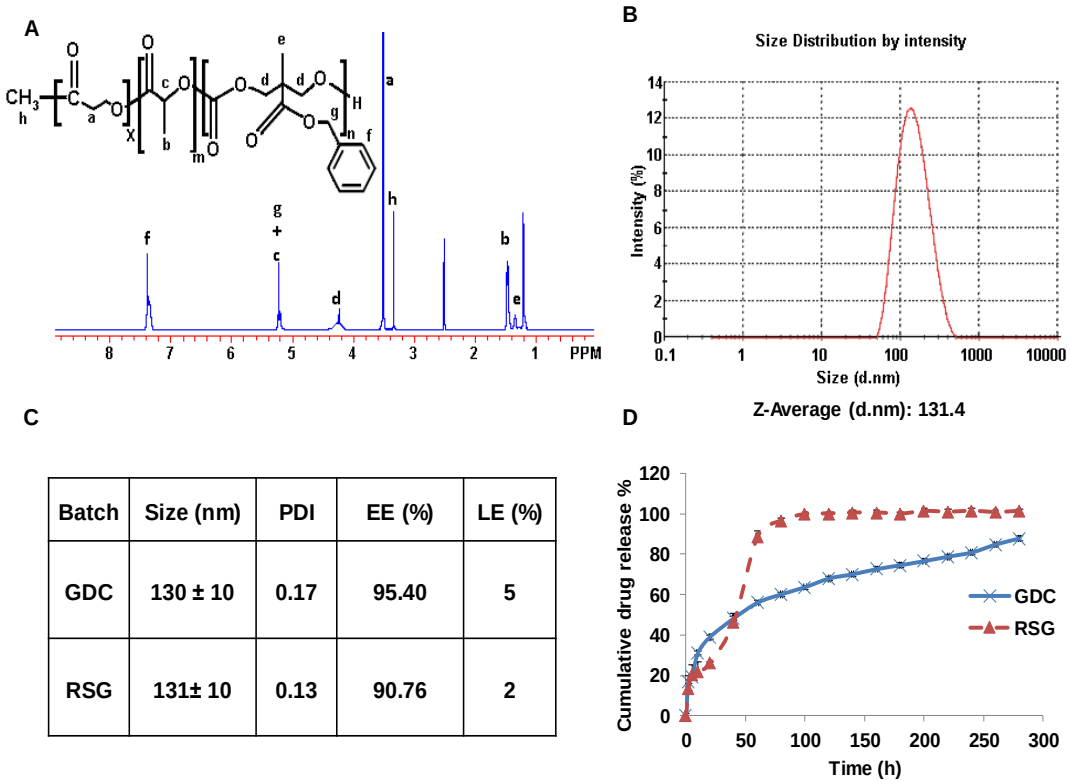

Batch	Size (nm)	PDI	EE (%)	LE (%)
GDC	130 ± 10	0.17	95.40	5
RSG	131± 10	0.13	90.76	2

Figure 2-1. Polymer synthesis, formulation and characterization of nanoparticles. (A) ^{1}H NMR spectra of $mPEG_{114}$-b-p(CB_{54}-co-LA_{160}) copolymer in DMSO-d6 (B) Particle size distribution of nanoparticles (C) Polydispersity index (PDI), Drug encapsulation efficiency (EE) and loading efficiency (LE) of nanoparticles (D) Release of GDC and RSG from nanoparticles at 37°C by dialysis in PBS (pH 7.4) containing 1.0% Tween 80. All data are presented as the mean ± S.D. (n = 3).

CBDL is known to cause an increase in intra-biliary pressure and leakage of bile into the liver parenchyma, which aggravates bile infarcts due to hepatocyte death [199]. Liver specimens from CBDL rats demonstrated extensive bile infarcts, while the number and area of infarction were significantly reduced upon administration of GDC-0449 or RSG loaded nanoparticles as evident from H&E staining. These results suggest that Hh inhibitor and PPAR-γ

agonist can attenuate liver injury and protect liver architecture **(Figure 2.2A)**. Liver sections were stained with Masson's trichrome stain for collagen. The increased deposition of collagen was evident by intense blue color staining for the interstitial collagen in CBDL rats **(Figure 2.2B)**.

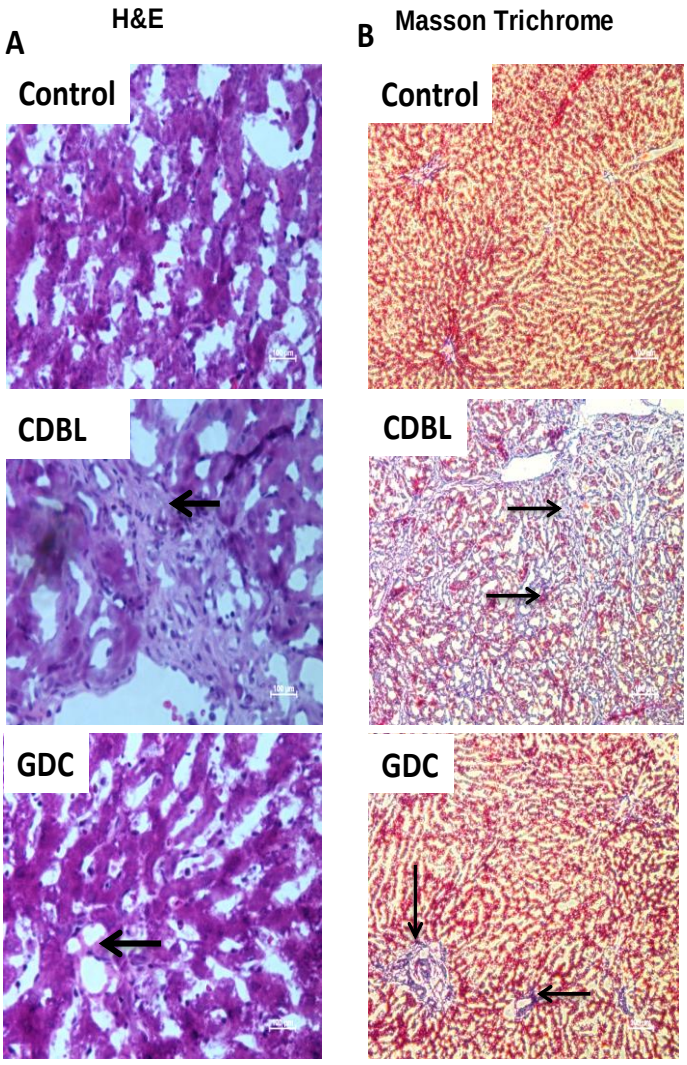

Figure 2-2. Hematoxylin & Eosin and Masson trichrome staining of liver sections of CBDL rats after systemic administration of nanoparticles loaded with GDC, RSG or combination. (A) Treatment with GDC and RSG loaded nanoparticles reduced histological liver injury, including bile infarcts. Geographic borders of infarcts indicated by black arrows were large in number and area in untreated CBDL rats and reduced upon treatment with nanoparticles carrying GDC and RSG (original magnification ×20). (B) Dark blue staining shows increased collagen deposition in CBDL rats (Black Arrows). Systemic administration of GDC and RSG loaded nanoparticles effectively reduced blue collagen

However, collagen staining was much weaker when nanoparticles loaded GDC-0449, RSG either alone or in combination were administered into CBDL rats, indicating significant inhibition of collagen accumulation in the enlarged periductal area and essentially no collagen accumulation in the liver interstitium.

2.3.3. Measurement of Liver Injury Markers

ALT, AST, and BIL are surrogate markers for liver injury, and their levels are known to increase upon bile duct ligation [200]. As evident from Figure 2.3, CBDL rat had many fold increase in serum AST, ALT, and BIL levels as compared to the sham-operated control rats. Treatment with GDC-0449 and RSG loaded nanoparticles resulted in decreased serum levels of all of these markers. These results indicate that the liver is susceptible to hepatocellular injury following CBDL, and GDC-0449 and RSG loaded-nanoparticles protected livers from the injury resulting in significant decrease in ALT, AST, and BIL (**Figure 2.3**, **P < 0.005).

2.3.4. Expression Levels of Hh Ligand and PPAR-γ

Hh signaling controls proliferation and migratory activities of Hh-responsive HSCs by promoting EMT [12]. Therefore, we measured Hh pathway ligands expression in CBDL rats after 7 days of systemic administration of GDC-0449 or RSG loaded nanoparticles and compared with the sham-operated control by RT-PCR and western blotting method. Shh mRNA was increased by 4.3 folds in CBDL rat livers. There was also a significant increase in transcription of Ptch-1 by 2.7 folds, SMO by 2.8 folds and Gli-1 by 3.6 folds as compared to the control **(Figure 2.4A)**.

Systemic administration of GDC-0449 loaded nanoparticles significantly decreased Shh expression levels. Ptch-1, SMO, and Gli-1 expressions were also significantly reduced in the liver when CBDL rats received nanoparticles carrying GDC-0449 alone or with RSG. Decrease

in mRNA expression of Shh and Gli-1 was confirmed by Western blot analysis of liver tissue protein extract **(Figure 2.4B)**.

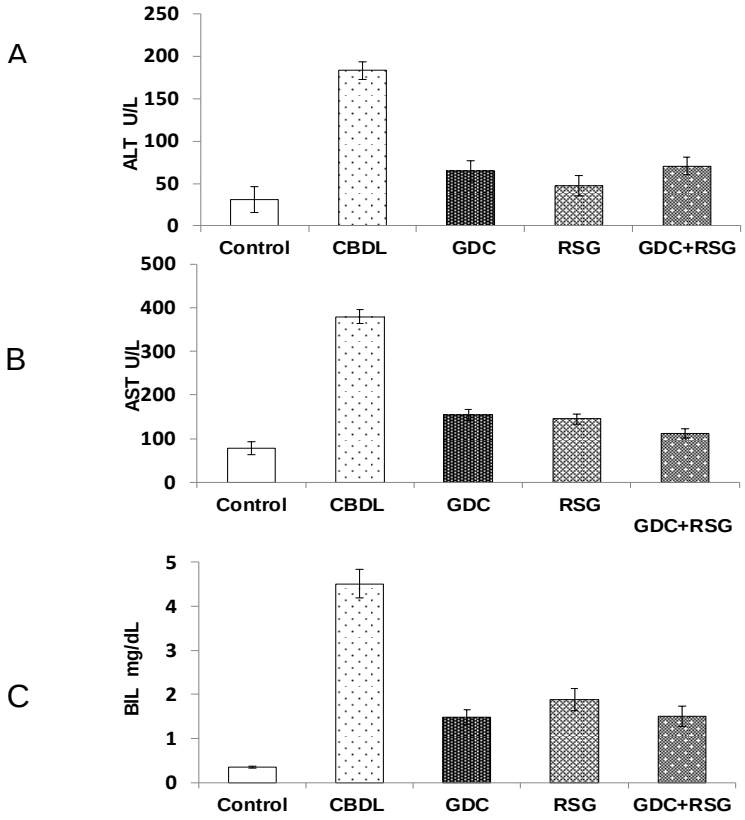

Figure 2-3. Serum biomarkers. Effect of GDC and RSG loaded nanoparticles on serum. (A) AST, (B) ALT, and (C) BIL levels. Serum markers in CBDL rats after systemic administration of GDC and RSG loaded nanoparticles were significantly lower than those in the CBDL rats. Results are presented as mean ± S.D. (n=5); (**p<0.001 treated rats as compared to CBDL).

In contrast to Hh signaling, PPAR-γ mRNA was significantly downregulated in CBDL rat livers, which is in good agreement with the literature [191]. Treatment of CBDL rats with RSG-loaded nanoparticles significantly restored PPAR-γ gene expression to the basal level **(Figure 2.4C)**. These results were also confirmed by Western blot analysis **(Figure 2.4D)**. Progression of liver fibrosis leads to an increase in the synthesis and deposition of ECM proteins, particularly collagen in the liver interstitium [201]. We determined mRNA expression level of collagen type-I (COL1A1) and observed 4.7 folds higher expression in the CBDL rats as compared to the

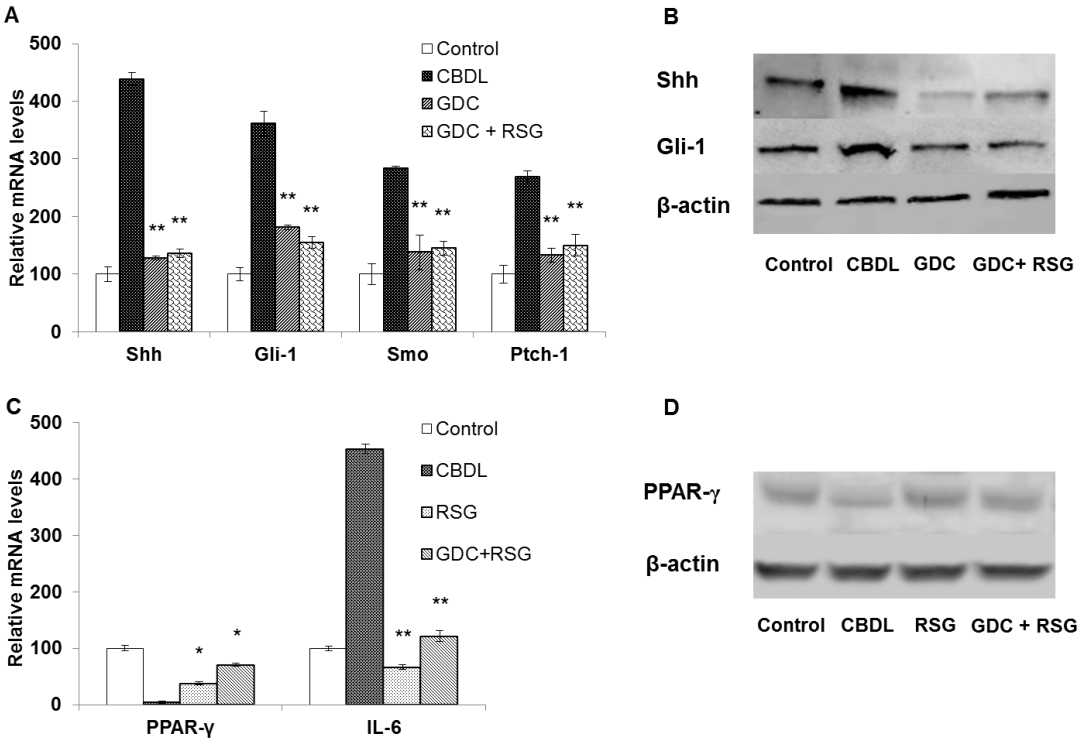

Figure 2-4. Real time RT-PCR and Western blot analysis of hedgehog ligands and PPAR-γ. (A) Systemic administration of GDC loaded nanoparticles into CBDL rats reduced gene expressions of Shh, Gli-1, Smo, and Ptch-1 as quantified by Real-Time RT-PCR. (B) Western blot analysis of liver tissues for Shh and Gli-1 proteins levels (C) mRNA expression levels of PPAR-γ and IL-6. (D) Western blot analysis of PPAR-γ protein. β-actin was used as an internal control. Results are presented as mean ± S.D. (n=3) (**p<0.001 compared to CBDL).

control, but its expression decreased upon treatment with nanoparticles carrying GDC-0449 (1.48 fold) or RSG alone (1.8 fold) or combination (1.34 fold) which is consistent with the results observed in Masson's trichrome staining **(Figure 2.5A)**.

α-SMA and FN-1 are characteristic markers of EMT [202]. Therefore, we determined transcription levels of α-SMA and FN-1 and found upregulation of their expression by 2.3 and 3.2-folds, respectively in CBDL rats **(Figure 2.5A)**. After systemic administration of nanoparticles carrying GDC-0449 or RSG either alone or in combination into CBDL rats, α-SMA and FN-1 expression decreased significantly both at mRNA and protein level **(Figures 2.5A, 5B)**. NF-kB promotes secretion of inflammatory factors, and its expression is known to be

elevated in liver fibrosis [189]. We found its level elevated in CBDL rats and upon treatment with nanoparticles containing drugs decreased its protein level **(Figure 2.5B)**.

TGF-β1 is involved in the early proliferation of HSCs through SMAD3 /SMAD7 signaling after CBDL [203]. Similarly, TGF-β1 expression was upregulated (3.64 folds) at mRNA level and significantly increased at proteins levels after CBDL, and was decreased in GDC-0449 or RSG alone or in combination treatment groups to the basal level **(Figures 2.5A, 2.5B)**. E-cadherin is a transmembrane glycoprotein found in most epithelial cells and promotes cell adhesion by forming a complex with β-catenin. Upon EMT, epithelial cells lose E-cadherin expression [204]. Therefore, we determined E-cadherin expression and found its expression was decreased to

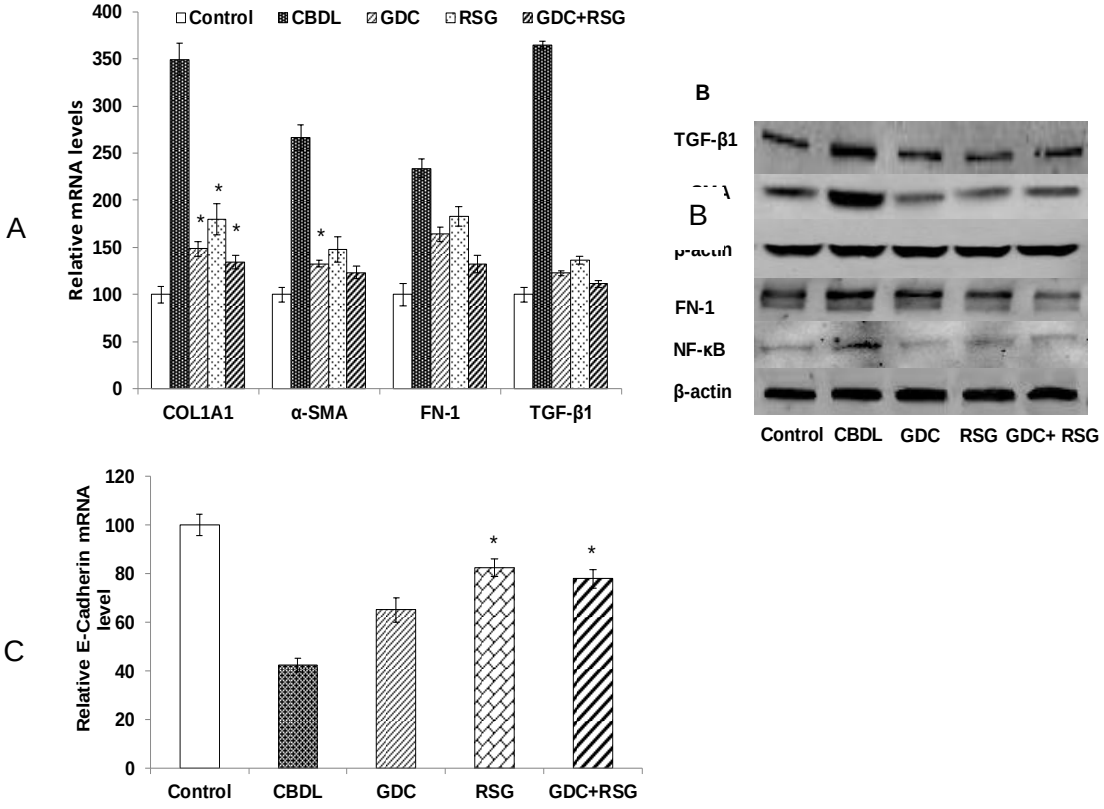

Figure 2-5. Real time RT-PCR and Western blot analysis of liver fibrosis markers. Systemic administration of RSG and GDC-0449 nanoparticles into CBDL rats reduced gene expression of Col1A1, α-SMA, FN-1, and TGF-β1. (A) RT-PCR (B) Western blot analysis of TGF-β1, α-SMA, FN-1 and NF-κB proteins from liver tissues of various groups. (C) RT-PCR of E-cadherin. Results are presented as mean ± S.D. (n=3) (*p<0.05, **p<0.001, treated vs. CBDL).

40% in CBDL rats as compared to the sham-operated control rats. After treatment with nanoparticles carrying GDC-0449 or RSG alone or in combination, we observed a significant increase in its mRNA level **(Figure 2.5C)**.

2.3.5. Expression of proinflammatory cytokines

Increased TGF-β1 induces IL-6 secretion at the site of injury [205]. We observed mRNA levels of IL-6 be significantly upregulated in CBDL rats compared to the control rats. Significant down-regulation of IL-6 mRNA was seen in the CBDL rats treated with GDC-0449 and RSG loaded nanoparticles **(Figure 2.4C)**. Moreover, we determined TNF-α expression which is an important proinflammatory cytokine in the progression of liver injuries and fibrosis [206]. RT-

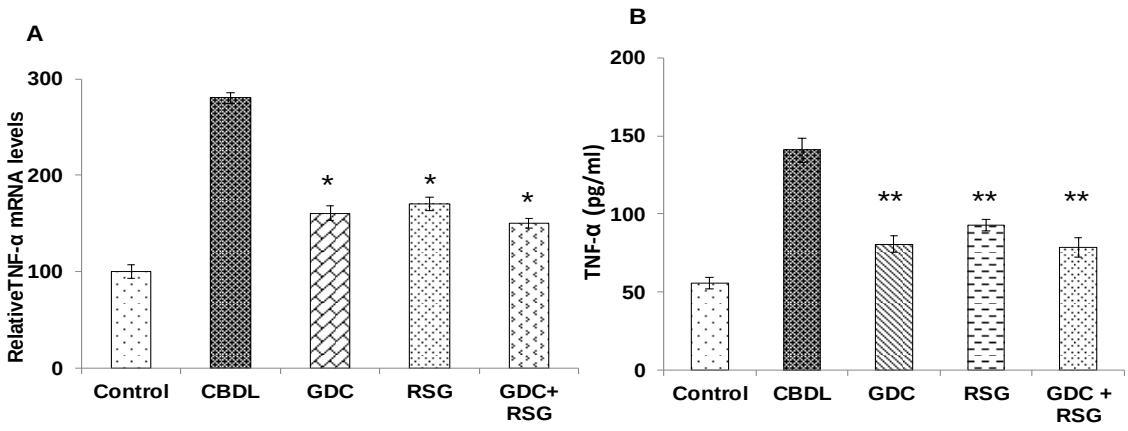

Figure 2-6. Real time RT-PCR and ELISA of inflammatory cytokine TNF-α. (A) mRNA level. (B) Serum TNF-α level. Results are presented as mean ± S.D. (n=3) (**p<0.001 treated vs CBDL).

PCR and ELISA results showed TNF-α mRNA and protein levels were significantly higher in CBDL rats as compared to the sham-operated control rats. Upon systemic administration of GDC-0449 or RSG alone or combination loaded nanoparticles to CBDL rats resulted in reduced TNF-α gene expression at both mRNA and protein level **(Figure 2.6A and B)**.

2.3.6. Immunofluorescent Staining

Immunofluorescence for a Hh-regulated transcription factor, Gli-1 overexpression was localized in the nucleus of the Hh-responsive cell population. This observation suggests that Hh ligands are highly activated in CBDL rats, resulting in intense immunofluorescent staining of Gli-1. However, Gli-1 expression was significantly reduced in CBDL rats after systemic administration of nanoparticles carrying GDC-0449 alone or with RSG **(Figure 2.7A)**. Immunoreactivity of mesenchymal cell markers, α-SMA and TGF-β1 correlate well with the progression of liver fibrosis**.** Immunofluorescent staining of the liver sections indicates that CBDL rats have increased the number of α-SMA expressing myofibroblasts in and around portal tracts **(Figure 2.7B)**. TGF-β1 positive cells were distributed with high density in the portal venule pericytes with perisinusoidal distribution. Treatment groups showed decreased the number of α-SMA and TGF-β1 producing cells in CBDL rats treated with nanoparticles carrying GDC-0449 or RSG. However, there was still fair a number of TGF-β1-positive cells in the liver sections of CBDL rats treated with GDC-0449 or RSG loaded nanoparticles, which distributed mainly at the fibrous septa-band **(Figure 2.7C)**.

2.4. DISCUSSION

Liver fibrosis is affecting millions of people and is a significant cause of morbidity and mortality worldwide. Liver fibrosis is the result of a wound-healing response to the liver injury, viral hepatitis or biliary tract disease. Fibrosis is characterized by the excessive production and deposition of ECM proteins. Chronic liver injuries result in the transformation of quiescent HSCs into active myofibroblasts [207]. Initiation and progression of liver fibrosis involve multiple regulatory events in the liver and coordinated changes in the activity of several transcription factors. A number of different approaches have been used earlier for treatment, including the inhibition of collagen synthesis, interruption of matrix deposition, stimulation of matrix degradation, modulation of HSC activation, induction of HSC apoptosis and modulation of

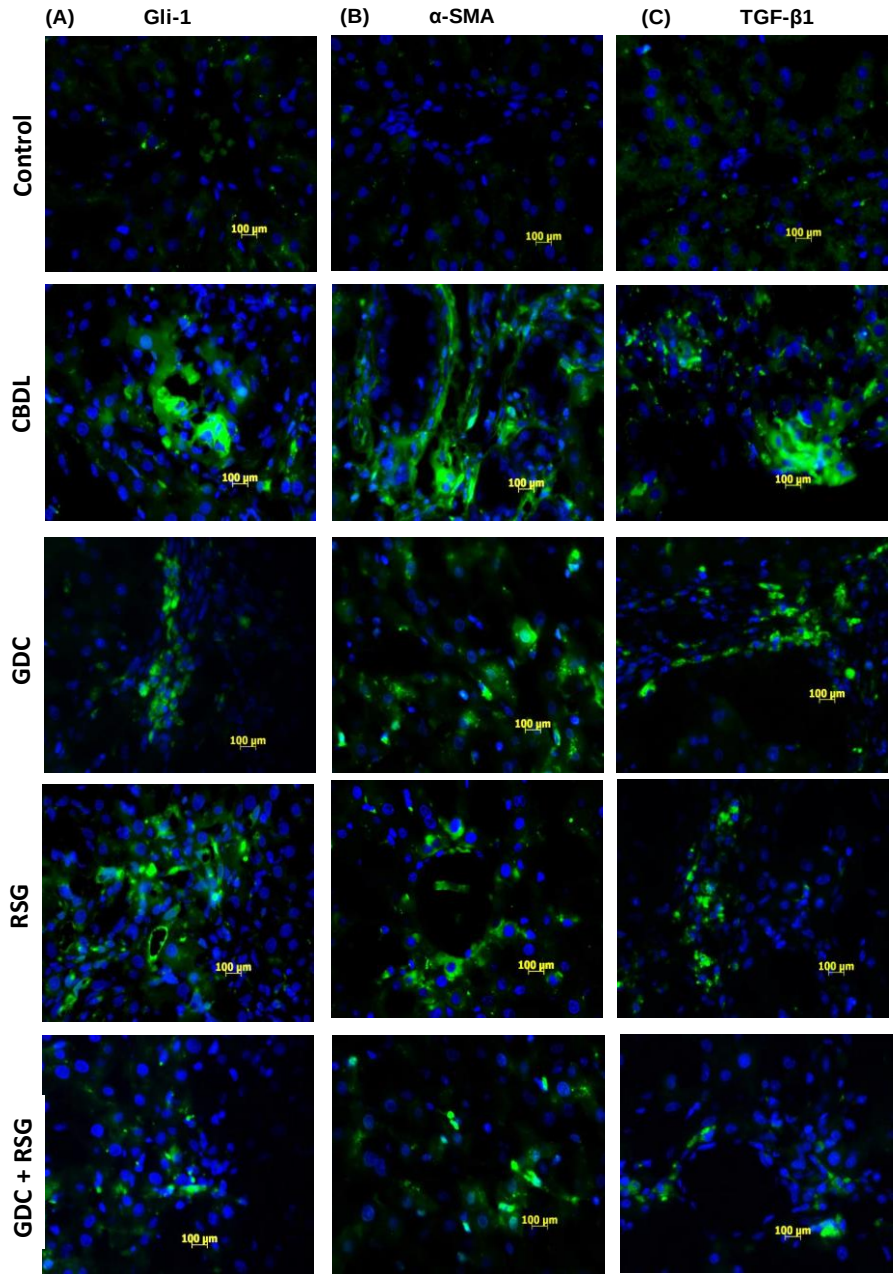

Figure 2-7. Immunofluorescent staining of liver sections: (A) Gli-1 expression in the liver sections of CBDL rats as reflected by intense green staining. GDC or combination treatment reduced Gli-1 expression as evident from faint green staining. (B) Sections from sham operated control rats do not express α-SMA, whereas CBDL rats showed strong fluorescent staining around the fibrous septa. α-SMA expression was decreased significantly after systemic administration of GDC and RSG loaded nanoparticles into CBDL rats. (C) Sham operated control rats showed weak staining for TGF- β1, whereas strong green staining can be seen in CBDL rats. Treatment groups showed weak staining for TGF-β1 as compared to CBDL group. Shown are representative images (original magnification, ×40).

progression of the disease requires the use of multipronged approach by targeting more than one factor. PPAR-γ is one of the key factors whose activity is decreased in activated HSCs. On the other hand, there is an increase in Hh activity in fibrotic livers. Therefore, inhibition of inflammation and EMT by combining of PPAR-γ agonist and Hh inhibitor can be a potential strategy to reverse liver fibrosis.

PPAR-γ agonist keeps HSCs in a quiescent state by blocking the profibrotic effects of TGF-β1 and reducing TNF-α activity. Thus, the loss of these receptors leads to transdifferentiation of HSCs from the retinoid storing state to the ECM-producing myofibroblasts [191,212,213]. RSG is a PPAR-γ agonist which is a thiazolidinediones derivative used as an anti-hyperglycemic agent [214]. In this study, RSG was chosen because it is non-toxic to the liver and does not induce cytochrome enzymes, like other members of this family [215]. Previously, we found that the progression of liver fibrosis is accompanied by the activation of Hh pathway leading to the proliferation and EMT of HSCs [39]. Treatment with Hh inhibitor, GDC-0449 ameliorated a fibrotic condition in CBDL rats [192]. However, administration of GDC-0449 required complex formation with β-CD (beta-cyclodextrin) at the low pH range, which is not suitable for systemic administration. Moreover, GDC-0449 shows poor complex formation with β-CD.

Taking care of their poor aqueous solubility and potential side effects of GDC-0449 and RSG, in this study we aimed to formulate nanoparticles encapsulating these two drugs using mPEG-b-p(CB-co-LA) copolymer. First, we synthesized amphiphilic mPEG-b-p(CB-co-LA) copolymer and characterized it using ^{1}H NMR **(Figure 2.1A)**. We have selected this copolymer because of its capacity to encapsulate poor water soluble drugs with high drug loading, biodegradable and nontoxic properties [196]. We have simultaneously encapsulated these drugs into nanoparticles successfully and tested this combination at half of their individual doses for treating liver fibrosis for minimizing any drug related toxicity. These nanoparticles were not

specifically targeted to liver. However, our group previously reported that micelles prepared from similar backbone copolymer PEG block- poly(2-methyl-2-benzoxycarbonyl-propylenecarbonate) tend to accumulate in the liver and spleen [216]. Based on these results, we expect nanoparticles containing GDC-0449 or RSG to be having same biodistribution profile.

Drug-loaded nanoparticles were formulated using o/w emulsification followed by solvent evaporation. Using this copolymer, we formulated uniform size distributed nanoparticle with high drug loading **(Figure 2.1B and 2.1C)**. The outer coating shell of mPEG prevents particles from aggregation and also provides stealth properties. This is necessary for nanoparticles to escape from the reticuloendothelial system (RES) and prolong systemic circulation. Owing to the differences in their hydrophobicity, their loading capacity in the formulated nanoparticle was different. At higher payload, the encapsulation capacity of both drugs decreased, which may be due to the saturation of the hydrophobic inner core. Nanoparticles carrying GDC-0449 and RSG were prepared at 5% and 2% w/w initial drug loading of GDC-0449 and RSG, respectively. Drug-loaded nanoparticles had a mean particle size of 130-140 nm. Nanoparticles provided sustained release with 80% drug release in 10 days and 96% in 4 days for GDC-0449 and RSG, respectively **(Figure 2.1D)**. We observed difference release profile for these two drugs as GDC-0449 is more hydrophobic than RSG, and thus GDC-0449 had slower release rate. PBS containing 1.0% Tween 80 was used as release medium to maintain the sink conditions and to prevent drug precipitation upon release.

CBDL rats showed large infarcts and intense blue collagen staining, whereas systemic treatment with nanoparticles containing GDC-0449, RSG or combination reduced the number as well as the area of infarcts and decreased the intensity of collagen-specific staining **(Figure 2.2A and 2.2B)**. Liver injury markers such as serum AST, ALT and BIL were found significantly elevated in CBDL rats as compared to GDC-0449, RSG or combination nanoparticles treated rats **(Figure 2.3)**. A significant increase in Hh ligand and Gli-1 expression in CBDL rats was

observed, as analyzed by RT-PCR, **(Figure 2.4A)** Western blot analysis **(Figure 2.4B)**, and immunofluorescence **(Figure 2.7A)**. Upon systemic administration of GDC-0449 and RSG loaded nanoparticles to CBDL rats, a significant decrease in HSC activation and liver fibrosis was observed.

There was a significant decrease in PPAR-γ expression in CBDL rats as compared to the sham control. This reduction is related to upregulation of TNF-α, which is known to inhibit PPAR-γ expression [188]. However, the treatment of CBDL rats with nanoparticles of RSG or in combination with GDC-0449 restored PPAR-γ expression at mRNA as well as protein levels, suggesting upregulation of this gene **(Figures 2.4C and 2.4D)**. There was a significant increase in TGF-β1 gene expression after CBDL in rats, possibly due to HSC activation **(Figures 2.5C and 2.7C)**. Moreover, activated HSCs showed an abundance of α-SMA proteins which is a well-known EMT marker and used to identify the early stages of liver fibrosis **(Figures 2.5AB and 2.7B)** [217]. Epithelial marker E-cadherin expression was decreased significantly in fibrotic livers **(Figure 2.5C)**. GDC-0449 and RSG carrying nanoparticles decreased TGF- β1 and α-SMA expression and also restored E-cadherin **(Figures 2.5 and 2.7B)** suggesting nanoparticles loaded with these drugs have prevented EMT. FN-1 is among the first ECM proteins which are upregulated after liver injury and mediates differentiation into myofibroblasts [218]. After CBDL, upregulation of TGF-β1 also resulted in increased FN-1 expression [219]. Treatment with GDC-0449 and RSG significantly abrogated FN-1 expression **(Figures 2.5A and 2.5B)**. Downregulation of these regulators is possibly the result of reduced activation of HSCs. The increase in collagen deposition was observed by Masson's trichrome staining and real-time RT-PCR. Following treatment with RSG and GDC-0449 carrying nanoparticles, reduced collagen level was observed in CBDL rats **(Figures 2.2B and 2.5C)**. Upon liver injury, Kupffer cells increase TNF-α production via NF-κB pathway and its increased activity is found in activated HSCs" [189]. TNF-α induces neutrophil infiltration and stimulates mitochondrial reactive oxygen

species (ROS) production in hepatocytes. These reactive oxidants activate HSCs and stimulate inflammatory as well as fibrogenic signals [220]. TNF-α was elevated in CBDL rats, which indicates the high inflammatory state in the liver. RSG decreased the expression of genes implicated in the inflammation of liver tissues during the progression of liver fibrosis. RSG negatively interferes with NF-κB inflammatory pathway by blocking its nuclear translocation and by reducing the production of TNF-α **(Figure 2.6)** and IL-6 **(Figure 2.4C)**.

2.5. CONCLUSIONS

In conclusion, mPEG-b-p (CB-co-LA) copolymer of 30,000 Da was synthesized and GDC-0449 and RSG loaded nanoparticles were prepared. Systemic administration of nanoparticles encapsulating GDC-0449 and RSG provided hepatoprotection by reducing Hh pathway ligands and increasing PPAR-γ activity, respectively. GDC-0449 was more effective than RSG in treating experimental liver fibrosis when the single drug was used. Combination therapy of GDC-0449 and RSG was able to treat early stage liver fibrosis even at a reduced dose and may provide a new strategy for treating liver fibrosis.

CHAPTER 3. CO-DELIVERY OF SMALL MOLECULE HEDGEHOG INHIBITOR AND miRNA FOR TREATING PANCREATIC CANCER

3.1. INTRODUCTION

Pancreatic ductal adenocarcinoma (PDAC) is a leading cause of cancer-related mortality with a dismal 2-5% five-year survival rate [221]. Due to its late-stage clinical manifestation, 85% of patients have metastatic disease at the time of diagnosis making surgical and therapeutic interventions ineffective. The current FDA-approved chemotherapeutic agent for pancreatic cancer is gemcitabine, which provides an only symptomatic improvement in a lesser proportion of patients. New combination therapy FOLFIRINOX (fluorouracil [5-FU], leucovorin, irinotecan, and oxaliplatin) showed improvement compared to gemcitabine alone; however, there was a significant rate of grade 3/4 toxicity in PDAC patients [222].

PDAC is characterized by a dense desmoplastic/ stromal reaction that consists of large fibroblasts, pancreatic stellate cells (PSCs), and ECM proteins including collagen I and fibronectin. PSCs form a niche for cancer stem cells (CSCs) and promote their self-renewal and invasiveness. CSCs are a subset of cancer cells that not only drive tumor growth but also resistant to chemotherapy and radiation. Hh signaling promotes desmoplasia causing PSC differentiation into myofibroblasts that result in poor delivery of therapeutic agents. Hh ligands also facilitate the maintenance of CSCs [223]. Blocking the Hh pathway decreases desmoplastic reactions, eliminates CSCs and increases tumor vascular density thus ultimately improves the chemotherapy [224]. GDC-0449 antagonizes Hh signaling by inhibiting the Smoothened (SMO) and Shh-Gli signaling selectively [225]. But due to poor aqueous solubility and low bioavailability, its clinical benefits are limited.

miRNAs are endogenous non‑coding single-stranded RNAs of 19-24 nt that regulate gene expression through mRNA cleavage or translational inhibition. miRNA plays a crucial role

in the initiation, progression, and maintenance of CSCs. Pancreatic CSCs express differential levels of miR-99a, miR-100, miR-125b, miR-192, and miR-429 compared with controls and miR-200c, miR-203, and miR-183 activity can lead to the downregulation of stem cell factors [226,227]. Expression levels of miRNAs correlate well with drug resistance, invasion, metastasis, and epithelial to mesenchymal transition (EMT) [185]. Despite their promise, the clinical potential of miRNAs has not been realized owing to the challenges involved in their in vivo delivery. Several barriers such as serum instability, non-specific accumulation, improper intracellular release and rapid excretion limit the clinical application of therapeutic miRNAs. Further, miRNAs are highly hydrophilic, which decreases their extravasation into the desmoplasmic PDAC tissue. Previous studies including our own show that miR-let7b is downregulated in pancreatic cancer cells and primary pancreatic cancer [228,229]. miR-let7b can target several tumor-promoting genes including K-RAS, MUC4, NCOA3, HMGA2, TGFβR1, and STAT3 phosphorylation [230-232]; thus its restoration can inhibit PDAC growth and progression.

A combination of two drugs having different mechanisms of action can inhibit tumor progression with synergistic or additive effects [233-235]. Previously, we have synthesized cationic polymer (mPEG-b-PCC-g-GEM-g-DC-g-CAT) for simultaneous delivery of miR-205 and gemcitabine, where gemcitabine was covalently attached to polymer backbone [180]. However, GDC-0449 has no functional group for chemical conjugation to the polymer. Therefore, in this study, we synthesized poly (ethylene glycol)-block-poly (2-methyl-2-carboxyl-propylenecarbonate-graft-dodecanol-graft tetraethylenepentamine) (PEG-b-PCC-g-DC-g-TAPA) which can self-assemble in micelles, form complex with miR-let7b, and encapsulate GDC-0449. These micelles were characterized for particle size, zeta potential, drug loading, miRNA complexation, stability, and transfection efficiency. The formulations were tested for the effect on proliferation of pancreatic cancer cell lines (HPAF-II, T3M4, CAPAN-1, and MIA PaCa-2).

Finally, these formulations were injected into subcutaneous pancreatic tumor bearing mice to determine whether there is synergism between these two drugs in inhibiting tumor growth.

3.2. MATERIALS & METHODS

3.2.1. Materials & Reagents

Benzyl bromide, 2, 2-bis (hydroxymethyl) propionic acid, methoxy poly (ethylene glycol) (mPEG, Mn = 5000, PDI= 1.03) and stannous 2-ethylhexanoate ($Sn(Oct)_2$) were purchased from Sigma-Aldrich (St. Louis, MO). Tetraethylenepentamine and dodecanol were purchased from Alfa-Aesar (Ward Hill, MA). TaqMan® reverse transcription reagent kit was purchased from Life Technologies (Grand Island, NY). Radioimmunoprecipitation assay (RIPA) buffer and SYBR green-1 were purchased from (Roche, Indianapolis, IN). miR-let7b (mature sequence UGAGGUAGUAGGUUGUGUGGUU) and scrambled miRNA were purchased from Invitrogen (Carlsbad, CA). All other reagents were purchased from Sigma-Aldrich and used without further purification.

3.2.2. Synthesis of Copolymer

For the synthesis of the mPEG-b-PCC-g-DC-g-TAPA copolymer, monomer 2-methyl-2-benzyloxycarbonyl-propylene carbonate (MBC) was synthesized by reacting 2, 2-bis (hydroxymethyl) propionic acid with benzyl bromide for 16h under nitrogen at 100°C [196]. mPEG-MBC was synthesized by ring opening polymerization in the presence of $Sn(Oct)_2$ as a catalyst at 100°C 8h. mPEG-MBC was then dissolved in THF: Methanol (1:1, v/v) and hydrogenated in the presence of 10 wt% palladium on carbon to obtain the copolymer containing pendant carboxyl groups (mPEG-PCC) [236]. Finally, tetraethylenepentamine (TEPA) and dodecanol were conjugated by carbodiimide coupling reaction at room temperature for 48h to obtain mPEG-b-PCC-g-DC-g-TEPA. This final product was purified by repeated

precipitation in isopropyl alcohol followed by diethyl ether. Copolymer mPEG-b-PCC-g-DC-g-TEPA was characterized using ^{1}H NMR (Bruker 400 MHz) after dissolving in DMSO-d_6.

3.2.3. Preparation of Micelles

Micelles encapsulating GDC-0449 and complexing miR-let7b were formulated by the film hydration method as reported earlier with slight modifications [180]. Briefly, 20 mg of mPEG-b-PCC-g-DC-g-TEPA was dissolved in chloroform in a glass vial, and a thin film was formed by solvent evaporation under reduced pressure. Chloroform was removed completely by placing the vial overnight in a vacuum desiccator. miR-let7b was added to 1 ml HEPES buffer (10 mM, pH 6.5) and mixed gently. HEPES buffer containing miR-let7b was then added to the copolymer film and vortexed for 5 min. The suspension was shaken for 30 min at 37°C to enable miRNA complexation. The formulation was then centrifuged at 5000 g for 5 min and filtered using 0.22 µm filter (Millipore) and lyophilized. miR-let7b and GDC-0449 combination formulations were prepared by dissolving the drug and copolymer in chloroform and then followed by film formation and hydration with HEPES buffer containing miR-let7b.

3.2.4. Characterization of Formulations

Micelles carrying miR-let7b and GDC-0449 were characterized by the particle size distribution and zeta potential using Malvern Zetasizer (NanoZS Series) and for morphology using Transmission electron microscope (TEM). Micelles containing miRNA and used for particle size characterization or drug release were formulated at N/P ratio of 32:1. Micellar drug loading was measured by HPLC-UV as reported earlier [237]. For the determination of the critical micelle concentration (CMC) of the cationic copolymer, pyrene fluorescence was used as previously described [238]. From pyrene stock solution of 2.6 mg/ml in chloroform, 19.23 µl (50 µg pyrene) aliquots were transferred to a series of clean, dry glass vials. The solvent was evaporated under vacuum while protected from light. Copolymer solutions were prepared at

concentrations ranging from 1X 10^{-9} -1.0 mg/ml in distilled water and added to each dry pyrene vials to obtain the final concentration of 6.18X 10^{-5} M. Vials containing mixtures were shaken for 24h at room temperature in the dark. Undissolved pyrene was removed by filtration and pyrene concentration solubilized in the micelles was determined by spectrofluorometer at wavelengths of excitation 339 nm and emission at 390 nm.

For the determination of the GDC-0449 release, a formulation containing 0.5 mg GDC-0449 was placed in a dialysis bag (MWCO 1000 Da) and suspended in PBS (pH 7.4) containing Tween 80 (1.0% w/v) at room temperature. 1 ml samples at a regular interval were withdrawn and replaced with fresh media (PBS + 1.0% Tween 80). Samples were analyzed using HPLC. Drug release was determined in the absence and presence of miR-let7b. Agarose gel retardation assay was used to evaluate miR-let7b condensation. Copolymer/miR-let7b complexes were prepared at different N/P ratios ranging from 4 to 64, and the complexes containing 1X loading buffer were loaded onto 1% agarose gel premixed with 0.05 mg/ml ethidium bromide. The mixture was separated in 1X Tris/Borate/EDTA (TBE) buffer at 100V for 30 minutes. miR-let7b bands were visualized using a UV Gel Doc EZ system (Bio-Rad, Hercules, CA).

miRNA release from GDC-0449 encapsulated and miR-let7b complexed micelles (N/P ratio: 32/1) was determined using heparin polyanion competition. Heparin sodium was added to miR-let7b at different weight ratios (0, 4, 8, 16, 32 and 64 µg) in 10 µl PBS were added to the nano-complex suspension and incubated at room temperature for 45 min. The miRNA released from the complex was analyzed by gel electrophoresis. miRNA stability within nano-complexes was determined by incubating the complexes (N/P ratio: 32/1) in 25% fetal bovine serum (FBS) for different time points at 37°C. After indicated time points, complexes were taken out and then incubated with heparin sulfate solution for 45 min. The mixture was then electrophoresed.

3.2.5. Transfection Efficiency

MIA PaCa-2 cells were seeded into Nunc Chamber Slides (Lab-Tek, Rochester, NY) at a density of 4 ×10^4 cells/well in serum free DMEM for Lipofectamine 2000® and DMEM with 10% serum for transfection with nano-complex for 24h. Copolymer/Block-IT™ fluorescent oligo complexes were prepared at the N/P ratio of 32:1. Lipofectamine transfection was carried out as per the manufacturer's instructions, and these cells were considered as the control. Nano-complexes were added to the respective wells (oligo 20pmol/well) with gentle shaking and incubated for 3h at 37°C. Cells were then washed twice with PBS containing Ca^{2+} and Mg^{2+}, fixed with 10% paraformaldehyde (PFA) in PBS for 15 min at room temperature. After fixing cells observed under a fluorescent microscope (Zeiss, Jena, Germany) and images were recorded.

3.2.6. Endosomal Escape Study

Cells were plated in Nunc Chamber slides at a density of 40,000 cells/well in 300µl DMEM. CellLight™ Early Endosomes-GFP was added for staining the endosomes as per the manufacturer's instructions. After overnight incubation, 50 µL of nano-complexes (20 µM) formulated from fluorescent Block-IT™ oligo were added to each well. After incubation for certain time points, cells were fixed with 10% PFA. For each time point, images were captured using Endosomes-GFP channel (excitation 488 nm, bandpass filter 500–550 nm) and Block-IT™ channel (excitation 543 nm, bandpass filter 560-615 nm). Image processing and analysis was conducted with ZEN software (Zeiss, Jena, Germany).

3.2.7. Cell Viability Assay

Cytotoxicity of the micelles carrying GDC-0449 and miR-let7b was determined by carrying out the cell viability assays. HPAF-2, M3T4, Capan-1, and MIA PaCa-2 cells (5000 cells/) were seeded 24h before transfection. Transfection was carried out using micelles

carrying GDC-0449 (1-10μM) and constant miR-let7b (10 pmol) concentration. Micelles carrying scrambled miRNA and GDC-0449 formulations were used as the positive control. Cell viability was assessed after 48h by MTT assay using a microplate reader (Epoch, BioTek Instruments Inc., Winooski, VT). % cell viability was calculated using equation:

$$\text{Cell viability } \% = \frac{\textbf{Absorbance Test}}{(\textbf{Absorbance Control})} \times 100 \quad (3.1)$$

3.2.8. In vivo Study

All animal experiments were performed in accordance with the protocol approved by the Institutional Animal Care and Use Committee (IACUC) at the University of Nebraska Medical Center (UNMC, Omaha, NE). Flank tumors were established in 8-10 week old male athymic nude mice by subcutaneous injection of $3X10^6$ MIA PaCa-2 cells suspended in a total 200 μl of 1:1 serum-free media and Matrigel® (BD Biosciences, CA). When the tumor volume reached 200-300mm^3, animals were randomly divided into five groups (n=5): blank micelles, micelles containing GDC-0449, GDC-0449 and scrambled miRNA (SCR), micelles containing miR-let7b, and micelles carrying miR-let7b and GDC-0449. Formulations were administered intratumorally thrice a week for two weeks at an equivalent dose of 10 mg/kg GDC-0449 and 2 mg/kg miR-let7b or the negative control (NC). Tumor size was measured at regular intervals using digital vernier calipers. Body weight of the animals was recorded three times a week. At the end of the study, tumor tissues were excised, weighed, and either fixed in formaldehyde or snapped frozen for further analysis.

3.2.9. Real-time RT-PCR

Gene expression levels of downstream targets of miR-let7b and GDC-0449 were determined using real-time RT-PCR. Total RNA from specimens was extracted using RNeasy RNA isolation kit (Qiagen, MD) as per manufacturer's protocol. mRNA was then reverse

transcribed into cDNA using TaqMan qRT-PCR kit (Life Technologies, Carlsbad, CA). cDNA templates were then amplified by real-time PCR on a Light Cycler 480 (Roche, Indianapolis, IN) using SYBR Green dye universal master mix. Primer sequences used were Shh (forward: CCAGAAACTCCGAGCGATTTA, reverse: TTTCACCGAGCA GTG GATATG) and GLI-1 (forward: CTACATCAACTCCGGCCAATAG reverse: GGT TGGGAGGTAAGGATCAAAG). β-actin (primer sequence forward: AGCCATGTACGTTGCTATCC, reverse: CGTAGCACAGCTTCTCCTTAAT) was used as a housekeeping gene, and the relative amount of mRNA was calculated using Crossing point (Cp) values.

3.2.10. Western Blot

Total proteins from tissues were extracted by homogenizing in RIPA buffer premixed with protease inhibitor cocktail (Sigma, St. Louis, MO). Proteins concentrations were determined using a BCA Protein Assay Kit (Thermo Scientific, Rockford, IL). Total protein (50 µg) was separated on 12 % Mini PROTEAN® polyacrylamide gels and then transferred to polyvinylidene fluoride (PVDF) (Life technologies Carlsbad, CA) using iBlot gel transfer system. The membrane was blocked using Odyssey blocking buffer for 1h at room temperature. Membranes were incubated overnight with rabbit polyclonal to Gli-1 (SC-20687), rabbit polyclonal to Shh (SC-h160), goat polyclonal to β-actin (SC-1616) (1:1000) (Santa Cruz Biotech., Dallas, TX) and mouse monoclonal to KRAS (ab-55391) (1:1000) (Abcam, Cambridge, MA). After washing with TBST buffer, the membrane was further incubated with their corresponding anti-rabbit, anti-goat and anti-mouse IR dye-conjugated secondary antibodies (1: 10,000) (LI-COR Biosciences, Lincoln, NE) for 60 min and visualized using the LI-COR imaging system. Expression levels of desired protein were normalized against β-actin (SC-1616) protein expression levels.

3.2.11. Histochemical and Immunofluorescence Assays

Tumors were excised, and specimens were fixed in 10% PFA overnight and embedded in paraffin. For the evaluation of the tissue morphology, sections (4µm) were stained with Hematoxylin & Eosin (H&E) and then analyzed blindly. For cell proliferation marker Ki-67, sections were probed with rabbit polyclonal Ki-67 antibody (1:50) (ab-15580). Sections were incubated for 45 min at room temperature with anti-rabbit horseradish peroxidase (HRP) conjugated secondary antibody diluted to 1:500 in 2% BSA/1×PBS solution. All stained slides were visualized under a microscope (Leica, Germany).

3.2.12. Terminal Deoxynucleotidyl Transferase nick end Labeling (TUNEL) Staining

DeadEnd® fluorometric TUNEL staining to identify apoptotic cells by fluorescein-12–dUTP labeling of fragmented DNA was carried out as per manufacture's protocol (Promega). Briefly, paraffin-embedded tumor tissue sections were deparaffinized by immersing in xylene and rehydrated by sequentially immersing the slides through graded ethanol. After washing with PBS, sections were fixed with 5% formaldehyde, washed with PBS and permeabilized by incubating with Proteinase K solution for 15 min. After fixing with 5% PFA and washing, slides were covered with 100µl of Equilibration Buffer for 15 min and washed with PBS. Subsequently, slides were coated with rTdT incubation buffer (equilibration buffer + nucleotide mix 5µl + rTdT enzyme) and incubated at 37°C for 60 min. For the negative control, incubation buffer was prepared without rTdT enzyme and incubated. Slides were then washed with 1X SSC buffer and PBS, and incubated in 1µg/ml propidium iodide (PI) in PBS for 20 min. Finally, slides were washed with deionized water twice and observed under confocal microscope.

3.2.13. Statistical Analysis

Student's unpaired t-test was used to compare the mean values of individual groups. A p-value <0.05 was considered as statistically significant.

3.3. RESULTS

Micelles containing miR-let7b and GDC-0449 were formulated and evaluated both in vitro and in vivo for treating pancreatic cancer. We have complexed hydrophilic miR-let7b and encapsulated hydrophobic GDC-0449 in our cationic polymeric micelles.

3.3.1. Copolymer Synthesis and Characterization

The cationic amphiphilic copolymer was synthesized by attaching dodecanol (DC) and TEPA to methoxy poly(ethylene glycol)-block-poly(2-methyl-2-carboxyl-propylene carbonate) (PEG-PCC) by carbodiimide coupling **(Figure 3.1A)**. mPEG-PCC was characterized with ^{1}HNMR and showed copolymer backbone peaks corresponding to PEG (–CH_2–CH_2–O) at δ 3.5, PCC (–CH_2–) at δ 4.2. After hydrogenation the characteristic peak of phenyl ring at δ 7.3 disappeared and a peak at δ 13 corresponding to exposed carboxyl group was observed which

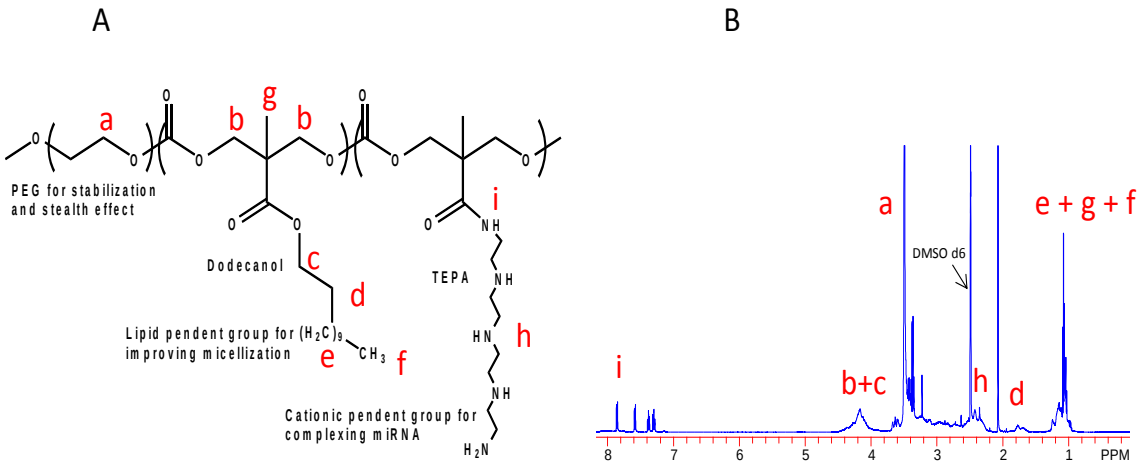

Figure 3-1. Design of amphiphilic copolymer for co-delivery of GDC-0449 and miR-let7b for treating for pancreatic cancer. (A) Schematic representation of copolymer (B) ^{1}H NMR.

indicates the complete removal of pendant benzyl group [236]. Based on the peak integrals of mPEG and PCC protons, a number average molecular weight (M_n) of the mPEG-PCC copolymer was calculated to be 10,370 g/mol with 31 PCC units. EDC/HOBt coupling reaction was used to conjugate, DC and TEPA chains to the copolymer. ^{1}HNMR characterization

showed peaks for TEPA at δ7–8 (–CO–NH–) and dodecanol peaks at δ of 1-2 (CH_2) **(Figure 3.1B)**.

The degree of polymerization (DP) of the copolymer was calculated based on ^{1}H NMR integration ratio of peaks assigned at δ 3.63 to ethylene protons of PEG backbone. Approximately 12 units of DC and 8 units of TEPA were present in the final copolymer with the disappearance of COOH peak and M_n calculated was approximately 14,000 g/mol. Gel permeation chromatography of the copolymer showed a unimodal peak with weight an average of 13776 g/mol (PDI of 2.0) and an increase in molecular weight compared to mPEG-MCC. This confirms the successful engraftment of DC and TEPA into the copolymer **(Figure 3.2)**. The CMC value of copolymer in the aqueous system as determined using pyrene was 5.5 X 10^{-4} (g/L) **(Figure 3.3)**.

A

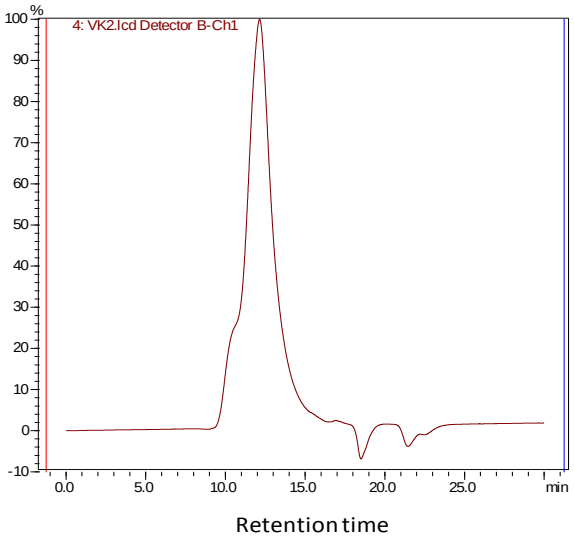

B

Number Average M.W.	Weight Ave.	Mw/Mn
6797	13776	2.02

Figure 3-2. Refractive index-gel permeation chromatography (RI-GPC) traces of mPEG-b-PCC-g-DC-g-TEPA copolymer and specifics of molecular weight data and characteristics.

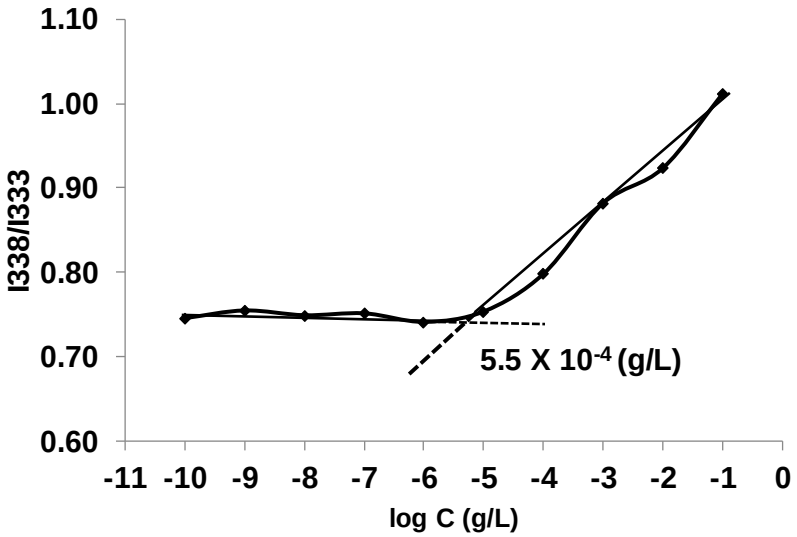

Figure 3-3. Plot of fluorescence intensity of pyrene vs. logarithm of the mPEG-b-PCC-g-DC-g-TEPA copolymer.

3.3.2. Formulation characterization

Mean particle size of micelles encapsulating GDC-0449 or in combination with miRNA was measured using DLS and TEM **(Figure 3.4 A&B)**. Micelles encapsulated only GDC-0449 showed a mean size of 95±10 nm (with PDI 0.11), while there was a slight decrease in the mean size (80±10 nm) (with PDI 0.10) when micelles contained both GDC-0449 and miRNA. TEM showed the morphology of GDC-0449 loaded miR-let7b complexed micelles as well-dispersed spherical particles. Compared to the hydrated state in DLS size of micelles (80±10 nm), TEM was carried out in the dried state, resulting in small size particles (60±10 nm). Zeta potential of miR-let7b polyplex micelles was in the range of 5 ± 2 mV compared to -15± 2 mV for a free miR-let7b solution.

These micelles carrying GDC-0449 and miR-let7b were fairly stable at room temperature, and thus there was little change in their particle size distribution even after a week (data not shown). There was the little release of miRNA from the polyplex, suggesting the high stability of this formulation. mPEG-b-PCC-b-DC-g-TEPA significantly increased solubilization of GDC-0449 up to 1560 ± 50 µg/ml, as determined by HPLC-UV. GDC-0449 release in the

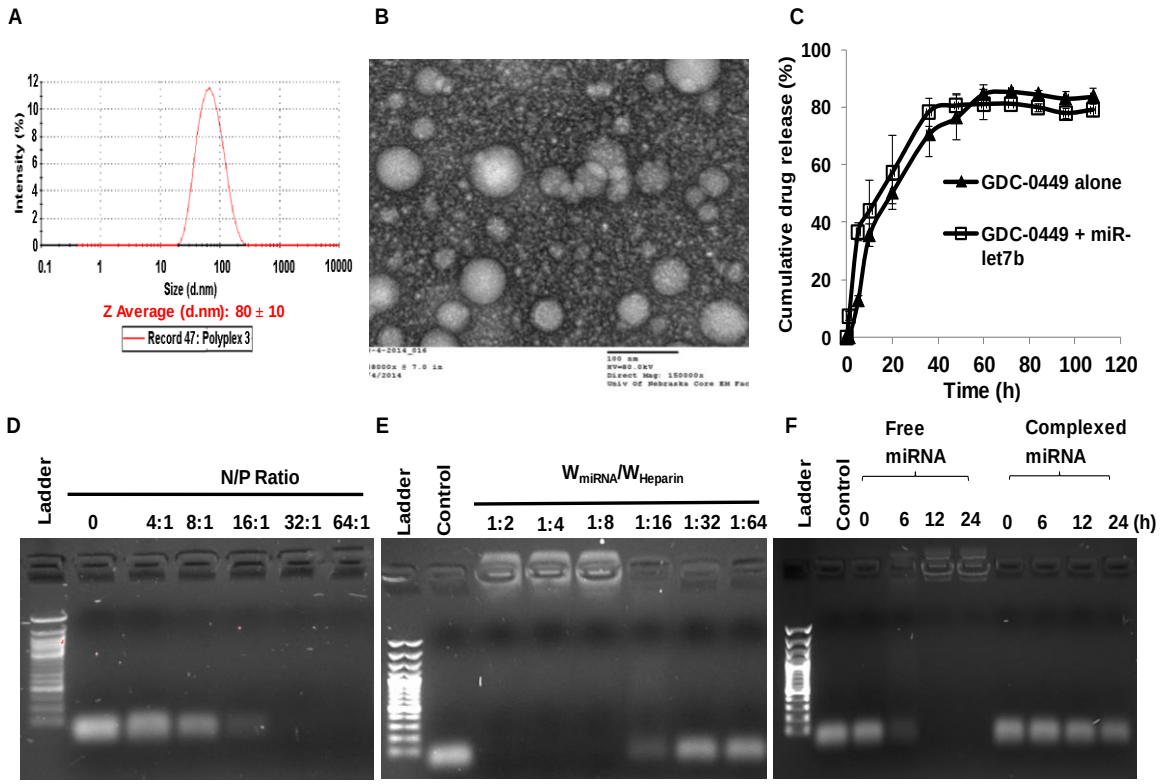

Figure 3-4. Micelle preparation and characterization. (A) Particle size distribution of miR-let7b complexed and GDC-0449 encapsulated micelles using dynamic light scattering; (B) Micelle morphology determined by transmission electron microscope (TEM); (C) GDC-0449 release profile from micelles with or without miRNA, (D) complex formation ability of micelles to miRNA at different N/P ratios, (E) miRNA dissociation from micelles by heparin; and (F) miRNA stability in presence of 25% FBS. Equal amount of each sample was incubated with 10 µL FBS at 37°C for 0, 6, 12 and 24h prior to gel electrophoresis.

presence and absence of miRNA from the combination formulations was determined at 7.4. Drug release showed a controlled release of 80% in 2 days, with no effect of the presence of miR-let7b on GDC-0449 release from the polyplexes **(Figure 3.4C)**.

To determine the effect of N/P ratio on miR-let7b complexation, miR-let7b was complexed with mPEG-b-PCC-b-DC-g-TEPA at N/P ratios ranging from 1:1 to 64:1. Complete retardation of miRNA was observed at N/P ratio of 32:1 **(Figure 3.4D)**. Heparin (170U/mg) was able to dissociate miR-let7b from the polyplexes at the ratio of 1:16 **(Figure 3.4F).** miR-let7b was stable in 25% FBS for 24h when formulated in micelles, while naked miRNA degraded within 1h, suggesting polyplex formation stabilizes miRNA against exonucleases **(Figure 3.4E)**.

Cellular uptake and intracellular distribution of these micelles were evaluated by confocal laser scanning microscopy. Although our cationic polymer showed transfection efficiency similar to Lipofectamine 2000® (**Figure 3.5**), significantly lesser cytotoxicity was observed based on the N/P (+/-) ratio of the complexes. Also, uptake study using our formulation was carried out using serum containing media, unlike Lipofectamine 2000® lipoplexes which required serum-free media for transfection. The N/P ratio of lipofectamine: miR-let7b was ~22:1 while our polymer was non-toxic even at N/P ratio of 64:1.

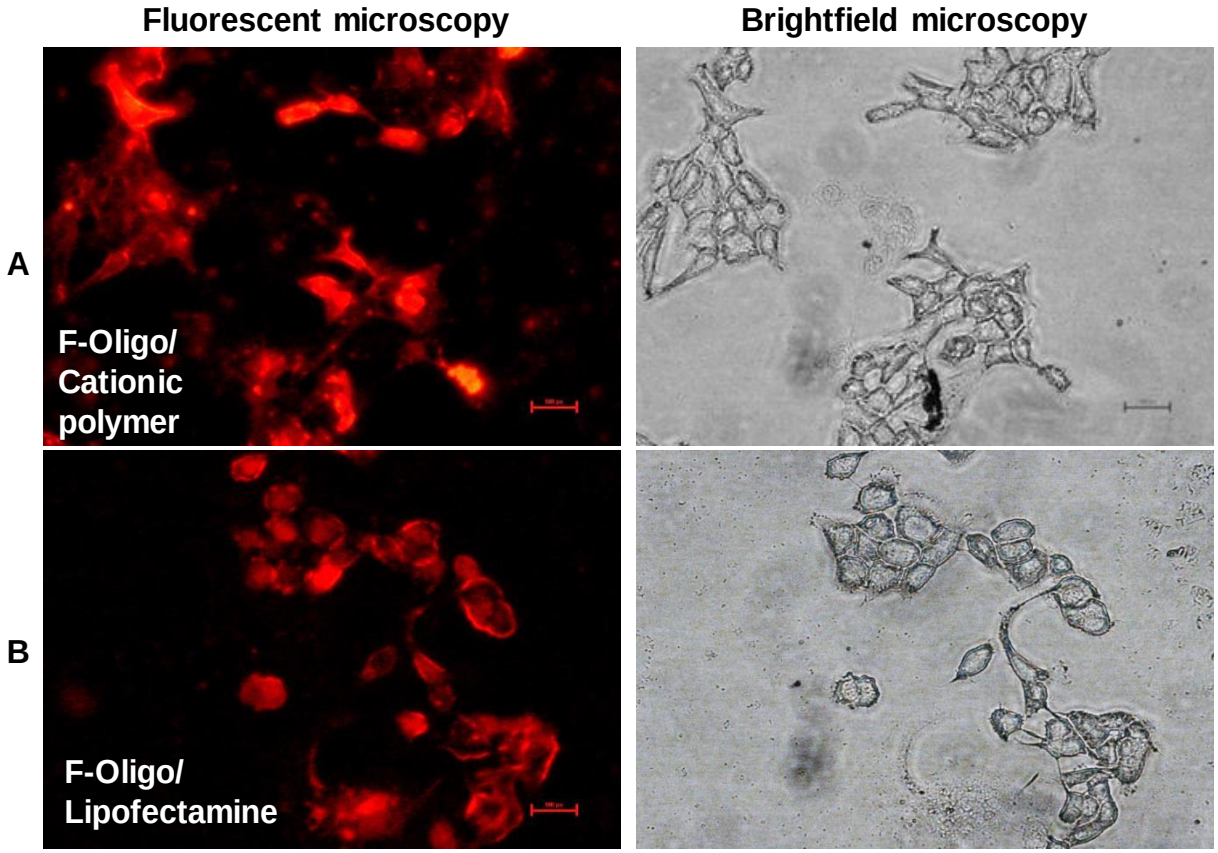

Figure 3-5. Transfection efficiency of fluorescent labeled Block-IT™ oligo loaded micelles into Capan-1 cells. (A) Oligo complexed micelles and (B) oligo/Lipofectamine-2000 complexes. Right panel is optical images of cells (DIC). After 4h post-transfection, cells were washed, fixed, and mounted for microscopy.

3.3.3. Transfection Efficiency and Lysosomal Escape

For endosomal escape study, MIA PaCa-2 cells were labeled with GFP and transfected with Cy3 labeled oligonucleotide formulation for different time points. After 1h of incubation, the co-localization of both fluorescent signals were observed, suggesting efficient uptake of micelles by the cells **(Figure 3.6A)**. The majority of fluorescence was localized in endosomal compartments and after 3h, both fluorescent colors were separated and clearly showed that micelles were not restricted to early endosomes **(Figure 3.6B)**, indicating its potential to be used as a miRNA carrier.

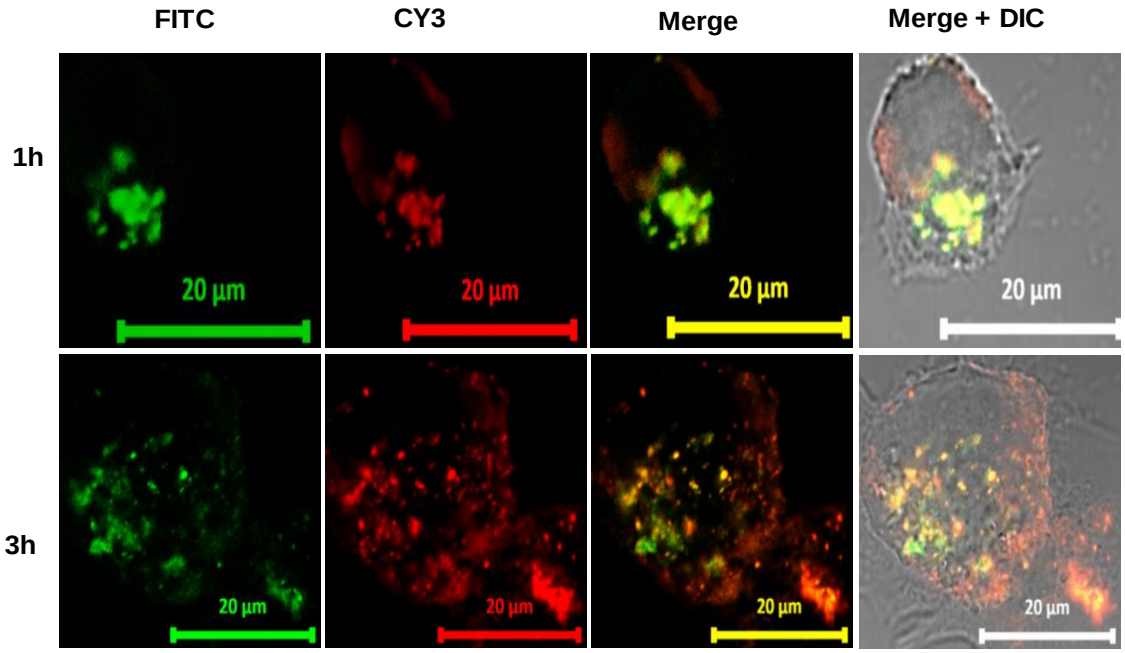

Figure 3-6. Confocal microscopy of MIA-PaCa-2 cells exposed to CY3 oligo complexed micelles. Cells were exposed to micelles for 1-5h. Fluorescence of the micellar core (red) and shell of the endosomes (green) is highly co-localized as indicated by the yellow signal in the merged images. (Scale bar: 20 µm.)

3.3.4. Cell Viability Assay

Cytotoxicity of micelles carrying GDC-0449 and miR-let7b were determined at N/P ratios of 32:1 with 10pmol miR-let7b. Cell viability was determined by MTT assay after 48h of

incubation and compared to the cells incubated with micelles carrying either GDC-0449 or miR-let7b alone or GDC-0449 and scrambled miRNA. The combination formulations reduced cell viability to 47% in HPAF-II, 20% in Capan-I, 30% in T3M4, and 37% in MIA PaCa-2 cells at the dose of 10 pmol miR-let7b and 10 µM GDC-0449 while both miR-let7b and GDC-0449 monotherapy failed to kill cells at the low doses **(Figure 3.7)**. Therefore, combination formulation was quite effective leading to a significant decrease in cell viability, suggesting synergism between these two drugs.

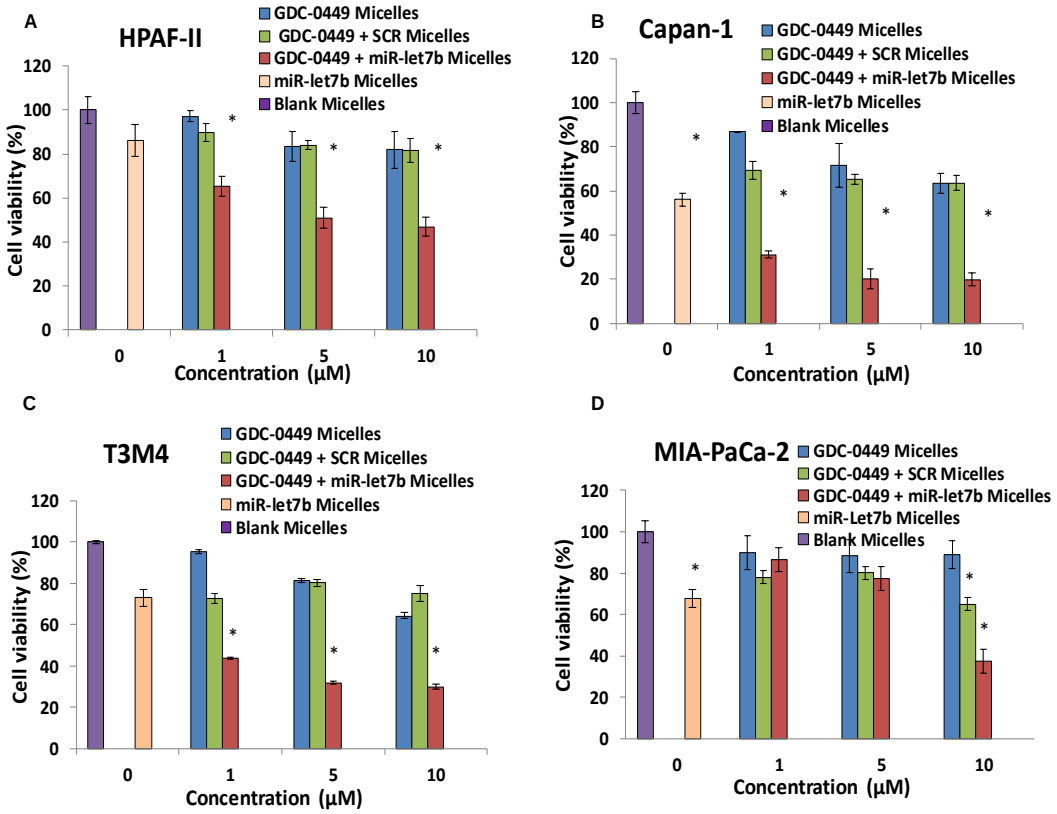

Figure 3-7. Effect of GDC-0449 and miR-let7b on cell viability in human pancreatic cancer cell line by micelles. (A) HPAF-II, (B) M3T4, (C) Capan-1 and (D) MIA PaCa-2 cells (5000/well) were treated with micelles containing (■) GDC-0449 (0, 1, 5 and 10 µM), (■) GDC-0449 and scrambled miRNA (■), GDC-0449 and miR-let7b (10pmol), (■) miR-let7b alone and (■) blank for 48h. Cell viability was measured by MTT assay at the end of incubation period. Data represent the mean ± S.D. (n=3)

3.3.5. In vivo Evaluation

The in vivo efficacy of micelles containing miR-let7b and GDC-0449 was determined in subcutaneous tumor bearing athymic nude mice generated using MIA PaCa-2 cells. All the animals did not show any signs of toxicity or loss in body weight during the treatment period **(Figure 3.8A)**. All the treatment groups had significantly low tumor growth

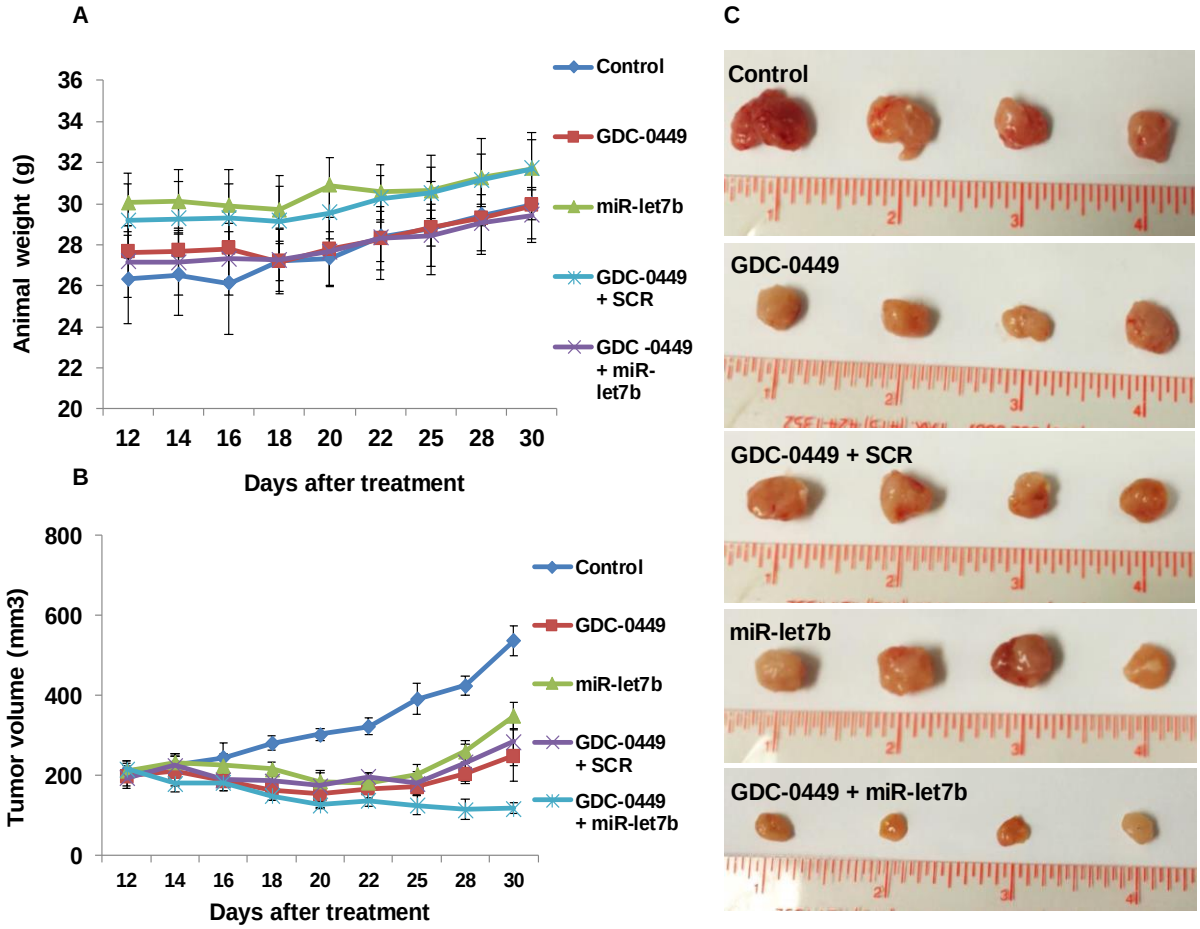

Figure 3-8. In vivo efficacy of mPEG-b-PCC-b-DC-b-TEPA micelles carrying GDC-0449 and miR-let7b in tumor bearing mice. Tumors were developed by subcutaneous injection of (3 X 10^6) MIA PaCa-2 cells in in the left flank of athymic mice. When the tumor size reached 200 mm^3, mice were injected intratumorally with one of the following formulations: blank micelles, micelles carrying GDC-0449, micelles carrying GDC-0449 and scrambled miRNA and micelles carrying GDC-0449 and miR-let7b. Dose was 10 mg/kg GDC-0449 and 2 mg/kg miR-let7b or scrambled miRNA. A) Animals body weight during treatment; B) tumor volume and C) representative tumor size of various treatment groups. GDC-0449/miR-let7b micelles decreased the rate of tumor growth compared to monotherapy. Data expressed as the mean ± S.E. (n= 5).

compared to the control group (537.30 ± 38.43 mm^3). However, significant tumor growth inhibition was observed in the mice which received micelles carrying miR-let7b and GDC-0449 (119.07 ± 13.25 m m^3) compared to the formulations containing miR-let7b (350.35 ± 64.15 mm^3) or GDC-0449 alone (249.19 ± 32.74) or formulations containing GDC-0449 and SCR miRNA (285.12 ± 58.63 mm^3) **(Figure 3.8B & C)**.

RT-PCR was used to determine the mRNA expression of Shh and Gli-1 in tumor tissues where relative expression of Shh mRNA was inhibited by GDC-0449 and GDC-0449 + SCR treatment groups to 59.15% ± 10.19 and 69.07 % ± 10.86 respectively, wherein its levels were 47.62% ± 7.05 in the combination treatment group. Relative Gli-1 mRNA also displayed the similar trend, where its transcripts were decreased to 63.45% ± 5.64 and 68.65 % ± 3.03 by GDC-0449 and GDC-0449 + SCR formulations respectively, and up to 31.82% ± 2.47 reductions by the combination treatment group **(Figure 3.9A)**. We did not observe any significant reduction in the level of either of these transcripts in mice treated with the formulations containing miR-let7b alone. Western blot analysis shows reduced Gli-1 and K-RAS protein expression in treatment groups **(Figure 3.9B)**.

Immunohistochemical analysis of tumor sections revealed that the treated mice displayed lower Ki-67 staining compared to untreated mice. Among treatment groups, mice treated with combination therapy had least Ki-67 staining **(Figure 3.10A)**. Treatment with micelles carrying GDC-0449 and miR-let7b resulted in loosened groups of epithelial cells, whereas the control group had dense cells within tumor mass **(Figure 3.10B)**. Tumor sections were examined for apoptosis of cancer cells using TUNEL assay. No apoptotic (TUNEL-positive green fluorescent) cells were observed in sections from the control mice. Mice treated with micelles containing miR-let7b or GDC-0449 alone showed an only modest increase in the number of apoptotic cells, while miR-le7b and GDC-0449 combination therapy significantly enhanced apoptosis **(Figure 3.10C)**.

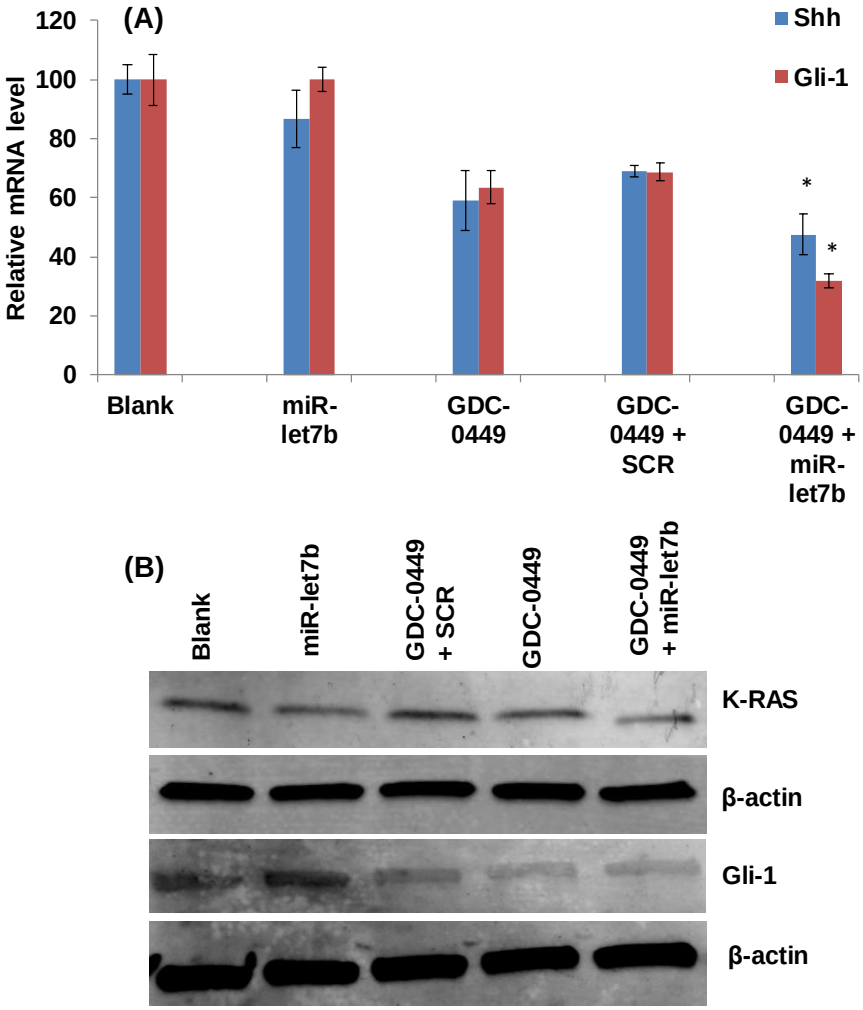

Figure 3-9. Real time RT-PCR and Western blot of tumor samples. A) GDC-0449/miR-let7b treated animals showed down regulated relative mRNA levels of Shh and Gli compared to control animals (n=3, $p<0.05$). B) Western blot of Gli-1 and K-RAS.

3.4. DISCUSSION

PDAC is among the most lethal human cancers and poses a medical challenge due to its insensitivity to the majority of proven chemotherapeutic agents. Hh signaling promotes proliferation of most cancer cell types including breast cancer, prostate cancer, colon cancer, brain tumors, pancreatic cancer, and basal cell carcinomas [165,239-243]. Hh signaling controls EMT and enhances cell proliferation by MAPK- and PI3-kinase-dependent manner decreases apoptosis by regulation of Bcl-2 and Bcl-X and also proliferates CSCs. Hh pathway also

promotes cell invasion, migration, and chemoresistance [244,245]. By inhibiting Hh signaling, GDC-0449 has shown the potential of reducing tumor cell growth [246].

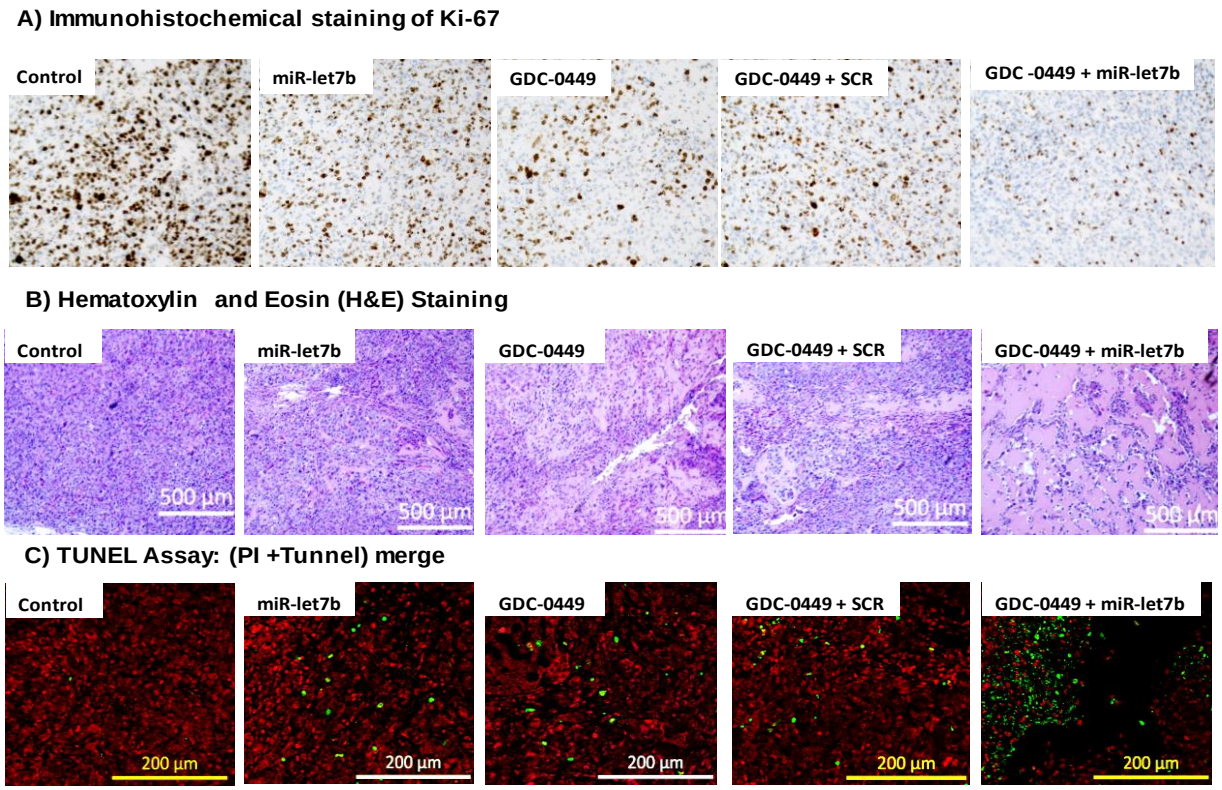

Figure 3-10. Analysis of tumor samples for Ki-67 staining, hematoxylin and eosin (H&E) staining and C) Tunnel Assay for apoptosis. A) Immunohistochemical staining of Ki-67; B) H & E staining of peripheral tumor regions; and C) apoptosis in tumor cells as indicated by the green fluorescence of TUNNEL, while red spots mark the cells with propidium iodide (PI) staining.

GDC-0449 and miR-let7b represent diverse physicochemical properties with GCD-0449 being a hydrophobic small molecule while miR-let7b is an oligonucleotide with high aqueous solubility. Therefore, we have synthesized an amphiphilic cationic mPEG-b-PCC-g-DC-g-TEPA copolymer, which self-assembles into micelles to encapsulate GDC-0449 and bears cationic pendant chains to form complexes with miR-let7b. Apart from co-delivery, our system offers distinct advantages in terms of a) PEG corona on the polymer imparting stealth property, b) small size of these micelles can take advantage of the EPR effect to maximize drug delivery to pancreatic tumor, and c) co-delivery will ensure similar biodistribution profiles of both the active

therapeutic moieties. Further, these nanomedicines are stable and scalable and hence bear high translational potential.

While miR-let7b has been reported to retard pancreatic cancer cell growth and proliferation in vitro, it failed to inhibit PDAC progression in vivo due to the lack of efficient delivery [247]. Therefore, there is a great need to develop an efficient delivery system for miRNAs. We complexed miR-let7b with cationic chains of mPEG-b-PCC-g-DC-g-TEPA copolymeric in micelles. This copolymer self-assembles into micelles and encapsulates GDC-0449 into its core and allows complex formation between miR-let7b and cationic pendant chains. The entrapment of miR-let7b into these micelles offers advantages of its improved in vivo stability, enhanced mean residence time and ensuring similar biodistribution of both GDC-0449 and miR-let7b. Cells of RES recognize particles of large size while particles smaller than 200 nm manage to escape. The mean particle size of our polyplexes ranged from 80 nm to 100 nm with spherical morphology **(Figure 3.4A and 4B)**. Moreover, mPEG corona on the polymer imparts stealth property for longer mean residence time at the tumor site [248]. By micellization, the aqueous solubility of GDC-0449 was increased from 0.1 µg/ml to 1560 ± 50 µg/ml.

Efficient miR-let7b complexation with the primary copolymer amines was observed at N/P ratio of 16/1 **(Figure 3.4D)**. Low zeta potential value of the formulations suggests that PEG corona surrounds the polyplex core [249]. Decrease in polyplex mean particle size was observed in the DLS analysis after miRNA addition, may be due to the strong interaction between miRNA and cationic chains leading to decrease in the inter-chains force of repulsion [250]. Complete displacement of miRNA from polyplexes observed in the presence of polyanionic heparin, demonstrating that miRNA can be effectively released from the carrier **(Figure 3.4E)**. Serum stability study shows that the naked miRNA degraded within 6h of incubation, while miRNA in the formulation was stable up to 24h **(Figure 3.4F)**.

We determined the effect of GDC-0449 and miR-let7b formulations on cell viability using four pancreatic cancer cell lines known to express high levels of Hh ligands [251]. miR-let7b or GDC-0449 alone in formulations was ineffective in reducing cell viability, whereas cytotoxicity was increased significantly when GDC-0449 and miR-let7b were used as combination formulations **(Figure 3.7)**. This synergy may be due to the fact that Hh signaling pathway works cooperatively with K-RAS in pancreatic cancer [164]. Thus, GDC-0449 reduces proliferation and induces apoptosis of these cells via Gli-1 dependent manner and chemosensitizers them to anti-K-RAS miR-let7b.

In vivo efficacy of the formulations was evaluated in athymic nude mice bearing ectopic tumor generated by subcutaneous implantation of MIA PaCa-2 cells. Treatment of these mice with micelles carrying miR-let7b and GDC-0449 resulted in a significant reduction in tumor growth rate and tumor weight compared to the control group **(Figure 3.8B and 8C)**. There was a significant reduction in Shh and Gli-1 expression as analyzed by RT-PCR and K-RAS expression as analyzed by Western blot **(Figure 3.9)**.

We observed a high expression of proliferation marker Ki-67 in control group showing a high cell growth, whereas treatment with miR-let7b and GDC-0449 combination reduced cellular proliferation to a significantly low level **(Figure 3.10A)**. Histological analysis of tumor specimens revealed a compact mass of epithelial cells in the control group, whereas combination treatment tumors appeared as loose epithelial cell aggregates with a larger amount of interspersed mesenchymal cells **(Figure 3.10B)**, which is in line with the literature [164]. TUNEL assays demonstrated that GDC-0449 and miR-let7b treatment resulted in increased number of apoptotic cells compared with the control or single drug-treated groups **(Figure 3.10C)**.

All of these observations conclude that by combining K-RAS targeting tumor suppressor miR-let7b with Hh inhibitor GDC-0449 reduces tumor growth synergistically. Although the precise mechanisms of this cooperation are subject to further investigation, it appears that

inhibition of Hh signaling sensitizes tumor cells to anti K-RAS therapy. This is in line with previous studies, where Hh pathway activation reduced sensitivity to treatment with therapeutics that target K-RAS signaling pathway. Further, targeting both Hh and anti-K-RAS pathways reduced pancreatic tumor initiation and growth [252].

We are aware of the outcome of a recent clinical trial, which revealed a remarkable decrease in Shh and proliferation marker Ki-67 after treatment with GDC-0449, but the combination of GDC-0449 and gemcitabine failed to improve the median survival of pancreatic cancer patients [253]. Furthermore, in a separate study, aggressive and undifferentiated tumor growth upon Hh deletion has been reported [254,255]. This tumor-promoting effect of Hh signaling suppression may be due to increased angiogenesis within tumor mass by a very high dose of GDC-0449 used (100 mg/kg) [256]. This is because, in a different clinical study, GDC-0449 in combination with gemcitabine and nab-paclitaxel showed higher overall survival compared to gemcitabine plus nab-paclitaxel [257]. Therefore, successful inhibition of tumor growth requires a delicate balance between the beneficial and harmful effects of Hh signaling [258].

3.5. CONCLUSIONS

In conclusion, we demonstrated that mPEG-b-PCC-g-DC-g-TEPA efficiently encapsulates GDC-0449 and forms complexes with miR-let7b, and this combination therapy has the potential to inhibit pancreatic cancer both in vitro and in vivo. This combination formulation represents a promising therapeutic approach to treat advanced pancreatic cancer with dense desmoplasia.

CHAPTER 4. CO-DELIVERY OF SMALL MOLECULE HEDGEHOG INHIBITOR AND MIRNA FOR TREATING LIVER FIBROSIS

4.1. INTRODUCTION

Recently, we demonstrated that Hh ligands are upregulated in the livers of the CBDL rats, and blockage of Hh signaling using small molecule Hh inhibitor, GDC-0449 can prevent early-stage liver fibrosis [192]. Our miRNA profiling has clearly shown that among various miRNAs, the miR-29 family is significantly downregulated during the activation of HSCs and progression of liver fibrosis. The mir-29 family is composed of four members: miR-29a, miR-29b1 (previously known as miR-29b), miR-29b2, and miR-29c. Their seed sequences are identical but have different flank regions [259]. Among them, miR-29b1 is gaining increasing attention for treating liver fibrosis.

Our in-silico analysis indicated that miR-29b1 targets several profibrotic genes like collagen type I & IV, c-MYC, platelets derived growth factor beta (PDGF-β), and PI3K/AKT through their 3'-UTR regions. Notably, miR-29b1 downregulates phosphorylation of protein kinase B (AKB) which is involved in growth and proliferation, adhesion, migration, and collagen production by HSCs [260,261]**.** TGF-β1 is upregulated in liver fibrosis and known to downregulate miR-29b1 through SMAD3 pathway [262,263]. Therefore, inhibition of fibrogenic signaling at multiple levels and inhibiting expression of ECM proteins by restoring intracellular levels of miR-29b1 could be an effective therapeutic strategy for liver fibrosis.

Due to the involvement of multiple signaling pathways and diverse cell type, the combination of two or more therapeutic agents with different mechanisms of action or targets is expected to show a synergistic antifibrotic effect [264]. Furthermore, profibrotic TGF-β is also known to induce Hh downstream transcription factor GLI proteins through SMAD pathway and activate Hh signaling independent from smoothened (SMO) [265]. Therefore, suppression of Hh

pathway alone without reduction of TGF-β or vice-versa is likely to result in partial treatment of liver fibrosis. Moreover, even when one or both types of suppressing agents are delivered separately, the only suboptimal effect can be expected. For spatial–temporal synchronization of hydrophobic GDC-0449 and hydrophilic miR-29b1, a specialized carrier system, capable of encapsulating and delivering them simultaneously, is required.

Recently, we have developed cationic polymer mPEG-b-PCC-g-DC-g-TEPA based micelles for simultaneous delivery of miR-let7b and GDC-0449, where GDC-0449 was encapsulated, and miRNA was complexed in the core of micelles. Micelles carrying miR-Let-7b and GDC-0449 were characterized by particle size, zeta potential, drug loading, miRNA complexation as well as stability and transfection efficiency, and evaluated for treating pancreatic cancer [179]. In this study, we extended our prior work by systemic delivery of GDC-0449 and miR-29b1 loaded micelles into CBDL mice to evaluate their anti-fibrotic efficacy. CBDL procedure induces proliferation and differentiation of intrahepatic biliary epithelial cells into myofibroblasts which result in overproduction and deposition of ECM [266]. Mechanistically, bile acid (BA) concentrations in animals act as pro-inflammatory signals, which trigger CXC chemokine formation in hepatocytes. These chemokines together with osteopontin derived from biliary epithelial cells recruit neutrophils to the areas of biliary leakage in the liver during obstructive cholestasis. Thus, CBDL-induced liver injury is caused by a neutrophil-mediated inflammatory response [267]. Here, we report micelles that are scalable, carry GDC-0449 and miR-29b1 simultaneously, and have high transfection efficiency with low cell toxicity. Systemic administration of micelles carrying miR-29b1 and GDC-0449 into CBDL mice resulted in a significant decrease in collagen deposition and serum injury markers as well as improvement in liver morphology. Further, we report a significantly upregulated expression of mature miR-29b1 following micelles mediated systemic delivery of miR-29b1 to CBDL mice. Finally, we demonstrated that systemic delivery of miR-29b1 and GDC-0449 containing micelles

significantly suppressed profibrotic genes like Shh, GLI, α-SMA, PDGFR-β and p-AKT in a mouse model of liver fibrosis. Our results suggest a new approach for co-delivery of miRNA and hydrophobic small molecule by biodegradable polymeric micelles.

4.2. MATERIALS AND METHODS

4.2.1. Materials and Reagents

Benzyl bromide, 2, 2-bis (hydroxymethyl) propionic acid, methoxy poly (ethylene glycol) (mPEG, Mn = 5000, PDI= 1.03) stannous 2-ethylhexanoate ($Sn(Oct)_2$) and radioimmunoprecipitation assay (RIPA) buffer were purchased from Sigma-Aldrich (St. Louis, MO). Tetraethylenepentamine (TEPA) and dodecanol (DC) were purchased from Alfa-Aesar (Ward Hill, MA). TaqMan® reverse transcription reagent kit was purchased from Life Technologies (Grand Island, NY) and SYBR green-1 was purchased from (Roche, Indianapolis, IN). miR-29b1 (mature sequence: GCUGGUUUCAUAUGGUGGUUUA) and scrambled miRNA were purchased from Invitrogen (Carlsbad, CA). miR-29b1 mimic is a double-stranded construct consisting of a guide and passenger strands. All other reagents were purchased from Sigma-Aldrich and used without further purification.

4.2.2. In silico miR-29b1 Target Prediction and miRNA Profiling

We used three algorithms computationally to predict potential targets of miR-29b1 including TargetScan, miRDB, and DIANA MicroT-CDS. The computationally predicted best miRNA-target pairs were selected by comparing the results from the three target prediction databases. miRNA profiling of liver samples from the sham control and CBDL fibrotic mice was done using our standardized protocols [229]. Briefly, total RNA including small non-coding miRNA was isolated from the liver tissues using miRNEasy RNA isolation kit (Qiagen, MD) with phenol-chloroform method. RNA quality was then determined using a microplate reader (Epoch, BioTek Instruments Inc., Winooski, VT) and converted to cDNA template using miScript II RT

Kit. miRNA PCR array was performed with a 96 well plate SYBR green based pathway-focused miScript miRNA PCR Array (Qiagen, MIMM-117ZF). This array profiles the expression of 84 miRNAs known to play a role in mouse liver fibrosis. This array includes 6 housekeeping genes (SNORD61, SNORD68, SNORD72, SNORD95, SNORD96A, RNU6B/RNU6-2) and quality controls assays. Roche Light Cycler 480® with thermo-cycle consisted of activation (95°C for 15 min) 45 cycle of denaturation (94°C for 15s) annealing (55°C for 30s) extension (70°C for 30s). Relative quantification was performed using miScript miRNA PCR Array Data Analysis web-based service (SA Biosciences, MD).

4.2.3. Synthesis of Copolymer and Preparation of Micelles

Copolymer mPEG-b-PCC-g-DC-g-TEPA was synthesized, and micelles were prepared by film hydration as previously described [179]. Briefly, GDC-0449 loaded micelles were prepared by dissolving GDC-0449 (1.5mg) and copolymer (30mg) in chloroform (0.5mL) and evaporated under reduced pressure to form a thin film and was further dried overnight in a desiccator. The film was then hydrated with HEPES buffer (1mL, pH 6.5) and vortexed for 5 min at room temperature. Micelles carrying GDC-0449 and miR-29b1 were prepared by hydrating the polymeric film containing GDC-0449 with HEPES buffer containing miR-29b1, vortexed for 5 min and suspension was shaken for 25-30 min at RT to enable miRNA complexation. The mixture was then centrifuged at 5000 rpm for 5 min and filtered using 0.22 µm filter (Millipore).

4.2.4. Characterization of Formulations

Micelles carrying GDC-0449 and miR-29b1 were characterized by the particle size distribution using a Malvern Zetasizer (NanoZS Series) and their morphology using transmission electron microscope (TEM) as described earlier [179]. All the formulations containing miRNA (used for characterization and as well as for in vivo studies) were formulated at N/P ratio of 32:1. The stability of micelles was assessed in PBS (pH 7.4) by monitoring changes in particle

size stored at RT with regular sampling for up to 6 days [268]. We determined the kinetic stability of micelles carrying GDC-0449 and miR-29b1 using two independent methods. Fluorescence resonance energy transfer (FRET)-based method was used to study the stability of micelles [269]. Briefly, 5mg mPEG-b-PCC-g-DC-g-TEPA, 250µg GDC-0449, 50µg Dil, and 50µg DiO were dissolved in 500 µL chloroform and dried to make a film. HEPES buffer (500 µl, pH 6.5) containing miR-29b1 was then added to the copolymer film, vortexed for 5 min and shaken for 30 min on an orbital shaker. Micelles were filtered through a microfilter (0.45 µm) and incubated with 100% FBS (1:4 volume ratio) at 37°C with gentle agitation, and time-resolved spectra were measured over 36h with an excitation wavelength at 484 nm. In the second method, the stability of the drug-containing micelles was probed in serum containing medium by size exclusion chromatography (SEC) [270]. The drug-containing micelles (1 mL) were incubated with 250 µl FBS at 37°C. At certain time intervals (0-24h), aliquots (100 µL) of the mixtures was withdrawn and analyzed by SEC (Ultrahydrogel 250, Waters, Japan) connected to a UV detector. Samples were eluted with 1× PBS (pH 7.4) at a flow rate of 1.0 mL/min.

4.2.5. Cellular Uptake Study

HSC-T6 cells were seeded in in 4-wells Nunc Chamber Slide (Lab-Tek, Rochester, NY) at a density of 4×10^4 cells per well and incubated in 500 µL DMEM with 10% FBS overnight. In Lipofectamine 2000/oligo complex transfected cells, the medium was removed by aspiration and replaced with serum free Optimum media. Lipofectamine2000/oligo complexes (20 pmol each well) were added to the respective wells and incubated for 3h. For micelle transfection, micelles loading oligo (20 pmol each well) were added to the wells directly, without removing the media (with serum) and incubated. For imaging, cells were washed twice with PBS containing Ca^{2+} and Mg^{2+}, fixed with 10% PFA in PBS for 10-15 min at room temperature and observed under a fluorescent microscope (Zeiss, Jena, Germany). Micelles containing 50 nmol/L of Cy5 labeled miR-29b1 (GE Dharmacon, Lafayette, CO) were formulated and incubated with HSC-T6 cells

for 4h to determine transfection efficiency as described before. Cells were then trypsinized and washed three times with heparin (20 U/ml heparin in PBS) and resuspended in 500 µl ice-cold PBS (0.2% BSA and 1 mmol/l ethylenediaminetetraacetic acid then analyzed by flow cytometry (BD FACSAria-II, San Jose, CA). The effect of GDC-0449-449 and miR-29b1 loaded micelles on cytotoxicity was determined by measuring cell viability and calculating as % of the cell viability of blank micelles treated cell samples. HSC-T6 cells were seeded in a 96-wells plate at a density of 3000 cells per well in DMEM medium containing 10% of FBS and grown overnight. After 48 h post-incubation of GDC-0449 and miR-29b1 containing micelles, MTT assay was carried out [179].

4.2.6. Animal Studies

C57BL/6J male mice (8-10 week old 20–25 g) were purchased from Charles River Laboratories, Inc. (Raleigh, NC). All animal experiments were performed in accordance with the protocol approved by the Institutional Animal Care and Use Committee (IACUC) at the University of Nebraska Medical Center (UNMC, Omaha, NE). CBDL was performed as described [192]. Intrahepatic bio-distribution of micelles containing GDC-0449 and miR-29b1 was determined at 30min in normal and fibrotic mice. Micelles containing GDC-0449 (10 mg/kg) and fluorescent cy5 dye labeled miR-29b1 (3 mg/kg) were injected intravenously after 7 days of CBDL. After 30 min, blood was collected via cardiac puncture, and livers were perfused with pronase E and collagenase P solutions, and cellular fractions (hepatocytes, HSCs and Kupffer + endothelial cells) were isolated as described earlier [271]. Cells were lysed with RIPA buffer. miR-29b1 and GDC-0449 were extracted, and their concentrations were determined using a fluorescent plate reader and LC–MS/MS, respectively [272-274].

Formulations were administered intravenously thrice a week for two weeks into sham-operated and CBDL mice to determine the therapeutic effect. During this period, survival was

>90% in all groups of mice. On day 14, post-surgery, blood was collected via cardiac puncture, mice were sacrificed, and livers were harvested and stored for further evaluation.

4.2.7. Serum Enzymes

Liver injury serum markers such as alanine transaminase (ALT), aspartate transaminase (AST), and total bilirubin (BIL) levels from various animal groups were measured using standard kits (Max Discovery™ Color Endpoint Assay kit. (Bioo Scientific Co. Austin, TX) following the manufacturer's instructions.

4.2.8. Histology

Liver tissue pieces from different animal groups were fixed in 10% PFA solution overnight and then embedded in paraffin. Sections of 5 µm thickness were cut and stained with H&E, Masson's trichrome (MT), and Sirius red by using standard protocols. Sections were scanned at 40X using iScan HT Slide Scanner (Ventana Medical Systems, Inc, AZ) and representative views of sections are shown. For quantitative analysis of the fibrous area, MT slides analyzed using Definiens Tissue Studio-4 software using four microscopic fields for each specimen.

4.2.9. Real Time RT-PCR

Total RNA from liver tissues was isolated using as described above. Two-step RT-PCR was performed to determine the levels of isolated mRNA. In the first step, Real- mouse liver RNA was converted to cDNA by using TaqMan reverse transcription reagents (Life Technologies) on S1000 Thermal Cycler (Bio-rad). Primers were designed using primer designing tool (Primer quest, IDT). Primer sequences used are given in table 4.1. Real-time amplification was then performed with SYBR® Green PCR master mix reagent (Applied Biosystems) using a LightCycler 480® machine (Roche). The expression level of mature miR-29b1 in mouse livers was analyzed by qRT-PCR using assay method and reagents from

Qiagen. First, the total RNA was reverse transcribed into cDNA using the miScript II RT kit. The qRT-PCR amplification of cDNA was then performed using miScript Primer Assays (Qiagen; MS00024703). The mature miR-29b1 expression was determined by the $\Delta\Delta C_T$ method and normalized to RNU6-2 (Qiagen; MS00033740), which is the endogenous control in the corresponding samples.

Table 4.1. Quantitative Real Time PCR primer sequences

Primer	Sequence	Name
GAPDH fwd GAPDH rev	GGGTGTGAACCACGAGAAATA GGGTCTGGGATGGAAATTGT	Glyceraldehyde-3-phosphate Dehydrogenase
Col1A1 fwd Col1A1 rev	AGACCTGTGTGTTCCCTACT GAATCCATCGGTCATGCTCTC	Collagen, type I, alpha 1
Shh fwd Shh rev	CGTCTTCTGTACTGCCTTCTT GTGCGT TAACAGTCTTGGTTTC	Sonic hedgehog
Gli-1 fwd Gli-1 rev	TCGACCTGCAAACCGTAATC CATCTGAGGTGGGAATCCTAAAG	Gli-1
FN1 fwd FN1 rev	TACGGAGAGACAGGAGGAAATA CATACAGGGTGATGGTGTAGTC	Fibronectin 1
α-SMA fwd α-SMA rev	CCATCATGCGTCTGGACTT GGCAGTAGTCACGAAGGAATAG	Alpha smooth muscle actin
TIMP-1 fwd TIMP-1 rev	CCCTTCGCATGGACATTTATTC AAGGTGGTCTCGTTGATTTCT	TIMP metallopeptidase inhibitor 1
mmu-miR-29b1	GCUGGUUUCAUAUGGUGGUUUA	Mus musculus miR-29b-1

4.2.10. Western Blot Analysis

Liver tissues (10 mg) were lysed in 1 mL RIPA buffer freshly supplemented with protease inhibitor cocktail using a tissue homogenizer keeping on ice. The lysates were then maintaining constant agitation for 2h keeping on the ice and then centrifuged for 20 min at 12000 rpm at 4°C. Supernatants were diluted with 4× Laemmli buffer, and samples were boiled for 5 min before gel loading. 30-50 µg proteins were separated on 7-15% SDS–polyacrylamide gel then transferred to PVDF membrane (Life Technologies) and blocked with Odyssey blocking

buffer (Li-Cor) for 1h at RT. Membranes were blotted with antibody against α-SMA (dilution 1:000; A-5228), antibody against GLI-1 (dilution 1:1000; SC-20687), antibody against collagen-1 (dilution 1:1000; nb600-408), antibody against total AKT (dilution 1:500; 9272S) antibody against p-AKT1/2/3 (dilution 1:1000; SC-101629), antibody against FN-1 (dilution 1:1000; SC-9068), and antibody against PGDFR-β (dilution 1: 1000; SC-432). The membranes were washed 3 × 5 min with washing buffer (TBS 1X + 0.05% Tween-20) and incubated with an infrared (IR) dye-conjugated secondary antibody (LI-COR) against the host IgGs. Subsequently, the blots were detected using Odyssey Clx imager (LI-COR). Membranes were probed with anti-β-actin (dilution 1:000; SC-1616) antibody for loading control.

4.2.11. Immunohistofluorescence (IHF)

For immunological detection of GLI-1, α-SMA, and p-AKT in the liver tissues, 5µm thick sections were first fixed with the pre-cooled acetone for 10 min rinsed 3-4 times in TBST (0.025% Triton X-100), and then blocked in 10% normal serum (host species of secondary antibody) with 1% BSA for 2h at RT. Next, slides were incubated with respective primary antibodies (dilution 1:200) against GLI-1, α-SMA, and p-AKT overnight at 4°C. After washing, slides were incubated with fluorescence dye conjugated secondary IgG against rabbit IgG (SC-2012) and goat IgG (ab-96932). Results were analyzed by fluorescence microscopy (Zeiss, Jena, Germany) and representative views of sections are shown. Fluorescent signal intensity was determined using Image-J software.

4.2.12. Statistical Analysis

Each in vitro experiment was performed in triplicate. In animal studies, data were typically obtained from 3-5 animals in each experimental group using duplicate or triplicate determinations for each animal. For the comparison of individual data points, student t-test was applied, and statistical significance set at $p < 0.05$.

4.3. RESULTS

4.3.1. In Silico miR-29b1 Target Prediction

29 family is predicted to target matrix-related genes (COL11A1, COL4A1, FN-1), HSC growth-related genes (PDGF-β, SMAD4), and ECM production related genes (MYC-N, SP-1) **(Figure 4.1)**.

4.3.2. miRNA PCR Array

miRNA expression profiling between sham-operated and CBDL livers revealed 38 differentially expressed miRNAs with greater than 2-fold change**,** wherein 24 miRNAs were

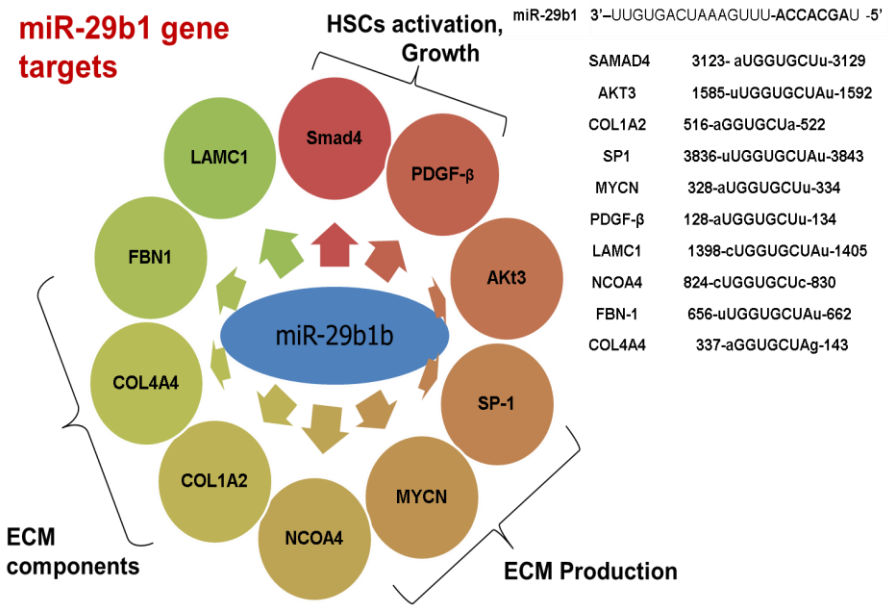

Figure 4-1. miR-29b1 target prediction. miRNA target gene prediction software revealed the downstream profibrotic targets of miR-29b1. Wherein, TargeScan predicts 828 conserved targets, with a total of 931 conserved sites and 196 poorly conserved sites, miRDB showed 426 targets and DIANA MicroT-CDS revealed 44 predicted targets (miTG score set at 0.9).

upregulated, and 14 miRNAs were downregulated **(Table 4.2)**. Based on previous reports, it was revealed that 7 of upregulated miRNAs were related to the progression of liver fibrosis (miR-199a, miR-200b, miR-497, miR-31a, miR-17, miR-222b and miR-27a) [118,275-279].

Among the downregulated miRNAs, 8 (miR-378, miR-29a/b/c, miR-19b, miR-335, miR-449, miR-132, miR-16, miR-126a, miR-495, and miR-196a) are reported in liver fibrosis [102,105,108,114,276,280,281]. In particular, the level of miR-29b-3p was found decreased significantly in mouse livers upon CBDL **(Figure 4.2)**. Therefore, the antifibrotic effect of miR-29b1 was investigated further using our formulations in CBDL mice.

Table 4.2. Differential miRNAs expressed in CBDL mice. More than 2 fold changed miRNAs are listed

Upregulated miRNAs	miR-338-5p, miR-146-5p, miR-122-5p, miR-874-3p, miR-205, miR-222-3p, miR-99a-5p, miR-34a-5p, miR-101a-3p, miR-142-3p, miR-27a-3p,miR-10a-5p, miR-223-3p miR-365-3p, miR-200b-3p, miR-31a-5p, miR-384-5p, miR-199a-5p, miR-192-5p, miR-19a-3p, miR-338-5p, miR-205-5p, miR-497-5p, miR-17-5p
Downregulated miRNAs	miR-145-5p, miR-93-5p, miR-19b-3p, miR-196a-5p, miR-495, miR-378a-3p, miR-132-3p, miR-29a-3p, miR-126a-3p, miR-16-5p, miR-335, miR-29c-3p, miR-449a-5p, miR-29b-3p

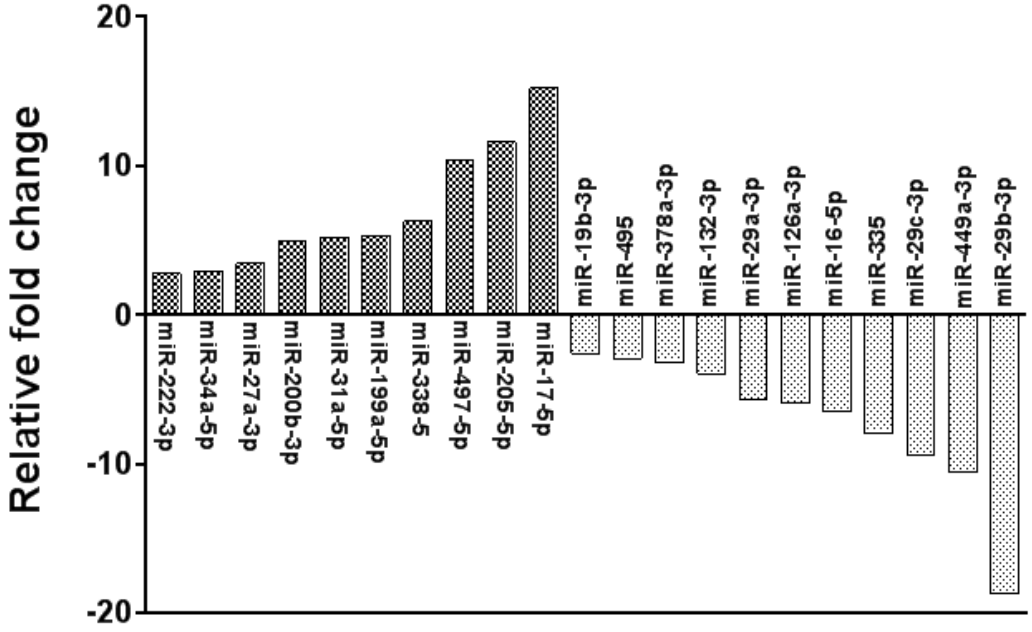

Figure 4-2. miRNA expression is changed in liver after CBDL induced liver fibrosis. 14 days after CBDL, mouse livers were harvested, RNA was isolated and miRNA array analysis was performed.

4.3.3. Micelle Formulation and Characterization

Micelles carrying GDC-0449 and miR-29b1 were well dispersed, spherical in shape and had the mean particle size of 80 ± 10 nm (with PDI 0.20) **(Figures 4.3 A and B)**. Zeta potential of these micelles was found to be in the range of negative 0.5 ± 5 mV compared to −15 ± 2 mV for a free miR-29b1 solution. These micelles carrying GDC-0449 and miR-29b1 maintained their size and narrow distribution in a physiological saline even after a week **(Figure 4.3C)**, suggesting that the micelles are stable for extended period of time.

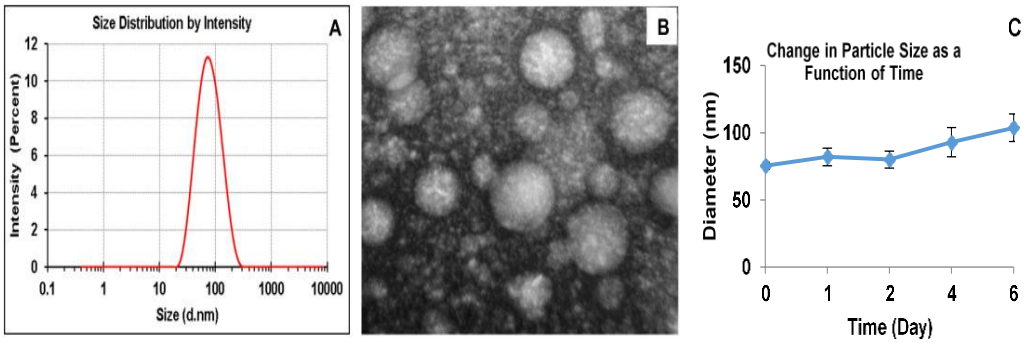

Figure 4-3. Characterization of micelles. (A) Particle size distribution of miR-29b1 complexed and GDC-0449 encapsulated micelles by dynamic light scattering (DLS). (B) Transmission Electron Microscope (TEM) image showing morphology of micelles. (C) mean particle size of micelles in PBS as a function of time.

The kinetic stability of FRET-micelles was determined in the presence of FBS over 36h. In the FRET experiment, an increase in the fluorescence intensity of DiO molecule and a decrease in fluorescence intensity of DiI molecule was observed over time **(Figure 4.4A)**, which suggested that FRET molecules were slowly released from the micelles when incubated with serum. The FRET ratio, I566/(I566 + I502), was calculated to determine the relative peak shift between I502 (the emission of DiO at 502 nm) and I566 (the emission of DiI at 566 nm). For micelles in serum, a decrease in the FRET ratio from 1 to 0.55 was observed over 36h **(Figure 4.4B)**. Micelle stability by SEC method over 24h also demonstrate that there was a minimal reduction of peak area at 17 min, suggesting micelles were not largely dissociated the following

incubation with FBS **(Figures 4.4C and D)**. Transfection efficiency of fluorescent Oligo (F-Oligo)/polymer complexes was determined at 32:1 N/P ratios in HSC-T6 cells. After 4h of incubation, cells were observed for the uptake of F-Oligo/cationic polymer complexes **(Figure 4.5A)**. Based on the N/P ratio of the complexes with Lipofectamine 2000 (22:1) and our cationic polymer (32:1), formulations showed similar cellular uptake. Transfection efficiency of micelles was determined my measuring fluorescence intensity of transfected cells by flow cytometry **(Figure 4.5B)**. Furthermore, our formulations have the advantage of being able to transfect cells in the presence of serum. In contrast, Lipofectamine needs serum free media, limiting its in vivo application. Moreover, these micelles carrying GDC-0449 and maintained their size and narrow distribution in a physiological saline even after a week **(Figure 4.3C)**,

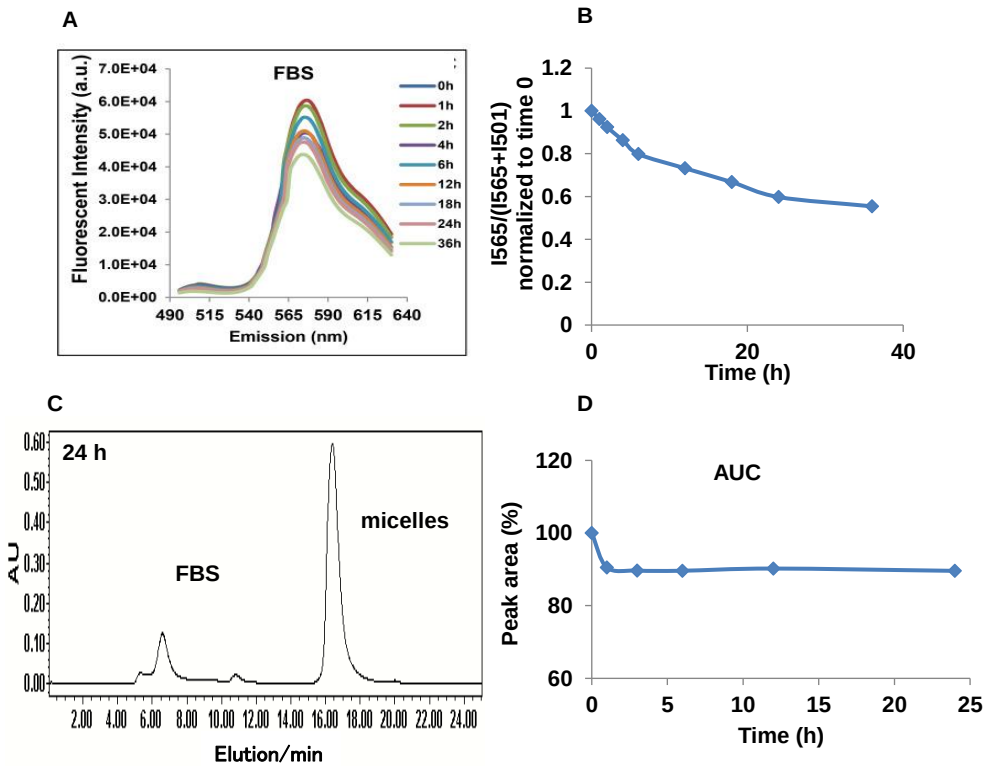

Figure 4-4. Stability of miR-29b1 and GDC-0449 containing micelles. (A) time-resolved spectra of FRET micelles in FBS (B) Time traces of the FRET ratio, I566/ (I5656+ I502), normalized to time 0, in FBS. (C) SEC traces of micelles incubated with 25 vol. % FBS. (D) Peak area of micelles as a function of incubation time.

suggesting that the micelles are stable enough for extended periods of time. In contrast, Lipofectamine 2000 lipoplexes need serum free media, limiting their in vivo application. These results demonstrate the capability of our micelles for carrying cargo in vivo. Cytotoxicity of micelles containing GDC-0449 at different concentrations and keeping miR-29b1 concentration constant (10pmol) was determined in HSC-T6 cells. We did not observe significant cell killing by micelles containing GDC-0449 alone, miR-29b1 alone or their combination as compared to the control **(Figure 4.6A)**.

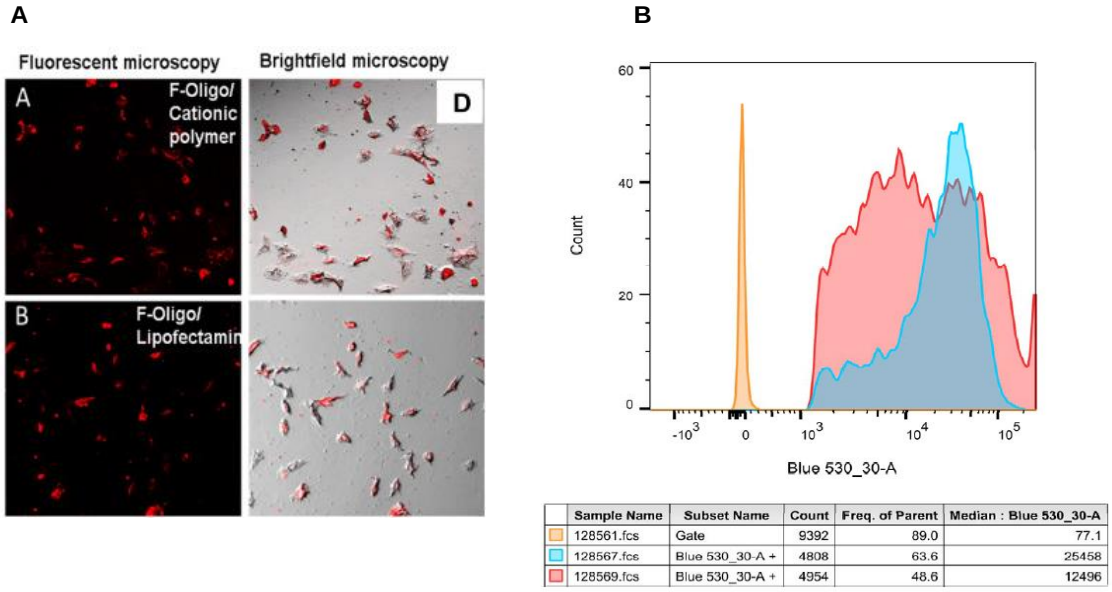

	Sample Name	Subset Name	Count	Freq. of Parent	Median : Blue 530_30-A
	128561.fcs	Gate	9392	89.0	77.1
	128567.fcs	Blue 530_30-A +	4808	63.6	25458
	128569.fcs	Blue 530_30-A +	4954	48.6	12496

Figure 4-5. Cellular uptake and transfection efficiency of the micelles. (A) Cellular uptake of fluorescent labeled Block-IT™ oligo loaded micelles into HSC-T6 cells. Left panel is oligo complexed micelles (upper panel) and oligo/Lipofectamine 2000 complexes (lower panel). Right panel is optical images of cells (DIC) (B) Flow cytometric analysis showing HSC-T6 cells transfected with Lipofectamine 2000 or micelles (Fluorescein-miR-29b1 (50 nmol/l) complexes in serum-free medium (blue curve, 63.6% positive) or complete medium (red curve 48.6% positive) for 6h and as compared with untreated cells (orange curve).

For determining the subcellular distribution of micelles containing GDC-0449 and miR-29b1, we perfused the liver at 30 min post administration and isolated different liver cells after in situ perfusion. A significant difference in the uptake of micelles by different liver cells was observed. GDC-0449 and miR-29b1 concentrations (µg/mg of cell protein) were in the following order:

Kupffer and endothelial cells ≥ HSCs ≥ hepatocytes **(Figures 4.6 B and C)**, whereas in liver fibrotic mice there were increased uptake by HSCs and hepatocytes but decreased uptake by Kupffer and endothelial cells. This observation is `similar to our previous publication for triplex forming oligonucleotides (TFOs) [271].

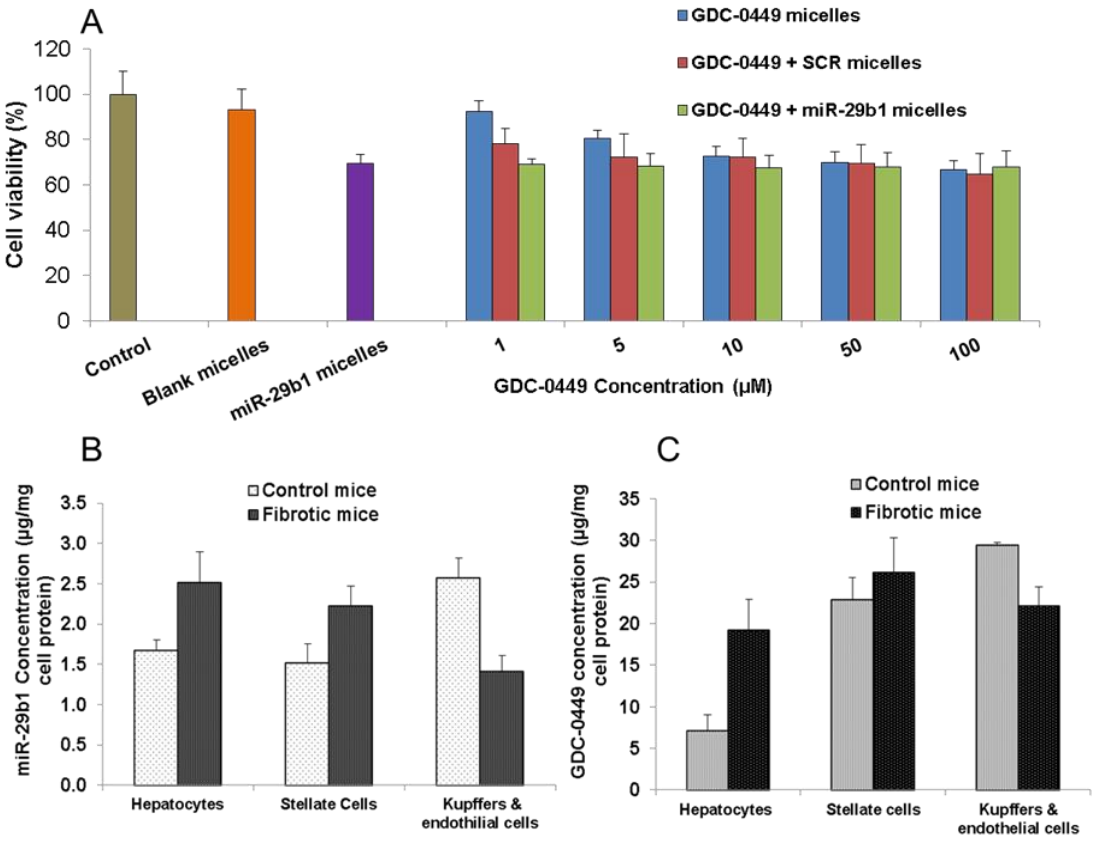

Figure 4-6. Cytotoxicity study and intrahepatic biodistribution of micelles in normal and common bile duct ligated (CBDL) mice after systemic administration. (A) % viability of HSC-T6 cells after treatment with GDC-0449 and miR-29b1 containing micelles. (B&C) amount of miR-29b1 and GDC-0449 found in each cell type. Data are presented as the mean (SD, combined cells types N = 3).

4.3.4. Liver Morphology

CBDL induced submaximal stimulation of hepatic fibrosis in all mice. We have tested our formulations in CBDL mice. At the time of sacrifice, livers of control animals showed normal

gross morphology while CBDL mouse livers were grossly enlarged and cholestatic with pitted and rough surface.

Treatment with GDC-0449 or miR-29b1 alone showed some improvement in liver condition, whereas combination treatment resulted in a smooth and shiny appearance as of the normal liver. Thus, combination treatment with GDC-0449 and miR-29b1 exerted a more potent anti-fibrotic effect than administration of either single agent **(Figure 4.7)**. Notably, the bile duct proliferation from the livers of the combination group was significantly less than those from the single agent therapy groups and untreated fibrotic group, suggesting low bile production in these animals [282].

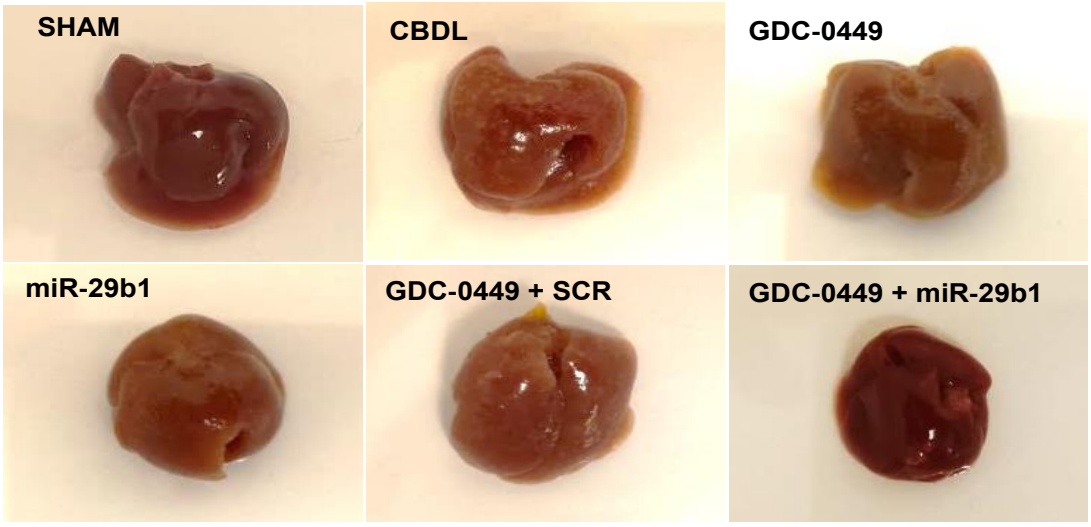

Figure 4-7. Liver morphology after common bile duct ligation (CBDL) and/or systemic delivery of micelles. Macroscopic images of mouse livers harvested after completion of treatment with micelles containing GDC-0449, miR-29b1, GDC-0449 + SCR or a combination of GDC-0449 + miR-29b1.

4.3.5. Liver Enzyme Level

We observed significantly higher serum levels of ALT (177±6.8 U/L), AST (779±60 U/L), and BIL (10±1.7 mg/dl) in CBDL mice compared to the sham controls. Systemic administration of micelles carrying miR-29b1 and GDC-0449 into CBDL mice led to significant decrease in ALT

(127±5.3, 108±10 U/L), AST (444±52, 348±25 U/L), and BIL (3±0.33, 5±1.96 mg/dl) levels. Among the various treatment groups, mice receiving the micelles carrying GDC-0449 and miR-29b1 had significantly lower levels of injury markers (ALT 38±12.1 U/L, AST 207±18.7 U/L and total BIL 2±0.51 mg/dl) than those receiving the GDC-0449 or miR-29b1 alone **(Figures 4.8)**.

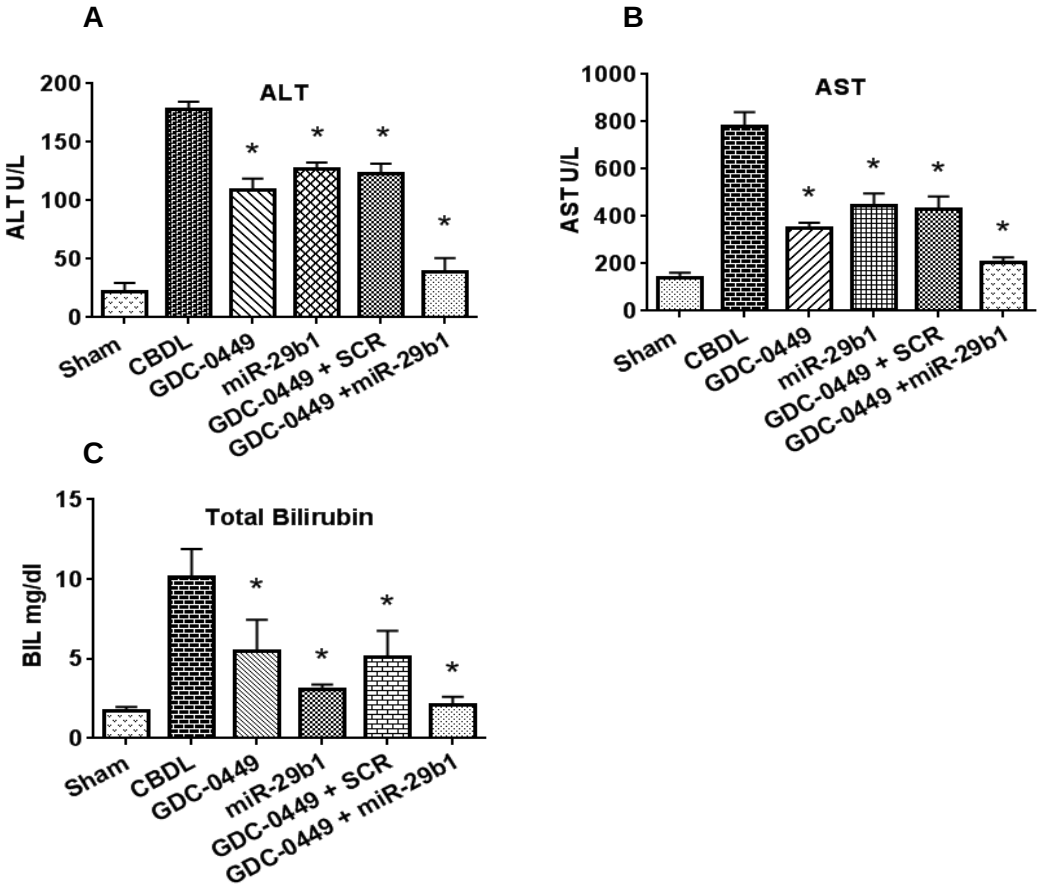

Figure 4-8. Effect of GDC-0449 and miR-29b1 loaded micelles on serum alanine transaminase (ALT), aspartate transaminase (AST), and total bilirubin (BIL) levels. Serum marker in common bile duct ligated (CBDL) mice after systemic administration of GDC-0449 and miR-29b1 loaded micelles were significantly lower than those in the CBDL mice. Results are presented as mean ± S.D. (*P < 0.05 versus CBDL, *n* = 4).

4.3.6. Histological Analysis

CBDL causes bile acid accumulation and exerts toxic effects on hepatocytes that result in the replacement of normal parenchyma with scary tissue and generates infarcts. Hematoxylin

and eosin (H & E) staining assessed bile infarcts in the liver and histological examination shows no fibrosis in the healthy liver, whereas confluent foci of infarcts around proliferating bile ducts were observed in CBDL animals. CBDL livers had edematous adjacent portal tracts with infiltrated neutrophils and disseminated liver cell necrosis representing hepatocellular injury. This difference was evident when liver sections were stained with H&E **(Figure 4.9A)**. The amount of collagen deposition in the liver sections was assessed by Masson's trichrome and Sirus red staining. Staining was significantly positive in CBDL mouse livers as compared to sham. Periportal fibrosis of the liver was reduced by treating with GDC-0449 and miR-29b1

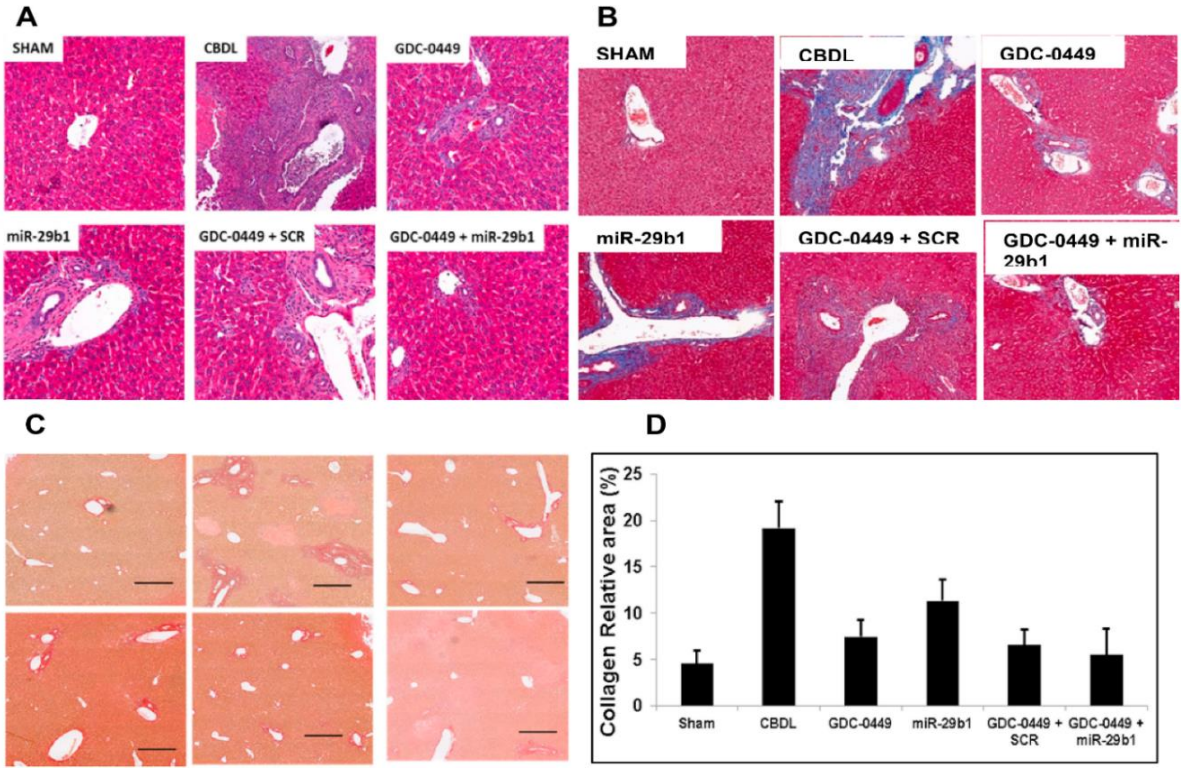

Figure 4-9. Hematoxylin & eosin (H & E), collagen specific Masson's Trichrome and Sirus red staining of liver sections of common bile duct ligated (CBDL) mice after systemic administration of micelles loaded with GDC-0449, miR-29b1 or their combination. (A) Treatment with micelles carrying GDC-0449 and miR-29b1 reduced histological liver injury, including bile infarcts. (B) Dark blue staining (C) Red staining shows increased collagen deposition in CBDL mice. (D) Systemic administration of GDC-0449 and miR-29b1 loaded micelles effectively reduced relative collagen level staining (original magnification, × 10, Scale bar 200 μM).

containing micelles and was seen a minimum in the livers treated with micelles carrying both GDC-0449 and miR-29b1 **(Figures 4.9 B, C and D)**.

4.3.7. Mature miR-29b1 Expression Levels

Compared to the sham control, there was a significant decrease in mature miR-29b1 expression in CBDL mice (42±10.8) while there was not much difference in miR-29b1 level in mice after treatment with micelles carrying GDC-0449 (89±9.3) or GDC-0449 and SCR (112.2±13.4). In contrast, there was a significant increase in the level of mature miR-29b1 (169± 6.4) when CBDL mice received micelles carrying miR-29b1 or GDC-0449 and miR-29b1 (165±11.5), respectively **(Figure 4.10)**. These results suggest that systemic administration of micelles carrying miR-29b1 either alone or with GDC-0449 could increase the levels of mature miR-29b1 in mice.

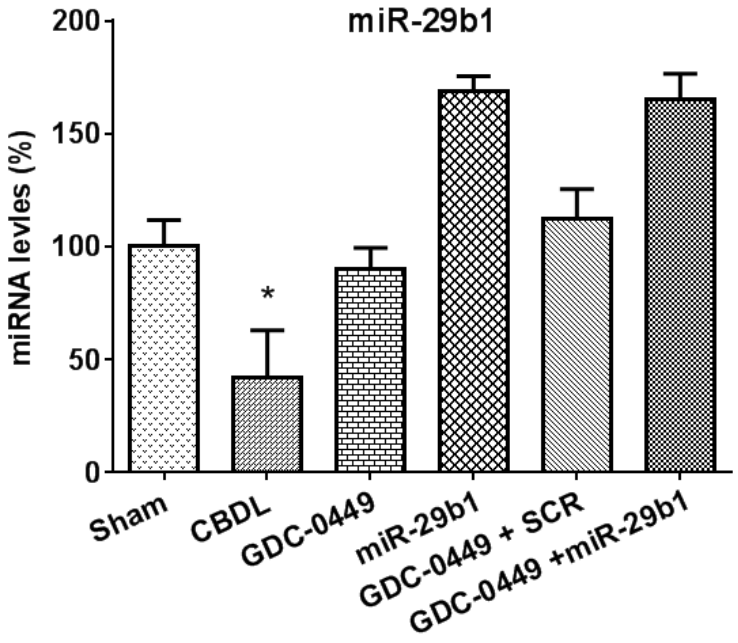

Figure 4-10. Expression level of mature miR-29b1. miR-29b1 was found down regulated in CBDL mice, and its level was restored upon treatment with micelles containing GDC-0449 and miR-29b1. (*P < 0.05 versus sham, n=3)

4.3.8. mRNA and Protein Expression Levels

To determine the influence of drug loaded micelles on the expression levels of profibrotic mediators such as Shh, GLI-1, and TIMP-1 as well as ECM components such as collagen and FN-1 and activation marker α-SMA in CBDL induced liver fibrosis were determined. Hepatic mRNA levels of these genes were verified by RT-PCR, which demonstrated that relative expression of Shh (1082±30.1), GLI-1 (645±51.6), Col1A1 (938±154.4) TIMP-1, (1664±209.8) α-SMA (446±19.14) and FN-1 (456±21.36) was greater in CBDL untreated mice compared to sham-operated mice **(Figure 4.11)**.

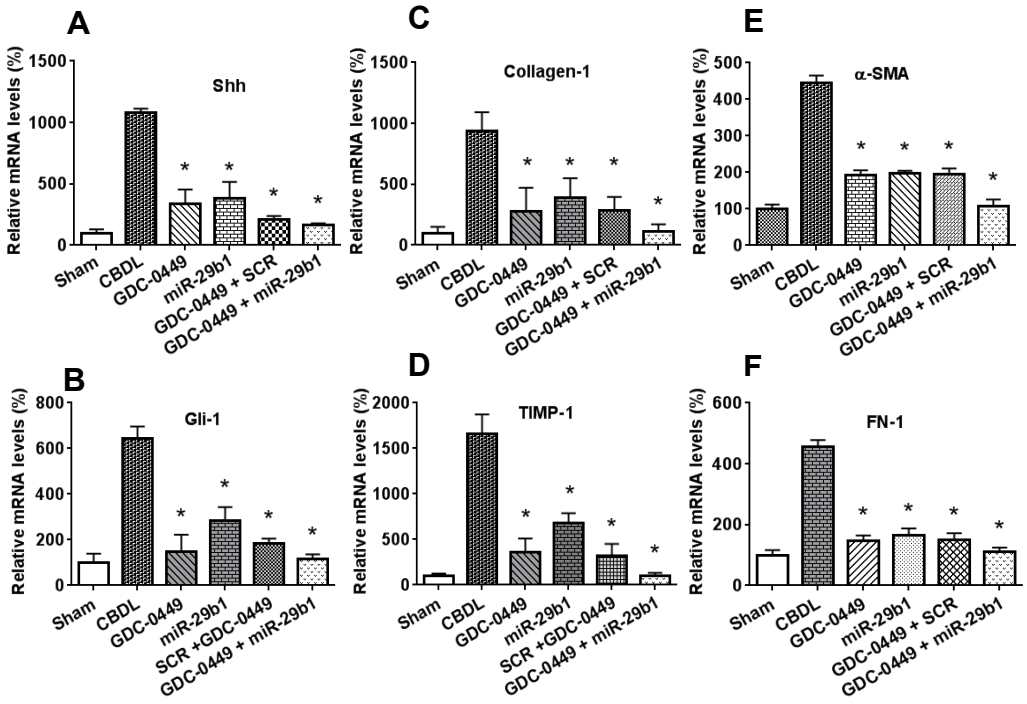

Figure 4-11. Real time RT-PCR and Western blot analysis of liver fibrosis markers. (**A-F**) mRNA levels. Systemic administration of micelles containing GDC-0449 and miR-29b1 into CBDL mice reduced mRNA expression of Shh, Gli-1, Collagen-1 TIMP-1, α-SMA and FN-1. (*P < 0.05 versus CBDL; data represented as mean of four animals).

Hepatic expression of all these mRNAs was lower in in mice treated with micelles carrying GDC-0449 (338±115.5, 148±74.4, 278±41.36, 361±150.1, 193±12.56, and 147±17.56), GDC-0449 + SCR (210±27.6, 182±23.8, 288±107.5, 323±128.6, 195±15.65, and 149±22.36), and miR-29b1 (384±130.9, 285±57.9, 386±98.2, 679±109.6, 196±8.35, and 165±22.23). By comparison, significant downregulation of all these genes was observed in CBDL mice treated with micelles carrying GDC-0449 and miR-29b1; Shh (163±16.4), GLI-1 (114±22.6), Col1A1 (110±60.3), TIMP-1(102±32.73), α-SMA (108±17.25), and FN-1 (111±13.25). Similarly, liver protein lysate from CBDL mice demonstrated an increase in GLI-1, α-SMA, Collagen-1, FN-1 PDGFR-β, and p-AKT levels compared to the sham operated mouse liver lysate as determined by Western blot analysis **(Figure 4.12)**.

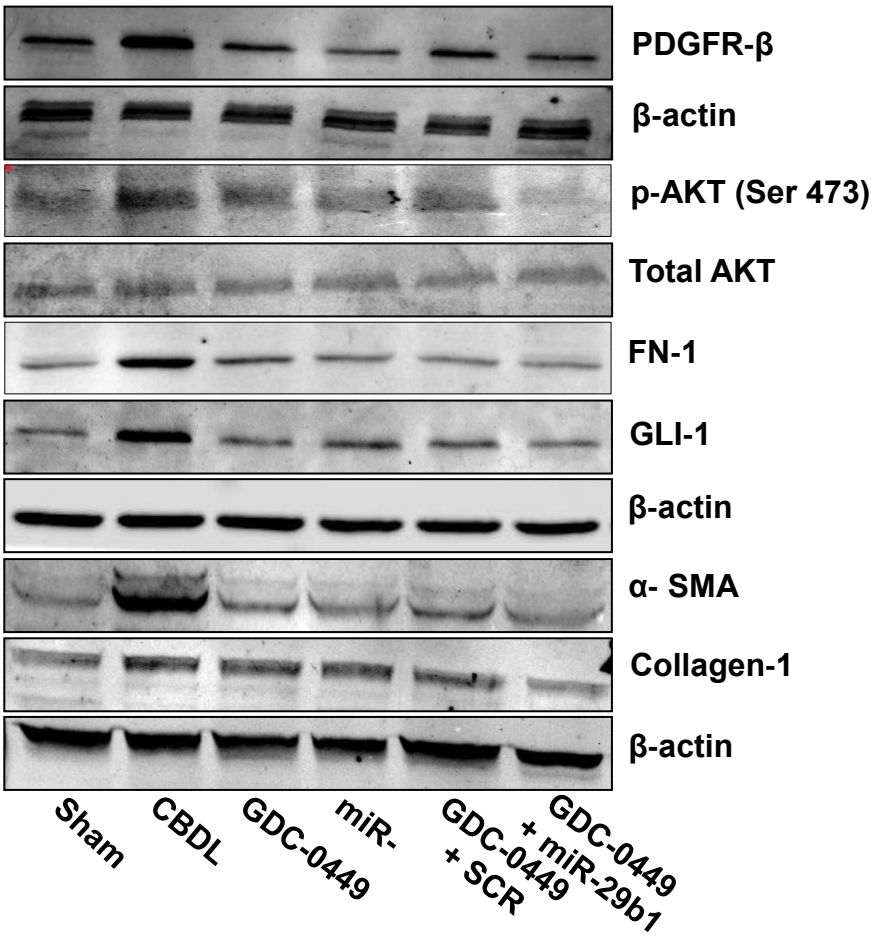

Figure. 4-12. Western blot analysis. Protein expression of PDGFR-β, p-AKT, FN-1, Gli-1, α-SMA, and collagen-1.

Liver lysates from the animals treated with drug-containing micelles showed a similar trend of decrease in GLI-1, α-SMA, Collagen-1, and FN-1 expression levels. miR- 29b1 reduces the phosphorylation of AKT and the effect of miR-29b1 containing micelles on protein expression of p-AKT [283]. As shown in Figure 4.12, protein expression of p-AKT was significantly high in the fibrotic liver tissues in CBDL mice. In contrast, CBDL mice supplemented with miR-29b1 showed significantly reduced expression of p-AKT without affecting the total AKT, indicating the improvement in histological severity of liver fibrosis.

4.3.9. Immunohistoflurescence

In response to liver injury, the activity of GLI-1, α-SMA, and p-AKT increased in the liver. Hence, immunofluorescence staining of GLI-1, α-SMA, and p-AKT showed an increase in CBDL mice **(Figure 4.13)**. Upon treatment with GDC-0449, and miR-29b1 containing micelles, a decrease in fluorescent intensity in the liver sections reflected their low expression levels.

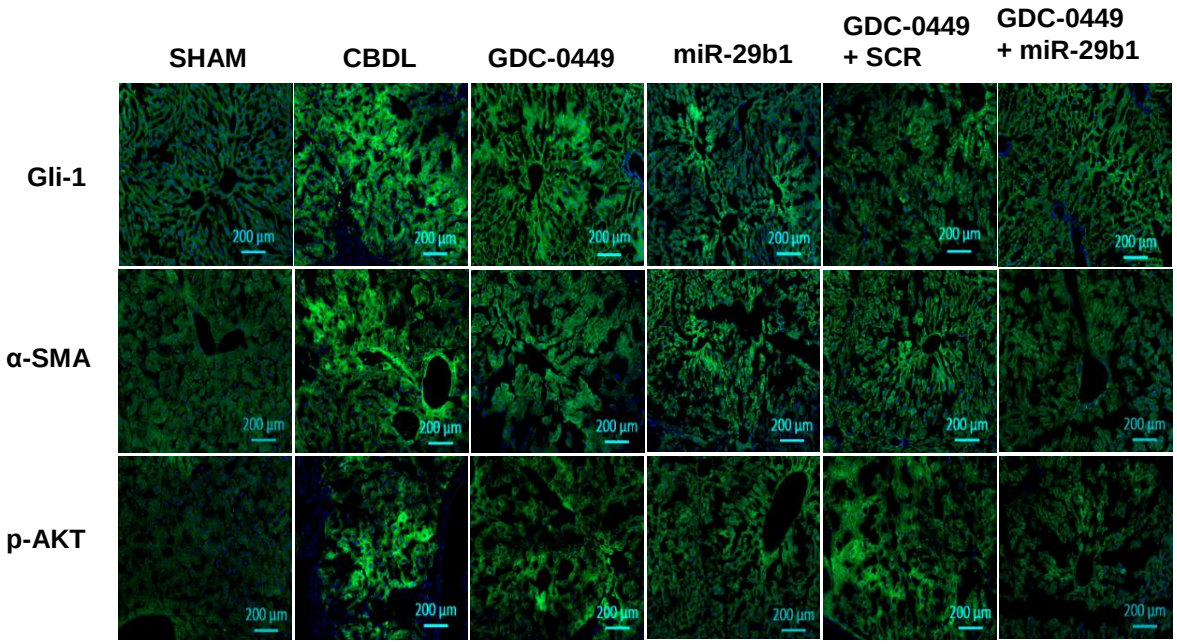

Figure 4-13. Immunohistofluorescence staining. CBDL results in increased GLI-1 a downstream mediator of Hh signaling, α-SMA a HSC activation marker and p-AKT a growth and ECM promoter expression. Staining was found highest in CDBL untreated mice whereas was reduced by treatment with GDC-0449 and miR-29b1 containing micelles.

4.4. DISCUSSION

Despite advancement in research on the molecular pathogenesis of liver fibrosis, monotherapy mostly results in a poor prognosis. In this setting, combination drug therapy has emerged as a potential treatment alternative for liver fibrosis. Previously, combination therapy of retinoic acid (TGF-β1 inhibitor) and ursodeoxycholic acid (immunomodulator), GDC-0449 (Hh inhibitor) and rosiglitazone (peroxisome proliferator-activated receptor agonist), imatinib mesylate (PDGF inhibitor) and perindopril (TGF-β1 inhibitor) and losartan (angiotensin II receptor inhibitor) and perindopril has been employed in preclinical studies to treat liver fibrosis [237,282,284,285]. However, treatment with conventional anti-fibrotic and anti-inflammatory drugs even in combination is not successful because of their poor efficacy or side effects. Our aim in this study was to evaluate the antifibrotic efficacy of micelles carrying GDC-0449 and miR-29b1 in a CBDL mouse model of obstructive cholestasis.

The Hh pathway plays a significant role in embryogenesis multiple species. However, its activity is usually reduced or absent in adult organisms [258]. Moreover, if in a healthy liver if any Hh ligand appears liver sinusoidal cells (e.g., endothelial cells and quiescent HSC) strongly express Hhip, and prevents its binding to Ptc receptors [286]. In CBDL cholestasis rodent model, a significant upregulation of Hh ligands is observed [39]. Hh pathway through its mediator transcription factor, GLI-1 promotes growth and viability of myofibroblasts, accumulation of which leads to abnormal liver repair and fibrosis [25]. Inhibition of Hh signaling with GDC-0449 substantially reduces the hepatic content of myofibroblasts and progenitors [287]. In good agreement with previous reports, in the current study, we have also found Hh components Shh and GLI-1 upregulated upon CBDL in mice.

miRNAs are known to repress target gene expression post-transcriptionally, and their role as a therapeutics is being accepted in a diverse array of diseases [288-290]. The use of miRNAs in liver fibrosis is advantageous in that a single miRNA can target multiple

genes/pathways involved in the progression of the disease, and due to their endogenous nature, they are safe to use. Recent studies have shown that miR-29b1 is downregulated in most of the liver fibrosis patients and animal models. miR-29b1 can target several genes involved in fibrosis including ECM production (collagen, fibronectin, elastin), HSC growth and proliferation/activation (PDGF-β, PI3/AKT) and immunomodulation through the intervening TGF-β1 (SMAD4) and NF-κB signaling [263,291]. Moreover, our web-based target prediction algorithm also confirmed that several of miR-29b1 targets are well known profibrotic genes **(Figure 4.1)**. We also analyzed the expression profile of miRNAs in CBDL mice and identified highly differential expression of miRNAs including miR-29b1 **(Table 4.2, Figure 4.2)**.

There is a cross-talk between TGF-β1 and Hh pathway as TGF-β1 activates transcription factor GLI via SMAD3 and increases Indian hedgehog (Ihh) production [292,293]. Therefore, it is of great interest to deliver GDC-0449 and miR-29b1 simultaneously for a complete shutdown of Hh signaling, resulting in the inhibition of liver fibrosis progression. However, in vivo use of both of these therapeutic agents is a challenge, because miRNA is highly unstable in biological fluids, and with high molecular weight and anionic charge do not cross cellular membrane, whereas GDC-0449 has low water solubility and bioavailability. Micellar encapsulation of miRNA is a viable approach to improve its half-life, tissue uptake and off-target issues [294]. Although several lipid-based carriers have been reported for siRNA/miRNA delivery, they are not suitable for co-delivery of miRNA with small hydrophobic molecules. Moreover, simultaneous encapsulation can ensure similar pharmacokinetic profiles needed for dual inhibition effect. We have successfully encapsulated both of these therapeutic agents simultaneously in the micelle formulated using our mPEG-b-PCC-g-DC-g-TEPA copolymer. Previously, we had used the similar approach for delivering GDC-0449 and miR-let7b simultaneously in ectopic tumor model of pancreatic cancer. After intratumoral injection, we observed a significant reduction in tumor growth [179].

Here, we extended our previous work and evaluated our system for co-delivery of miRNA and small molecule systemically. Micelles were prepared with mPEG-b-PCC-g-DC-g-TEPA copolymer by film hydration. TEM image showed micelles are of spherical shape and well-dispersed particles with the mean diameter of 60±10nm **(Figure 4.3B)**. The Smaller size of micelles can be advantageous for penetration into fibrotic liver tissue as reported earlier [295,296]. Cellular uptake study indicated that micelles can transfect miRNA efficiently in HSC-T6 cells even in the presence of serum, which indicates the in vivo applicability of these micelles over many of the commercially available transfection reagents **(Figure 4.5)**. For pharmaceutical use, the stability of the formulations is one of the critical parameters, and we investigated the storage stability of miR-29b1 and GDC-0449 containing micelles. We found that the micelles formulations were stable for least a week at work bench storage **(Figure 4.3C)**. We did not observe any significant cell killing with micelle formulations, which indicate that Hh inhibition does not produce cytotoxicity in HSCs and also confirms micelles itself are nontoxic and safe to use in vivo **(Figure 4.6A)**. Previous reports indicate higher uptake of TFOs by different liver cells, with higher concentration in HSCs and other liver cells. In this study, there was also similar intrahepatic biodistribution of GDC-0449 and miR-29b1 in different liver cells [271]. Moreover, the similar distribution profile of GDC-0449 and miR-29b1 confirms that the micelles are stable in vivo **(Figure 4.6BC).**

We evaluated antifibrotic properties of these micelles in CBDL mice. Repeated systemic administration of micelles containing miR-29b1 and GDC-0449 did not impact the normal behavior of animals nor did it produce any histological evidence of toxicity at any of dose tested. The ability to deliver multiple anti-fibrotic agents and favorable safety profiles suggest that the micelles might be effective as a targeted therapy for liver fibrosis [294]. As shown in Figure 4.8, untreated CBDL mice demonstrated consistently higher serum ALT, AST and BIL levels, in keeping with other evidence that CBDL provokes chronic hepatocyte injury [297]. Gross

morphology of the normal livers exhibited ordinary reddish color and smooth surface, whereas CBDL livers showed, abnormal color, and an uneven, pitted surface with evident mixed-sized fibrotic nodules **(Figure 4.7)**. Histology also confirmed that the sham control animals had an intact lobular architecture with no inflammation or deposited collagen around the portal areas, whereas CBDL mice exhibited signs of liver damage, a high number of infarcts with signs of neutrophil infiltration and ductal proliferation **(Figure 4.9A)**. In CBDL untreated mice, collagen accumulation was evident in hepatic lobules mostly around the bile ducts, resulting from increased fibrosis **(Figure 4.9B)**. miR-29b1 and GDC-0449 both are anti-fibrotic agents and inhibitors of collagen deposition in vitro and in vivo [298-300]. Therefore, the antifibrotic effect of micelle treatment in mice was evident, as liver tissues from mice receiving GDC-0449 and miR-29b1 containing micelles represented a significantly decreased number of infarcts, reduced inflammation, which is accompanied by depletion of collagen in the liver. Additionally, it is noteworthy that our combination therapy showed the complete reversal of fibrotic signs and bile duct proliferation.

After systemic administration of micelles containing miR-29b1, we observed a significant increase in mature miR-29b1 level in the liver samples, which indicate that these micelles are capable of delivering miRNA in vivo **(Figure 4.10)**. Transcript of collagen-1 and TIMP-1 were significantly higher in CBDL mice and were correlated with the progression of liver fibrosis. The upregulation of TIMP-1 in activated HSCs inhibits the activity of interstitial collagenases such as matrix metalloproteases (MMPs), which additionally favors the accumulation of ECM [301]. Reduced TIMP-1 mRNA levels after micelle treatment is an indicator of the resolution of liver fibrosis and increased matrix degradation. However, reduction in the TIMP-1 transcript was low with miR-29b1 alone treatment, which is in agreement with previous reports [263] α-SMA protein is expressed by activated HSCs and is an early marker of hepatic fibrogenesis. α-SMA reflects their myofibroblast-like phenotypes and is in direct correlation to experimental liver fibrogenesis

[217]. We observed high mRNA and protein expression level of α-SMA in untreated CBDL mice when compared to the sham mice. Herein, a combination of miR-29b1 and GDC-0449 treatment reduced the mRNA of TIMP-1, α-SMA, and FN-1 as well as proteins levels of α-SMA, and FN-1 to a significantly low level indicating the resolution of liver fibrosis. Collagen-1 and FN-1 are ECM components, and their decreased expression after micelle treatment is in agreement with previous reports [302,303]. Previously, we have shown that GDC-0449 loaded micelle treatment decreased Hh component in an in vivo model, and we observed similar trend after systemic delivery of micelles containing GDC-0449 **(Figures 4.11, 12 and 13)**. Consistently, the current study showed that combination therapy decreased expression of profibrotic mRNAs and proteins in CBDL mice.

Previous studies demonstrate that there is a putative GLI binding site at 424 (50 GCCCGCCCA) in the human miR-29b1 promoter sequence. GLI transcription factor binds directly to this site in the miR-29b1 promoter region and decreases its activity in H69 non-malignant cholangiocytes [304]. We observed expression level of mature miR-29b1 in mice liver samples is in good correlation with the degree of liver fibrosis, as determined by immunohistochemistry. Therefore, after treatment CBDL mice showed increased levels of mature miR-29b1 not only in miRNA-treated but also in GDC-0449-449 treated mice. The possible reason could be by inhibiting Hh signaling with GDC-0449 reduced accumulation of myofibroblasts and decreased expression of GLI-1 and its miR-29b1 suppression effect. This is in agreement with the other reports suggesting miR-29b1 is in negative correlation with TGF-β1 expression, and Hh inhibitors are a well-known suppressor of TGF-β1 [305,306].

During the recovery phase of liver fibrosis, one of the potential fates of activated HSCs is apoptosis [307]. PI3K/Akt signaling pathway regulates HSC activation, proliferation and also reduces their apoptosis by inactivating downstream of apoptogenic factors [261,308]. In this study, we found increased AKT phosphorylation in untreated CBDL mouse livers. Moreover,

our search of databases and recent reports suggest that miR-29b1 can target PDGF ligands and receptor family [309]. PDGFR upregulation in liver fibrosis is known to trigger HSC proliferation and activation onto myofibroblasts. Overexpression of miR-29b1 by systemic administration of miR-29b1 containing micelles resulted in decreased p-AKT and PDGFR-β levels **(Figure 4.12)** and explained the antifibrotic mechanism of miR-29b1 through negatively regulating PI3K/AKT and PDGFR signaling pathway. This work provides evidence that our micelle carrier system is efficient in delivering physicochemically diverse miRNA and small hydrophobic molecules in the cholestatic induced fibrotic liver.

4.5. CONCLUSIONS

In conclusion, the present study demonstrates that our cationic polymer based micelles can be a new strategy for co-delivery of small hydrophobic molecules and miRNA. The presence of cationic chains protects miRNA from enzymatic degradation without showing any signs of toxicity, which was a major concern in previously reported RNAi delivery vehicles. Co-delivery ensured similar biodistribution profiles of both the therapeutics and improved the outcome of anti-fibrotic therapy. Blocking the Hh and AKT pathway simultaneously along with decreasing the ECM component like collagen and FN-1 reduced the fibrosis severity. Thus, the combination of GDC-0449 and miR29b1 can be a promising strategy to treat liver fibrosis. Further, these nanomedicines are stable, scalable and hence bear high translational potential.

CHAPTER 5. SUMMERY AND FUTURE DIRECTIONS

5.1. SUMMARY

Liver fibrosis is excessive scarring process resulting from chronic insults of heterogeneous etiology. Together with primary liver cancer, it represents the end-stage liver pathology with high mortality. The major hallmark of liver fibrosis is deposition of fibrous ECM with the main culprit being the HSCs. Various growth factors and inflammatory cytokines are known to be involved in the induction and progression of this disease. Hh and PPAR-γ are major signaling pathways involved in the pathogenesis of liver fibrosis. We synthesized biodegradable mPEG-b-p(CB-co-LA) copolymer (30,000 Da) and formulated nanoparticles encapsulating Hh inhibitor, GDC-0449 and PPAR-γ agonist, RSG for treating liver fibrosis. Nanoparticles were prepared using emulsification/solvent evaporation. Nanoparticles were monodispersed with a mean particle size of 120–130 nm. Drug loading was 5% and 2% w/w for GDC-0449 and RSG, respectively. Nanoparticles carrying both GDC-0449 and RSG were formulated at half of their individual drug loading. Anti-liver fibrotic efficacy of drug loaded nanoparticles was evaluated after tail vein injection into CBDL fibrotic rats. Drug-loaded nanoparticles protected liver injury in CBDL rats by suppressing the activation of HSCs and decreasing inflammatory cytokines. Combination drug containing nanoparticles have the potential to treat liver fibrosis by intervening complex fibrotic cascade.

Successful treatment of PDAC remains a challenge due to its poor diagnosis, metastasis, and resistance to chemotherapy. Recent advances in cancer biology have revealed that several miRNAs take part in processes associated with pancreatic cancer initiation and progression including cell cycle, DNA repair, apoptosis, invasivity, and metastasis. While Hh levels are increased in pancreatic cancer cells, the level of tumor suppressor miR-let7b is downregulated. We inhibited Hh pathway with GDC-0449 and restored miR-let7b level by its synthetic mimic simultaneously for treating PDAC synergistically. miR-let7b and GDC-0449

were co-formulated into micelles using mPEG-b-PCC-g-DC-g-TEPA. This copolymer self-assembled into micelles of <100 nm and encapsulated hydrophobic GDC-0449 into its core with 5% w/w drug loading and allowed complex formation between miR-let7b and its cationic pendant chains. miR-let7b and GDC-0449 inhibited the proliferation of human pancreatic cancer cells, synergistically. miRNA in the micelle formulation was stable for up to 36h in the presence of serum, and high uptake efficiency was achieved with low cytotoxicity. This combination therapy effectively inhibited tumor growth when injected into athymic nude mice bearing ectopic tumor generated using MIA PaCa-2 cells compared to micelles carrying GDC-0449 or miR-let7b alone.

Decreased expression of miR-29b1 is observed in liver fibrosis. Our in-silico analysis indicated that miR-29b1 targets several profibrotic genes like collagen type I & IV, c-MYC, PDGF-β, and PI3K/AKT. From previous studies, we found that GDC-0449 has great potential for treating liver fibrosis. We co-formulated miR-29b1 and GDC-0449 into micelles using mPEG-b-PCC-g-DC-g-TEPA copolymer and injected systemically into CBDL mice. High concentrations of GDC-0449 and miR-29b1 were delivered to liver cells as determined by in situ liver perfusion at 30 min post systemic administration of their micelle formulation. There was a significant decrease in collagen deposition in the liver and serum injury markers, leading to improvement in liver morphology. Combination therapy was more effective in providing hepatoprotection, lowering liver injury related serum enzyme levels, reducing fibrotic protein markers such as collagen, α-SMA, FN-1, and p-AKT compared to monotherapy.

5.2. FUTURE DIRECTIONS

The findings presented in this thesis demonstrated that micelles prepared with cationic amphiphilic polymers can simultaneously upload hydrophobic drug(s) in their hydrophobic cores and form complex with RNA molecules. Systemic administration of these micelles significantly increased the circulation time of miRNA and small drug molecule, leading to their enhanced

accumulation to the target organ (tumor in case of pancreatic cancer and liver in case of liver fibrotic mice). Since our copolymers consist of ester bonds and polycarbonate as a backbone, these polymers will degrade into carbon oxide and aliphatic alcohols.

To further increase the drug loading and prolong their release, we will synthesize polymer with different lipids and different cationic chains including spermine and N, N-dimethyldipropylenetriamine to optimize formulation characteristics such as complexation, stability, release, and endosomal escape of miRNA. We will also evaluate whether changes in these parameters affect downstream target genes of miR-29b1.

Successful treatment of liver fibrosis and pancreatic cancer requires site-specific drug delivery to target cells. In the case of liver fibrosis conjugate mannose -6-phosphate (M6P), vitamin A, and C1-3 short chain fragment variable (ScFv) to our amphiphilic polymer to maximize delivery to HSCs of liver fibrotic mice. Similarly, in the case of pancreatic cancer, micelles will be decorated with anti-EGFR ScFv antibody. Since miRNA is known to be unstable in vivo, we will test the effect of backbone modifications of serum and thermodynamic stability of these miRNAs (miR-29b1, miR-let7b). We will also check if backbone modifications also affect the efficacy of miRNAs in vivo. Since high cationic component needed for a high dose of miRNA can have toxic effects, we will evaluate various cationic components for minimum toxic effects. We would like to determine pharmacokinetic, and biodistribution of targeted vs. non targeted micellar formulations both in pancreatic cancer and liver fibrosis.

BIBLIOGRAPHY

1. M. K. Connolly, A. S. Bedrosian, J. Mallen-St Clair, A. P. Mitchell, J. Ibrahim, A. Stroud, et al **In liver fibrosis, dendritic cells govern hepatic inflammation in mice via TNF-alpha** J Clin Invest, 119 (2009), pp. 3213-3225.

2. L. Giannitrapani, M. Soresi, M. L. Bondi, G. Montalto, M. Cervello **Nanotechnology applications for the therapy of liver fibrosis** World J Gastroenterol, 20 (2014), pp. 7242-7251.

3. K. Cheng, R. I. Mahato **Gene modulation for treating liver fibrosis** Crit Rev Ther Drug Carrier Syst, 24 (2007), pp. 93-146.

4. G. Szabo, S. Bala **MicroRNAs in liver disease** Nat Rev Gastroenterol Hepatol, 10 (2013), pp. 542-552.

5. V. Sanchez-Valle, N. C. Chavez-Tapia, M. Uribe, N. Mendez-Sanchez **Role of oxidative stress and molecular changes in liver fibrosis: a review** Curr Med Chem, 19 (2012), pp. 4850-4860.

6. S. Hemmann, J. Graf, M. Roderfeld, E. Roeb **Expression of MMPs and TIMPs in liver fibrosis - a systematic review with special emphasis on anti-fibrotic strategies** J Hepatol, 46 (2007), pp. 955-975.

7. U. E. Lee, S. L. Friedman **Mechanisms of hepatic fibrogenesis** Best Pract Res Clin Gastroenterol, 25 (2011), pp. 195-206.

8. J. Wiegand, T. Berg **The etiology, diagnosis and prevention of liver cirrhosis: part 1 of a series on liver cirrhosis** Dtsch Arztebl Int, 110 (2013), pp. 85-91.

9. R. G. Wells **Cellular sources of extracellular matrix in hepatic fibrosis** Clin Liver Dis, 12 (2008), pp. 759-68, viii.

10. J. X. Jiang, K. Mikami, S. Venugopal, Y. Li, N. J. Torok **Apoptotic body engulfment by hepatic stellate cells promotes their survival by the JAK/STAT and Akt/NF-kappaB-dependent pathways** J Hepatol, 51 (2009), pp. 139-148.

11. R. G. Wells **The role of matrix stiffness in hepatic stellate cell activation and liver fibrosis** J Clin Gastroenterol, 39 (2005), pp. S158-61.

12. A. Omenetti, A. Porrello, Y. Jung, L. Yang, Y. Popov, S. S. Choi, et al **Hedgehog signaling regulates epithelial-mesenchymal transition during biliary fibrosis in rodents and humans** J Clin Invest, 118 (2008), pp. 3331-3342.

13. Y. Jung, R. P. Witek, W. K. Syn, S. S. Choi, A. Omenetti, R. Premont, et al **Signals from dying hepatocytes trigger growth of liver progenitors** Gut, 59 (2010), pp. 655-665.

14. M. M. Richardson, J. R. Jonsson, E. E. Powell, E. M. Brunt, B. A. Neuschwander-Tetri, P. S. Bhathal, et al **Progressive fibrosis in nonalcoholic steatohepatitis: association with altered regeneration and a ductular reaction** Gastroenterology, 133 (2007), pp. 80-90.

15. T. A. Wynn, L. Barron **Macrophages: master regulators of inflammation and fibrosis** Semin Liver Dis, 30 (2010), pp. 245-257.

16. F. Meng, K. Wang, T. Aoyama, S. I. Grivennikov, Y. Paik, D. Scholten, et al **Interleukin-17 signaling in inflammatory, Kupffer cells, and hepatic stellate cells exacerbates liver fibrosis in mice** Gastroenterology, 143 (2012), pp. 765-76.e1-3.

17. D. P. Higgins, S. Hemsley, P. J. Canfield **Association of uterine and salpingeal fibrosis with chlamydial hsp60 and hsp10 antigen-specific antibodies in Chlamydia-infected koalas** Clin Diagn Lab Immunol, 12 (2005), pp. 632-639.

18. Y. Popov, D. Y. Sverdlov, K. R. Bhaskar, A. K. Sharma, G. Millonig, E. Patsenker, et al **Macrophage-mediated phagocytosis of apoptotic cholangiocytes contributes to reversal of experimental biliary fibrosis** Am J Physiol Gastrointest Liver Physiol, 298 (2010), pp. G323-34.

19. C. Aloman, F. Tacke **Dendritic cells in liver fibrosis: conductor of the inflammatory orchestra?**Hepatology, 51 (2010), pp. 1070-1072.

20. D. Kershenobich Stalnikowitz, A. B. Weissbrod **Liver fibrosis and inflammation. A review** Ann Hepatol, 2 (2003), pp. 159-163.

21. N. N. Kabil, H. A. Seddiek, N. A. Yassin, M. M. Gamal-Eldin **Effect of ghrelin on chronic liver injury and fibrogenesis in male rats: possible role of nitric oxide** Peptides, 52 (2014), pp. 90-97.

22. Y. Kojima, S. Suzuki, Y. Tsuchiya, H. Konno, S. Baba, S. Nakamura **Regulation of pro-inflammatory and anti-inflammatory cytokine responses by Kupffer cells in endotoxin-enhanced reperfusion injury after total hepatic ischemia** Transpl Int, 16 (2003), pp. 231-240.

23. A. Canbay, A. E. Feldstein, H. Higuchi, N. Werneburg, A. Grambihler, S. F. Bronk, et al **Kupffer cell engulfment of apoptotic bodies stimulates death ligand and cytokine expression** Hepatology, 38 (2003), pp. 1188-1198.

24. Y. Chen, S. S. Choi, G. A. Michelotti, I. S. Chan, M. Swiderska-Syn, G. F. Karaca, et al **Hedgehog controls hepatic stellate cell fate by regulating metabolism** Gastroenterology, 143 (2012), pp. 1319-29.e1-11.

25. S. S. Choi, A. Omenetti, R. P. Witek, C. A. Moylan, W. K. Syn, Y. Jung, et al **Hedgehog pathway activation and epithelial-to-mesenchymal transitions during myofibroblastic transformation of rat hepatic cells in culture and cirrhosis** Am J Physiol Gastrointest Liver Physiol, 297 (2009), pp. G1093-106.

26. A. Leask, D. J. Abraham **TGF-beta signaling and the fibrotic response** FASEB J, 18 (2004), pp. 816-827.

27. N. Yang, R. I. Mahato **GFAP promoter-driven RNA interference on TGF-beta1 to treat liver fibrosis** Pharm Res, 28 (2011), pp. 752-761.

28. X. L. Zhang, N. Topley, T. Ito, A. Phillips **Interleukin-6 regulation of transforming growth factor (TGF)-beta receptor compartmentalization and turnover enhances TGF-beta1 signaling** J Biol Chem, 280 (2005), pp. 12239-12245.

29. H. Yoshiji, S. Kuriyama, J. Yoshii, Y. Ikenaka, R. Noguchi, D. J. Hicklin, et al **Vascular endothelial growth factor and receptor interaction is a prerequisite for murine hepatic fibrogenesis** Gut, 52 (2003), pp. 1347-1354.

30. K. Sakata, S. Eda, E. S. Lee, M. Hara, M. Imoto, S. Kojima **Neovessel formation promotes liver fibrosis via providing latent transforming growth factor-beta** Biochem Biophys Res Commun, 443 (2014), pp. 950-956.

31. M. Pinzani **PDGF and signal transduction in hepatic stellate cells** Front Biosci, 7 (2002), pp. d1720-6.

32. F. Zhang, C. Ni, D. Kong, X. Zhang, X. Zhu, L. Chen, et al **Ligustrazine attenuates oxidative stress-induced activation of hepatic stellate cells by interrupting platelet-derived growth factor-beta receptor-mediated ERK and p38 pathways** Toxicol Appl Pharmacol, 265 (2012), pp. 51-60.

33. G. Son, I. N. Hines, J. Lindquist, L. W. Schrum, R. A. Rippe **Inhibition of phosphatidylinositol 3-kinase signaling in hepatic stellate cells blocks the progression of hepatic fibrosis** Hepatology, 50 (2009), pp. 1512-1523.

34. F. Zhang, Y. Z. Zhuge, Y. J. Li, J. X. Gu **S-adenosylmethionine inhibits the activated phenotype of human hepatic stellate cells via Rac1 and matrix metalloproteinases** Int Immunopharmacol, 19 (2014), pp. 193-200.

35. F. R. Murphy, R. Issa, X. Zhou, S. Ratnarajah, H. Nagase, M. J. Arthur, et al **Inhibition of apoptosis of activated hepatic stellate cells by tissue inhibitor of metalloproteinase-1 is mediated via effects on matrix metalloproteinase inhibition: implications for reversibility of liver fibrosis** J Biol Chem, 277 (2002), pp. 11069-11076.

36. C. Uchida, T. L. Haas **Endothelial cell TIMP-1 is upregulated by shear stress via Sp-1 and the TGFbeta1 signaling pathways** Biochem Cell Biol, 92 (2014), pp. 77-83.

37. L. A. O'Neill, C. Kaltschmidt **NF-kappa B: a crucial transcription factor for glial and neuronal cell function** Trends Neurosci, 20 (1997), pp. 252-258.

38. B. Sun, M. Karin **NF-kappaB signaling, liver disease and hepatoprotective agents** Oncogene, 27 (2008), pp. 6228-6244.

39. A. Pratap, R. Panakanti, N. Yang, R. Lakshmi, K. A. Modanlou, J. D. Eason, et al **Cyclopamine attenuates acute warm ischemia reperfusion injury in cholestatic rat liver: hope for marginal livers** Mol Pharm, 8 (2011), pp. 958-968.

40. N. Nikolaidis, J. Kountouras, O. Giouleme, V. Tzarou, O. Chatzizisi, K. Patsiaoura, et al **Colchicine treatment of liver fibrosis** Hepatogastroenterology, 53 (2006), pp. 281-285.

41. Y. Finkelstein, S. E. Aks, J. R. Hutson, D. N. Juurlink, P. Nguyen, G. Dubnov-Raz, et al **Colchicine poisoning: the dark side of an ancient drug** Clin Toxicol (Phila), 48 (2010), pp. 407-414.

42. J. H. Tsai, J. Y. Liu, T. T. Wu, P. C. Ho, C. Y. Huang, J. C. Shyu, et al **Effects of silymarin on the resolution of liver fibrosis induced by carbon tetrachloride in rats** J Viral Hepat, 15 (2008), pp. 508-514.

43. C. C. Li, C. Y. Hsiang, S. L. Wu, T. Y. Ho **Identification of novel mechanisms of silymarin on the carbon tetrachloride-induced liver fibrosis in mice by nuclear factor-kappaB bioluminescent imaging-guided transcriptomic analysis** Food Chem Toxicol, 50 (2012), pp. 1568-1575.

44. W. H. Hsu, B. H. Lee, Y. W. Hsu, T. M. Pan **Peroxisome proliferator-activated receptor-gamma activators monascin and rosiglitazone attenuate carboxymethyllysine-induced fibrosis in hepatic stellate cells through regulating the oxidative stress pathway but independent of the receptor for advanced glycation end products signaling** J Agric Food Chem, 61 (2013), pp. 6873-6879.

45. L. Gobejishvili, S. Barve, K. Breitkopf-Heinlein, Y. Li, J. Zhang, D. V. Avila, et al **Rolipram attenuates bile duct ligation-induced liver injury in rats: a potential pathogenic role of PDE4** J Pharmacol Exp Ther, 347 (2013), pp. 80-90.

46. I. O. Sherif, M. M. Al-Gayyar **Antioxidant, anti-inflammatory and hepatoprotective effects of silymarin on hepatic dysfunction induced by sodium nitrite** Eur Cytokine Netw, 24 (2013), pp. 114-121.

47. L. Garcia, I. Hernandez, A. Sandoval, A. Salazar, J. Garcia, J. Vera, et al **Pirfenidone effectively reverses experimental liver fibrosis** J Hepatol, 37 (2002), pp. 797-805.

48. W. Yang, H. Chen, Y. Jiang **Inhibitive effect of curcumin and amiloride on the fibrosis of rat hepatic stellate cells induced by oxidative stress** Zhong Yao Cai, 26 (2003), pp. 795-798.

49. A. Benedetti, A. Di Sario, A. Casini, F. Ridolfi, E. Bendia, P. Pigini, et al **Inhibition of the NA(+)/H(+) exchanger reduces rat hepatic stellate cell activity and liver fibrosis: an in vitro and in vivo study** Gastroenterology, 120 (2001), pp. 545-556.

50. W. L. Kuo, M. C. Yu, J. F. Lee, C. N. Tsai, T. C. Chen, M. F. Chen **Imatinib mesylate improves liver regeneration and attenuates liver fibrogenesis in CCL4-treated mice** J Gastrointest Surg, 16 (2012), pp. 361-369.

51. Y. Kim, M. I. Fiel, E. Albanis, H. I. Chou, W. Zhang, G. Khitrov, et al **Anti-fibrotic activity and enhanced interleukin-6 production by hepatic stellate cells in response to imatinib mesylate** Liver Int, 32 (2012), pp. 1008-1017.

52. K. D. Lindor, E. R. Dickson, W. P. Baldus, R. A. Jorgensen, J. Ludwig, P. A. Murtaugh, et al **Ursodeoxycholic acid in the treatment of primary biliary cirrhosis** Gastroenterology, 106 (1994), pp. 1284-1290.

53. R. E. Poupon, P. M. Huet, R. Poupon, A. M. Bonnand, J. T. Nhieu, E. S. Zafrani **A randomized trial comparing colchicine and ursodeoxycholic acid combination to ursodeoxycholic acid in primary biliary cirrhosis. UDCA-PBC Study Group** Hepatology, 24 (1996), pp. 1098-1103.

54. C. Corpechot, P. Benlian, V. Barbu, O. Chazouilleres, R. E. Poupon, R. Poupon **Apolipoprotein E polymorphism, a marker of disease severity in primary biliary cirrhosis?**J Hepatol, 35 (2001), pp. 324-328.

55. S. Reif, B. Weis, H. Aeed, M. Gana-Weis, L. Zaidel, Y. Avni, et al **The Ras antagonist, farnesylthiosalicylic acid (FTS), inhibits experimentally-induced liver cirrhosis in rats** J Hepatol, 31 (1999), pp. 1053-1061.

56. P. Aguilar-Melero, A. Luque, M. M. Machuca, M. P. Perez de Obanos, R. Navarrete, I. C. Rodriguez-Garcia, et al **Cardiotrophin-1 reduces ischemia/reperfusion injury during liver transplant** J Surg Res, 181 (2013), pp. e83-91.

57. C. J. Parsons, B. U. Bradford, C. Q. Pan, E. Cheung, M. Schauer, A. Knorr, et al **Antifibrotic effects of a tissue inhibitor of metalloproteinase-1 antibody on established liver fibrosis in rats** Hepatology, 40 (2004), pp. 1106-1115.

58. H. Ling, E. Roux, D. Hempel, J. Tao, M. Smith, S. Lonning, et al **Transforming growth factor beta neutralization ameliorates pre-existing hepatic fibrosis and reduces cholangiocarcinoma in thioacetamide-treated rats** PLoS One, 8 (2013), pp. e54499.

59. S. Ogawa, T. Ochi, H. Shimada, K. Inagaki, I. Fujita, A. Nii, et al **Anti-PDGF-B monoclonal antibody reduces liver fibrosis development** Hepatol Res, 40 (2010), pp. 1128-1141.

60. I. J. Ezquerro, J. J. Lasarte, J. Dotor, I. Castilla-Cortazar, M. Bustos, I. Penuelas, et al **A synthetic peptide from transforming growth factor beta type III receptor inhibits liver fibrogenesis in rats with carbon tetrachloride liver injury** Cytokine, 22 (2003), pp. 12-20.

61. R. G. Bennett, D. G. Heimann, S. Singh, R. L. Simpson, D. J. Tuma **Relaxin decreases the severity of established hepatic fibrosis in mice** Liver Int, (2013), .

62. J. K. Sicklick, Y. X. Li, S. S. Choi, Y. Qi, W. Chen, M. Bustamante, et al **Role for hedgehog signaling in hepatic stellate cell activation and viability** Lab Invest, 85 (2005), pp. 1368-1380.

63. S. Takashimizu, S. Kojima, Y. Nishizaki, T. Kagawa, K. Shiraishi, T. Mine, et al **Effect of endothelin A receptor antagonist on hepatic hemodynamics in cirrhotic rats. Implications for endothelin-1 in portal hypertension** Tokai J Exp Clin Med, 36 (2011), pp. 37-43.

64. A. Y. Hui, A. J. Dannenberg, J. J. Sung, K. Subbaramaiah, B. Du, P. Olinga, et al **Prostaglandin E2 inhibits transforming growth factor beta 1-mediated induction of collagen alpha 1(I) in hepatic stellate cells** J Hepatol, 41 (2004), pp. 251-258.

65. T. Van Bergen, D. Marshall, S. Van de Veire, E. Vandewalle, L. Moons, J. Herman, et al **The role of LOX and LOXL2 in scar formation after glaucoma surgery** Invest Ophthalmol Vis Sci, 54 (2013), pp. 5788-5796.

66. A. M. Gewirtz, D. L. Sokol, M. Z. Ratajczak **Nucleic acid therapeutics: state of the art and future prospects** Blood, 92 (1998), pp. 712-736.

67. G. Zon **Antisense phosphorothioate oligodeoxynucleotides: introductory concepts and possible molecular mechanisms of toxicity** Toxicol Lett, 82-83 (1995), pp. 419-424.

68. K. D. Raney **Chemical modifications of DNA for study of helicase mechanisms** Bioorg Med Chem, (2014), .

69. M. D. Frank-Kamenetskii, S. M. Mirkin **Triplex DNA structures** Annu Rev Biochem, 64 (1995), pp. 65-95.

70. R. Panakanti, A. Pratap, N. Yang, J. S. Jackson, R. I. Mahato **Triplex forming oligonucleotides against type alpha1(I) collagen attenuates liver fibrosis induced by bile duct ligation** Biochem Pharmacol, 80 (2010), pp. 1718-1726.

71. N. Yang, Z. Ye, F. Li, R. I. Mahato **HPMA polymer-based site-specific delivery of oligonucleotides to hepatic stellate cells** Bioconjug Chem, 20 (2009), pp. 213-221.

72. S. A. Angaji, S. S. Hedayati, R. H. Poor, S. Madani, S. S. Poor, S. Panahi **Application of RNA interference in treating human diseases** J Genet, 89 (2010), pp. 527-537.

73. B. Czech, G. J. Hannon **Small RNA sorting: matchmaking for Argonautes** Nat Rev Genet, 12 (2011), pp. 19-31.

74. T. Kawamata, Y. Tomari **Making RISC** Trends Biochem Sci, 35 (2010), pp. 368-376.

75. M. S. Shim, Y. J. Kwon **Efficient and targeted delivery of siRNA in vivo** FEBS J, 277 (2010), pp. 4814-4827.

76. L. Zhu, R. I. Mahato **Targeted delivery of siRNA to hepatocytes and hepatic stellate cells by bioconjugation** Bioconjug Chem, 21 (2010), pp. 2119-2127.

77. D. D. Rao, J. S. Vorhies, N. Senzer, J. Nemunaitis **siRNA vs. shRNA: similarities and differences** Adv Drug Deliv Rev, 61 (2009), pp. 746-759.

78. K. Cheng, N. Yang, R. I. Mahato **TGF-beta1 gene silencing for treating liver fibrosis** Mol Pharm, 6 (2009), pp. 772-779.

79. S. L. Chen, M. H. Zheng, K. Q. Shi, T. Yang, Y. P. Chen **A new strategy for treatment of liver fibrosis: letting MicroRNAs do the job** BioDrugs, 27 (2013), pp. 25-34.

80. D. Didiano, O. Hobert **Perfect seed pairing is not a generally reliable predictor for miRNA-target interactions** Nat Struct Mol Biol, 13 (2006), pp. 849-851.

81. A. Q. Gomes, S. Nolasco, H. Soares **Non-coding RNAs: multi-tasking molecules in the cell** Int J Mol Sci, 14 (2013), pp. 16010-16039.

82. L. He, G. J. Hannon **MicroRNAs: small RNAs with a big role in gene regulation** Nat Rev Genet, 5 (2004), pp. 522-531.

83. M. A. Valencia-Sanchez, J. Liu, G. J. Hannon, R. Parker **Control of translation and mRNA degradation by miRNAs and siRNAs** Genes Dev, 20 (2006), pp. 515-524.

84. S. Gu, L. Jin, F. Zhang, Y. Huang, D. Grimm, J. J. Rossi, et al **Thermodynamic stability of small hairpin RNAs highly influences the loading process of different mammalian Argonautes** Proc Natl Acad Sci U S A, 108 (2011), pp. 9208-9213.

85. J. Elmen, H. Thonberg, K. Ljungberg, M. Frieden, M. Westergaard, Y. Xu, et al **Locked nucleic acid (LNA) mediated improvements in siRNA stability and functionality** Nucleic Acids Res, 33 (2005), pp. 439-447.

86. H. Kume, K. Hino, J. Galipon, K. Ui-Tei **A-to-I editing in the miRNA seed region regulates target mRNA selection and silencing efficiency** Nucleic Acids Res, (2014), .

87. A. Khvorova, A. Reynolds, S. D. Jayasena **Functional siRNAs and miRNAs exhibit strand bias** Cell, 115 (2003), pp. 209-216.

88. N. Hibio, K. Hino, E. Shimizu, Y. Nagata, K. Ui-Tei **Stability of miRNA 5'terminal and seed regions is correlated with experimentally observed miRNA-mediated silencing efficacy** Sci Rep, 2 (2012), pp. 996.

89. T. Kawamata, H. Seitz, Y. Tomari **Structural determinants of miRNAs for RISC loading and slicer-independent unwinding** Nat Struct Mol Biol, 16 (2009), pp. 953-960.

90. F. Frank, N. Sonenberg, B. Nagar **Structural basis for 5'-nucleotide base-specific recognition of guide RNA by human AGO2** Nature, 465 (2010), pp. 818-822.

91. H. Hamzeiy, J. Allmer, M. Yousef **Computational methods for microRNA target prediction** Methods Mol Biol, 1107 (2014), pp. 207-221.

92. Y. Watanabe, M. Tomita, A. Kanai **Computational methods for microRNA target prediction** Methods Enzymol, 427 (2007), pp. 65-86.

93. S. Yoon, G. De Micheli **Computational identification of microRNAs and their targets** Birth Defects Res C Embryo Today, 78 (2006), pp. 118-128.

94. J. Brennecke, A. Stark, R. B. Russell, S. M. Cohen **Principles of microRNA-target recognition** PLoS Biol, 3 (2005), pp. e85.

95. A. J. Enright, B. John, U. Gaul, T. Tuschl, C. Sander, D. S. Marks **MicroRNA targets in Drosophila** Genome Biol, 5 (2003), pp. R1.

96. B. P. Lewis, I. H. Shih, M. W. Jones-Rhoades, D. P. Bartel, C. B. Burge **Prediction of mammalian microRNA targets** Cell, 115 (2003), pp. 787-798.

97. H. Min, S. Yoon **Got target? Computational methods for microRNA target prediction and their extension** Exp Mol Med, 42 (2010), pp. 233-244.

98. D. Grun, Y. L. Wang, D. Langenberger, K. C. Gunsalus, N. Rajewsky **microRNA target predictions across seven Drosophila species and comparison to mammalian targets** PLoS Comput Biol, 1 (2005), pp. e13.

99. J. Zheng, Z. Lin, P. Dong, Z. Lu, S. Gao, X. Chen, et al **Activation of hepatic stellate cells is suppressed by microRNA-150** Int J Mol Med, 32 (2013), pp. 17-24.

100. Y. Sekiya, T. Ogawa, K. Yoshizato, K. Ikeda, N. Kawada **Suppression of hepatic stellate cell activation by microRNA-29b** Biochem Biophys Res Commun, 412 (2011), pp. 74-79.

101. Y. Sekiya, T. Ogawa, K. Yoshizato, K. Ikeda, N. Kawada **Suppression of hepatic stellate cell activation by microRNA-29b** Biochem Biophys Res Commun, 412 (2011), pp. 74-79.

102. J. Mann, D. C. Chu, A. Maxwell, F. Oakley, N. L. Zhu, H. Tsukamoto, et al **MeCP2 controls an epigenetic pathway that promotes myofibroblast transdifferentiation and fibrosis** Gastroenterology, 138 (2010), pp. 705-14, 714.e1-4.

103. N. J. Sarma, V. Tiriveedhi, V. Subramanian, S. Shenoy, J. S. Crippin, W. C. Chapman, et al **Hepatitis C virus mediated changes in miRNA-449a modulates inflammatory biomarker YKL40 through components of the NOTCH signaling pathway** PLoS One, 7 (2012), pp. e50826.

104. J. Li, M. Ghazwani, Y. Zhang, J. Lu, J. Li, J. Fan, et al **miR-122 regulates collagen production via targeting hepatic stellate cells and suppressing P4HA1 expression** J Hepatol, 58 (2013), pp. 522-528.

105. C. Chen, C. Q. Wu, Z. Q. Zhang, D. K. Yao, L. Zhu **Loss of expression of miR-335 is implicated in hepatic stellate cell migration and activation** Exp Cell Res, 317 (2011), pp. 1714-1725.

106. C. J. Guo, Q. Pan, D. G. Li, H. Sun, B. W. Liu **miR-15b and miR-16 are implicated in activation of the rat hepatic stellate cell: An essential role for apoptosis** J Hepatol, 50 (2009), pp. 766-778.

107. X. H. Gong, C. Chen, P. Hou, S. C. Zhu, C. Q. Wu, C. L. Song, et al **Overexpression of miR-126 Inhibits the Activation and Migration of HSCs through Targeting CRK** Cell Physiol Biochem, 33 (2014), pp. 97-106.

108. A. M. Lakner, N. M. Steuerwald, T. L. Walling, S. Ghosh, T. Li, I. H. McKillop, et al **Inhibitory effects of microRNA 19b in hepatic stellate cell-mediated fibrogenesis** Hepatology, 56 (2012), pp. 300-310.

109. X. Tu, H. Zhang, J. Zhang, S. Zhao, X. Zheng, Z. Zhang, et al **MicroRNA-101 suppresses liver fibrosis by targeting the TGFbeta signalling pathway** J Pathol, (2014), .

110. N. J. Sarma, V. Tiriveedhi, J. S. Crippin, W. C. Chapman, T. Mohanakumar **Hepatitis C virus-induced changes in microRNA 107 (miRNA-107) and miRNA-449a modulate CCL2 by targeting the interleukin-6 receptor complex in hepatitis** J Virol, 88 (2014), pp. 3733-3743.

111. J. J. Yang, H. Tao, W. Hu, L. P. Liu, K. H. Shi, Z. Y. Deng, et al **MicroRNA-200a controls Nrf2 activation by target Keap1 in hepatic stellate cell proliferation and fibrosis** Cell Signal, (2014), .

112. L. Chen, A. Charrier, Y. Zhou, R. Chen, B. Yu, K. Agarwal, et al **Epigenetic regulation of connective tissue growth factor by MicroRNA-214 delivery in exosomes from mouse or human hepatic stellate cells** Hepatology, 59 (2014), pp. 1118-1129.

113. F. Li, N. Ma, R. Zhao, G. Wu, Y. Zhang, Y. Qiao, et al **Overexpression of miR-483-5p/3p cooperate to inhibit mouse liver fibrosis by suppressing the TGF-beta stimulated HSCs in transgenic mice** J Cell Mol Med, 18 (2014), pp. 966-974.

114. Y. Sekiya, T. Ogawa, M. Iizuka, K. Yoshizato, K. Ikeda, N. Kawada **Down-regulation of cyclin E1 expression by microRNA-195 accounts for interferon-beta-induced inhibition of hepatic stellate cell proliferation** J Cell Physiol, 226 (2011), pp. 2535-2542.

115. Z. J. Li, P. H. Ou-Yang, X. P. Han **Profibrotic effect of miR-33a with Akt activation in hepatic stellate cells** Cell Signal, 26 (2014), pp. 141-148.

116. S. Ramachandran, H. Ilias Basha, N. J. Sarma, Y. Lin, J. S. Crippin, W. C. Chapman, et al **Hepatitis C virus induced miR200c down modulates FAP-1, a negative regulator of Src signaling and promotes hepatic fibrosis** PLoS One, 8 (2013), pp. e70744.

117. W. Q. Li, C. Chen, M. D. Xu, J. Guo, Y. M. Li, Q. M. Xia, et al **The rno-miR-34 family is upregulated and targets ACSL1 in dimethylnitrosamine-induced hepatic fibrosis in rats** FEBS J, 278 (2011), pp. 1522-1532.

118. J. Ji, J. Zhang, G. Huang, J. Qian, X. Wang, S. Mei **Over-expressed microRNA-27a and 27b influence fat accumulation and cell proliferation during rat hepatic stellate cell activation** FEBS Lett, 583 (2009), pp. 759-766.

119. J. Wei, L. Feng, Z. Li, G. Xu, X. Fan **MicroRNA-21 activates hepatic stellate cells via PTEN/Akt signaling** Biomed Pharmacother, 67 (2013), pp. 387-392.

120. W. J. Shen, R. Dong, G. Chen, S. Zheng **microRNA-222 modulates liver fibrosis in a murine model of biliary atresia** Biochem Biophys Res Commun, 446 (2014), pp. 155-159.

121. T. Ogawa, M. Enomoto, H. Fujii, Y. Sekiya, K. Yoshizato, K. Ikeda, et al **MicroRNA-221/222 upregulation indicates the activation of stellate cells and the progression of liver fibrosis** Gut, 61 (2012), pp. 1600-1609.

122. W. Tan, Y. Li, S. G. Lim, T. M. Tan **miR-106b-25/miR-17-92 clusters: polycistrons with oncogenic roles in hepatocellular carcinoma** World J Gastroenterol, 20 (2014), pp. 5962-5972.

123. B. Wang, W. Li, K. Guo, Y. Xiao, Y. Wang, J. Fan **miR-181b promotes hepatic stellate cells proliferation by targeting p27 and is elevated in the serum of cirrhosis patients** Biochem Biophys Res Commun, 421 (2012), pp. 4-8.

124. H. M. El Tayebi, K. A. Hosny, G. Esmat, K. Breuhahn, A. I. Abdelaziz **miR-615-5p is restrictedly expressed in cirrhotic and cancerous liver tissues and its overexpression alleviates the tumorigenic effects in hepatocellular carcinoma** FEBS Lett, 586 (2012), pp. 3309-3316.

125. J. Mann, D. A. Mann **Transcriptional regulation of hepatic stellate cells** Adv Drug Deliv Rev, 61 (2009), pp. 497-512.

126. F. Ebrahimi, V. Gopalan, R. A. Smith, A. K. Lam **miR-126 in human cancers: clinical roles and current perspectives** Exp Mol Pathol, 96 (2014), pp. 98-107.

127. Y. He, C. Huang, X. Sun, X. R. Long, X. W. Lv, J. Li **MicroRNA-146a modulates TGF-beta1-induced hepatic stellate cell proliferation by targeting SMAD4** Cell Signal, 24 (2012), pp. 1923-1930.

128. A. W. Rachfal, D. R. Brigstock **Connective tissue growth factor (CTGF/CCN2) in hepatic fibrosis** Hepatol Res, 26 (2003), pp. 1-9.

129. T. Ogawa, N. Kawada, K. Ikeda **Effect of natural interferon alpha on proliferation and apoptosis of hepatic stellate cells** Hepatol Int, 3 (2009), pp. 497-503.

130. R. T. Marquez, S. Bandyopadhyay, E. B. Wendlandt, K. Keck, B. A. Hoffer, M. S. Icardi, et al **Correlation between microRNA expression levels and clinical parameters associated with chronic hepatitis C viral infection in humans** Lab Invest, 90 (2010), pp. 1727-1736.

131. K. A. Lennox, M. A. Behlke **Chemical modification and design of anti-miRNA oligonucleotides** Gene Ther, 18 (2011), pp. 1111-1120.

132. H. Inoue, Y. Hayase, A. Imura, S. Iwai, K. Miura, E. Ohtsuka **Synthesis and hybridization studies on two complementary nona(2'-O-methyl)ribonucleotides** Nucleic Acids Res, 15 (1987), pp. 6131-6148.

133. J. Stenvang, A. Petri, M. Lindow, S. Obad, S. Kauppinen **Inhibition of microRNA function by antimiR oligonucleotides** Silence, 3 (2012), pp. 1-907X-3-1.

134. K. A. Lennox, J. L. Sabel, M. J. Johnson, B. G. Moreira, C. A. Fletcher, S. D. Rose, et al **Characterization of modified antisense oligonucleotides in Xenopus laevis embryos** Oligonucleotides, 16 (2006), pp. 26-42.

135. J. Krutzfeldt, N. Rajewsky, R. Braich, K. G. Rajeev, T. Tuschl, M. Manoharan, et al **Silencing of microRNAs in vivo with 'antagomirs'** Nature, 438 (2005), pp. 685-689.

136. M. Takahashi, N. Yamada, H. Hatakeyama, M. Murata, Y. Sato, N. Minakawa, et al **In vitro optimization of 2'-OMe-4'-thioribonucleoside-modified anti-microRNA oligonucleotides and its targeting delivery to mouse liver using a liposomal nanoparticle** Nucleic Acids Res, 41 (2013), pp. 10659-10667.

137. G. Meister, M. Landthaler, Y. Dorsett, T. Tuschl **Sequence-specific inhibition of microRNA- and siRNA-induced RNA silencing** RNA, 10 (2004), pp. 544-550.

138. J. Elmen, M. Lindow, S. Schutz, M. Lawrence, A. Petri, S. Obad, et al **LNA-mediated microRNA silencing in non-human primates** Nature, 452 (2008), pp. 896-899.

139. W. P. Kloosterman, A. K. Lagendijk, R. F. Ketting, J. D. Moulton, R. H. Plasterk **Targeted inhibition of miRNA maturation with morpholinos reveals a role for miR-375 in pancreatic islet development** PLoS Biol, 5 (2007), pp. e203.

140. Y. Shu, F. Pi, A. Sharma, M. Rajabi, F. Haque, D. Shu, et al **Stable RNA nanoparticles as potential new generation drugs for cancer therapy** Adv Drug Deliv Rev, 66 (2014), pp. 74-89.

141. A. T. Qureshi, W. T. Monroe, V. Dasa, J. M. Gimble, D. J. Hayes **miR-148b-nanoparticle conjugates for light mediated osteogenesis of human adipose stromal/stem cells** Biomaterials, 34 (2013), pp. 7799-7810.

142. S. H. Hsu, B. Yu, X. Wang, Y. Lu, C. R. Schmidt, R. J. Lee, et al **Cationic lipid nanoparticles for therapeutic delivery of siRNA and miRNA to murine liver tumor** Nanomedicine, 9 (2013), pp. 1169-1180.

143. P. de Antonellis, L. Liguori, A. Falanga, M. Carotenuto, V. Ferrucci, I. Andolfo, et al **MicroRNA 199b-5p delivery through stable nucleic acid lipid particles (SNALPs) in tumorigenic cell lines** Naunyn Schmiedebergs Arch Pharmacol, 386 (2013), pp. 287-302.

144. D. Pramanik, N. R. Campbell, C. Karikari, R. Chivukula, O. A. Kent, J. T. Mendell, et al **Restitution of tumor suppressor microRNAs using a systemic nanovector inhibits pancreatic cancer growth in mice** Mol Cancer Ther, 10 (2011), pp. 1470-1480.

145. R. S. Gomes, R. P. das Neves, L. Cochlin, A. Lima, R. Carvalho, P. Korpisalo, et al **Efficient pro-survival/angiogenic miRNA delivery by an MRI-detectable nanomaterial** ACS Nano, 7 (2013), pp. 3362-3372.

146. Y. Endo-Takahashi, Y. Negishi, A. Nakamura, S. Ukai, K. Ooaku, Y. Oda, et al **Systemic delivery of miR-126 by miRNA-loaded Bubble liposomes for the treatment of hindlimb ischemia** Sci Rep, 4 (2014), pp. 3883.

147. A. F. Ibrahim, U. Weirauch, M. Thomas, A. Grunweller, R. K. Hartmann, A. Aigner **MicroRNA replacement therapy for miR-145 and miR-33a is efficacious in a model of colon carcinoma** Cancer Res, 71 (2011), pp. 5214-5224.

148. Y. Pan, Y. Zhang, T. Jia, K. Zhang, J. Li, L. Wang **Development of a microRNA delivery system based on bacteriophage MS2 virus-like particles** FEBS J, 279 (2012), pp. 1198-1208.

149. Y. Chen, X. Zhu, X. Zhang, B. Liu, L. Huang **Nanoparticles modified with tumor-targeting scFv deliver siRNA and miRNA for cancer therapy** Mol Ther, 18 (2010), pp. 1650-1656.

150. X. Q. Liu, W. J. Song, T. M. Sun, P. Z. Zhang, J. Wang **Targeted delivery of antisense inhibitor of miRNA for antiangiogenesis therapy using cRGD-functionalized nanoparticles** Mol Pharm, 8 (2011), pp. 250-259.

151. Q. L. Hu, Q. Y. Jiang, X. Jin, J. Shen, K. Wang, Y. B. Li, et al **Cationic microRNA-delivering nanovectors with bifunctional peptides for efficient treatment of PANC-1 xenograft model** Biomaterials, 34 (2013), pp. 2265-2276.

152. C. L. Esposito, L. Cerchia, S. Catuogno, G. De Vita, J. P. Dassie, G. Santamaria, et al **Multifunctional Aptamer-miRNA Conjugates for Targeted Cancer Therapy** Mol Ther, 22 (2014), pp. 1151-1163.

153. J. Krutzfeldt, N. Rajewsky, R. Braich, K. G. Rajeev, T. Tuschl, M. Manoharan, et al **Silencing of microRNAs in vivo with 'antagomirs'** Nature, 438 (2005), pp. 685-689.

154. N. Mercatelli, V. Coppola, D. Bonci, F. Miele, A. Costantini, M. Guadagnoli, et al **The inhibition of the highly expressed miR-221 and miR-222 impairs the growth of prostate carcinoma xenografts in mice** PLoS One, 3 (2008), pp. e4029.

155. J. Hou, L. Lin, W. Zhou, Z. Wang, G. Ding, Q. Dong, et al **Identification of miRNomes in human liver and hepatocellular carcinoma reveals miR-199a/b-3p as therapeutic target for hepatocellular carcinoma** Cancer Cell, 19 (2011), pp. 232-243.

156. **American Cancer Society, Pancreatic Cancer** 5 (2016), .

157. D. Ciliberto, C. Botta, P. Correale, M. Rossi, M. Caraglia, P. Tassone, et al **Role of gemcitabine-based combination therapy in the management of advanced pancreatic cancer: a meta-analysis of randomised trials** Eur J Cancer, 49 (2013), pp. 593-603.

158. S. Jones, X. Zhang, D. W. Parsons, J. C. Lin, R. J. Leary, P. Angenendt, et al **Core signaling pathways in human pancreatic cancers revealed by global genomic analyses** Science, 321 (2008), pp. 1801-1806.

159. Y. Miyamoto, A. Maitra, B. Ghosh, U. Zechner, P. Argani, C. A. Iacobuzio-Donahue, et al **Notch mediates TGF alpha-induced changes in epithelial differentiation during pancreatic tumorigenesis** Cancer Cell, 3 (2003), pp. 565-576.

160. N. Rivlin, R. Brosh, M. Oren, V. Rotter **Mutations in the p53 Tumor Suppressor Gene: Important Milestones at the Various Steps of Tumorigenesis** Genes Cancer, 2 (2011), pp. 466-474.

161. F. H. Sarkar, S. Banerjee, Y. Li **Pancreatic cancer: pathogenesis, prevention and treatment** Toxicol Appl Pharmacol, 224 (2007), pp. 326-336.

162. Z. Wang, D. Kong, S. Banerjee, Y. Li, N. V. Adsay, J. Abbruzzese, et al **Down-regulation of platelet-derived growth factor-D inhibits cell growth and angiogenesis through inactivation of Notch-1 and nuclear factor-kappaB signaling** Cancer Res, 67 (2007), pp. 11377-11385.

163. P. Buchler, A. Gazdhar, M. Schubert, N. Giese, H. A. Reber, O. J. Hines, et al **The Notch signaling pathway is related to neurovascular progression of pancreatic cancer** Ann Surg, 242 (2005), pp. 791-800, discussion 800-1.

164. S. P. Thayer, M. P. di Magliano, P. W. Heiser, C. M. Nielsen, D. J. Roberts, G. Y. Lauwers, et al **Hedgehog is an early and late mediator of pancreatic cancer tumorigenesis** Nature, 425 (2003), pp. 851-856.

165. M. Pasca di Magliano, S. Sekine, A. Ermilov, J. Ferris, A. A. Dlugosz, M. Hebrok **Hedgehog/Ras interactions regulate early stages of pancreatic cancer** Genes Dev, 20 (2006), pp. 3161-3173.

166. M. Miyaki, T. Kuroki **Role of Smad4 (DPC4) inactivation in human cancer** Biochem Biophys Res Commun, 306 (2003), pp. 799-804.

167. M. Scaltriti, J. Baselga **The epidermal growth factor receptor pathway: a model for targeted therapy** Clin Cancer Res, 12 (2006), pp. 5268-5272.

168. Clifford J., Whatcott RG, Posner DD, Von H., Haiyong H. **Desmoplasia and chemoresistance in pancreatic cancer**. In: Grippo P.J., Munshi H.G., editors. **Pancreatic Cancer and Tumor Microenvironment**: Transworld Research Network, 2012.

169. J. J. Pan, M. H. Yang **The role of epithelial-mesenchymal transition in pancreatic cancer** J Gastrointest Oncol, 2 (2011), pp. 151-156.

170. Y. Wu, B. P. Zhou **New insights of epithelial-mesenchymal transition in cancer metastasis** Acta Biochim Biophys Sin (Shanghai), 40 (2008), pp. 643-650.

171. A. N. Shah, J. M. Summy, J. Zhang, S. I. Park, N. U. Parikh, G. E. Gallick **Development and characterization of gemcitabine-resistant pancreatic tumor cells** Ann Surg Oncol, 14 (2007), pp. 3629-3637.

172. Z. Du, R. Qin, C. Wei, M. Wang, C. Shi, R. Tian, et al **Pancreatic cancer cells resistant to chemoradiotherapy rich in "stem-cell-like" tumor cells** Dig Dis Sci, 56 (2011), pp. 741-750.

173. E. E. Merika, K. N. Syrigos, M. W. Saif **Desmoplasia in pancreatic cancer. Can we fight it?**Gastroenterol Res Pract, 2012 (2012), pp. 781765.

174. D. L. Schwartz, J. A. Bankson, R. Lemos Jr, S. Y. Lai, A. K. Thittai, Y. He, et al **Radiosensitization and stromal imaging response correlates for the HIF-1 inhibitor PX-478 given with or without chemotherapy in pancreatic cancer** Mol Cancer Ther, 9 (2010), pp. 2057-2067.

175. T. Halkova, R. Cuperkova, M. Minarik, L. Benesova **MicroRNAs in Pancreatic Cancer: Involvement in Carcinogenesis and Potential Use for Diagnosis and Prognosis** Gastroenterol Res Pract, 2015 (2015), pp. 892903.

176. J. Xia, F. H. Sarkar, Z. Wang **Emerging Role of MicroRNA in Pancreatic Cancer** Pancreatic disorders & therapy, 2 (2) (2012), pp. e114.

177. S. Arora, S. K. Swaminathan, A. Kirtane, S. K. Srivastava, A. Bhardwaj, S. Singh, et al **Synthesis, characterization, and evaluation of poly (D,L-lactide-co-glycolide)-based nanoformulation of miRNA-150: potential implications for pancreatic cancer therapy** Int J Nanomedicine, 9 (2014), pp. 2933-2942.

178. R. Subramani, L. Gangwani, S. B. Nandy, A. Arumugam, M. Chattopadhyay, R. Lakshmanaswamy **Emerging roles of microRNAs in pancreatic cancer diagnosis, therapy and prognosis (Review)** Int J Oncol, 47 (2015), pp. 1203-1210.

179. V. Kumar, G. Mondal, P. Slavik, S. Rachagani, S. K. Batra, R. I. Mahato **Codelivery of small molecule hedgehog inhibitor and miRNA for treating pancreatic cancer** Mol Pharm, 12 (2015), pp. 1289-1298.

180. A. Mittal, D. Chitkara, S. W. Behrman, R. I. Mahato **Efficacy of gemcitabine conjugated and miRNA-205 complexed micelles for treatment of advanced pancreatic cancer** Biomaterials, 35 (2014), pp. 7077-7087.

181. S. Dangi-Garimella, M. J. Strouch, P. J. Grippo, D. J. Bentrem, H. G. Munshi **Collagen regulation of let-7 in pancreatic cancer involves TGF-beta1-mediated membrane type 1-matrix metalloproteinase expression** Oncogene, 30 (2011), pp. 1002-1008.

182. N. Bitarte, E. Bandres, V. Boni, R. Zarate, J. Rodriguez, M. Gonzalez-Huarriz, et al **MicroRNA-451 is involved in the self-renewal, tumorigenicity, and chemoresistance of colorectal cancer stem cells** Stem Cells, 29 (2011), pp. 1661-1671.

183. H. Cheng, S. Shi, X. Cai, J. Long, J. Xu, C. Liu, et al **microRNA signature for human pancreatic cancer invasion and metastasis** Exp Ther Med, 4 (2012), pp. 181-187.

184. B. Bao, Z. Wang, S. Ali, D. Kong, Y. Li, A. Ahmad, et al **Notch-1 induces epithelial-mesenchymal transition consistent with cancer stem cell phenotype in pancreatic cancer cells** Cancer Lett, 307 (2011), pp. 26-36.

185. D. Chitkara, A. Mittal, R. I. Mahato **miRNAs in pancreatic cancer: Therapeutic potential, delivery challenges and strategies** Adv Drug Deliv Rev, 81C (2014), pp. 34-52.

186. BeachyPhilip A., KarhadkarSunil S., BermanDavid M. **Tissue repair and stem cell renewal in carcinogenesis** Nature, 432 (2004), pp. 324-331.

187. A. Omenetti, A. M. Diehl **The adventures of sonic hedgehog in development and repair. II. Sonic hedgehog and liver development, inflammation, and cancer** Am J Physiol Gastrointest Liver Physiol, 294 (2008), pp. G595-8.

188. T. Miyahara, L. Schrum, R. Rippe, S. Xiong, H. F. Yee Jr, K. Motomura, et al **Peroxisome proliferator-activated receptors and hepatic stellate cell activation** J Biol Chem, 275 (2000), pp. 35715-35722.

189. T. Luedde, R. F. Schwabe **NF-kappaB in the liver--linking injury, fibrosis and hepatocellular carcinoma** Nat Rev Gastroenterol Hepatol, 8 (2011), pp. 108-118.

190. A. Omenetti, Y. Popov, Y. Jung, S. S. Choi, R. P. Witek, L. Yang, et al **The hedgehog pathway regulates remodelling responses to biliary obstruction in rats** Gut, 57 (2008), pp. 1275-1282.

191. A. Galli, D. W. Crabb, E. Ceni, R. Salzano, T. Mello, G. Svegliati-Baroni, et al **Antidiabetic thiazolidinediones inhibit collagen synthesis and hepatic stellate cell activation in vivo and in vitro** Gastroenterology, 122 (2002), pp. 1924-1940.

192. A. Pratap, S. Singh, V. Mundra, N. Yang, R. Panakanti, J. D. Eason, et al **Attenuation of early liver fibrosis by pharmacological inhibition of smoothened receptor signaling** J Drug Target, 20 (2012), pp. 770-782.

193. H. Chen, Y. W. He, W. Q. Liu, J. H. Zhang **Rosiglitazone prevents murine hepatic fibrosis induced by Schistosoma japonicum** World J Gastroenterol, 14 (2008), pp. 2905-2911.

194. C. M. Rudin, C. L. Hann, J. Laterra, R. L. Yauch, C. A. Callahan, L. Fu, et al **Treatment of medulloblastoma with hedgehog pathway inhibitor GDC-0449** N Engl J Med, 361 (2009), pp. 1173-1178.

195. A. Cheng-Lai, A. Levine **Rosiglitazone: an agent from the thiazolidinedione class for the treatment of type 2 diabetes** Heart Dis, 2 (2000), pp. 326-333.

196. M. Danquah, T. Fujiwara, R. I. Mahato **Self-assembling methoxypoly(ethylene glycol)-b-poly(carbonate-co-L-lactide) block copolymers for drug delivery** Biomaterials, 31 (2010), pp. 2358-2370.

197. V. Mundra, Y. Lu, M. Danquah, W. Li, D. D. Miller, R. I. Mahato **Formulation and characterization of polyester/polycarbonate nanoparticles for delivery of a novel microtubule destabilizing agent** Pharm Res, 29 (2012), pp. 3064-3074.

198. M. Wagner, P. Fickert, G. Zollner, A. Fuchsbichler, D. Silbert, O. Tsybrovskyy, et al **Role of farnesoid X receptor in determining hepatic ABC transporter expression and liver injury in bile duct-ligated mice** Gastroenterology, 125 (2003), pp. 825-838.

199. P. Fickert, M. J. Pollheimer, D. Silbert, T. Moustafa, E. Halilbasic, E. Krones, et al **Differential effects of norUDCA and UDCA in obstructive cholestasis in mice** J Hepatol, 58 (2013), pp. 1201-1208.

200. Y. Yamaura, M. Nakajima, S. Takagi, T. Fukami, K. Tsuneyama, T. Yokoi **Plasma microRNA profiles in rat models of hepatocellular injury, cholestasis, and steatosis** PLoS One, 7 (2012), pp. e30250.

201. N. Yang, S. Singh, R. I. Mahato **Targeted TFO delivery to hepatic stellate cells** J Control Release, 155 (2011), pp. 326-330.

202. A. Jiroutova, L. Majdiakova, M. Cermakova, R. Kohlerova, J. Kanta **Expression of cytoskeletal proteins in hepatic stellate cells isolated from normal and cirrhotic rat liver** Acta Medica (Hradec Kralove), 48 (2005), pp. 137-144.

203. M. H. Branton, J. B. Kopp **TGF-beta and fibrosis** Microbes Infect, 1 (1999), pp. 1349-1365.

204. S. Y. Chaw, A. A. Majeed, A. J. Dalley, A. Chan, S. Stein, C. S. Farah **Epithelial to mesenchymal transition (EMT) biomarkers--E-cadherin, beta-catenin, APC and Vimentin--in oral squamous cell carcinogenesis and transformation** Oral Oncol, 48 (2012), pp. 997-1006.

205. G. J. Seong, S. Hong, S. A. Jung, J. J. Lee, E. Lim, S. J. Kim, et al **TGF-beta-induced interleukin-6 participates in transdifferentiation of human Tenon's fibroblasts to myofibroblasts** Mol Vis, 15 (2009), pp. 2123-2128.

206. R. F. Schwabe, D. A. Brenner **Mechanisms of Liver Injury. I. TNF-alpha-induced liver injury: role of IKK, JNK, and ROS pathways** Am J Physiol Gastrointest Liver Physiol, 290 (2006), pp. G583-9.

207. J. Rosenbloom, F. A. Mendoza, S. A. Jimenez **Strategies for anti-fibrotic therapies** Biochim Biophys Acta, 1832 (2013), pp. 1088-1103.

208. P. Muriel **Alpha-interferon prevents liver collagen deposition and damage induced by prolonged bile duct obstruction in the rat** J Hepatol, 24 (1996), pp. 614-621.

209. Z. Ye, K. Cheng, R. V. Guntaka, R. I. Mahato **Receptor-mediated hepatic uptake of M6P-BSA-conjugated triplex-forming oligonucleotides in rats** Bioconjug Chem, 17 (2006), pp. 823-830.

210. M. Bickel, K. H. Baringhaus, M. Gerl, V. Gunzler, J. Kanta, L. Schmidts, et al **Selective inhibition of hepatic collagen accumulation in experimental liver fibrosis in rats by a new prolyl 4-hydroxylase inhibitor** Hepatology, 28 (1998), pp. 404-411.

211. M. C. Wright, R. Issa, D. E. Smart, N. Trim, G. I. Murray, J. N. Primrose, et al **Gliotoxin stimulates the apoptosis of human and rat hepatic stellate cells and enhances the resolution of liver fibrosis in rats** Gastroenterology, 121 (2001), pp. 685-698.

212. C. W. Wu, E. S. Chu, C. N. Lam, A. S. Cheng, C. W. Lee, V. W. Wong, et al **PPARgamma is essential for protection against nonalcoholic steatohepatitis** Gene Ther, 17 (2010), pp. 790-798.

213. J. Yu, S. Zhang, E. S. Chu, M. Y. Go, R. H. Lau, J. Zhao, et al **Peroxisome proliferator-activated receptors gamma reverses hepatic nutritional fibrosis in mice and suppresses activation of hepatic stellate cells in vitro** Int J Biochem Cell Biol, 42 (2010), pp. 948-957.

214. H. Hauner **The mode of action of thiazolidinediones** Diabetes Metab Res Rev, 18 Suppl 2 (2002), pp. S10-5.

215. J. A. Balfour, G. L. Plosker **Rosiglitazone** Drugs, 57 (1999), pp. 921-30; discussion 931-2.

216. W. Lu, F. Li, R. I. Mahato **Poly(ethylene glycol)-block-poly(2-methyl-2-benzoxycarbonyl-propylene carbonate) micelles for rapamycin delivery: in vitro characterization and biodistribution** J Pharm Sci, 100 (2011), pp. 2418-2429.

217. G. Carpino, S. Morini, S. Ginanni Corradini, A. Franchitto, M. Merli, M. Siciliano, et al **Alpha-SMA expression in hepatic stellate cells and quantitative analysis of hepatic fibrosis in cirrhosis and in recurrent chronic hepatitis after liver transplantation** Dig Liver Dis, 37 (2005), pp. 349-356.

218. A. L. Olsen, B. K. Sackey, C. Marcinkiewicz, D. Boettiger, R. G. Wells **Fibronectin extra domain-A promotes hepatic stellate cell motility but not differentiation into myofibroblasts** Gastroenterology, 142 (2012), pp. 928-937.e3.

219. B. Guo, D. Koya, M. Isono, T. Sugimoto, A. Kashiwagi, M. Haneda **Peroxisome proliferator-activated receptor-gamma ligands inhibit TGF-beta 1-induced fibronectin expression in glomerular mesangial cells** Diabetes, 53 (2004), pp. 200-208.

220. J. J. Maher, S. Zia, C. Tzagarakis **Acetaldehyde-induced stimulation of collagen synthesis and gene expression is dependent on conditions of cell culture: studies with rat lipocytes and fibroblasts** Alcohol Clin Exp Res, 18 (1994), pp. 403-409.

221. Wolfgang CL, Herman JM FAU - Laheru,Daniel A., Laheru DA FAU - Klein,Alison P., Klein AP FAU - Erdek,Michael A., Erdek MA FAU - Fishman,Elliot K., Fishman EK FAU - Hruban,Ralph H., et al. Recent progress in pancreatic cancer.

222. S. Mohammed, G. Van Buren 2nd, W. E. Fisher **Pancreatic cancer: advances in treatment** World J Gastroenterol, 20 (2014), pp. 9354-9360.

223. F. T. Huang, Y. X. Zhuan-Sun, Y. Y. Zhuang, S. L. Wei, J. Tang, W. B. Chen, et al **Inhibition of hedgehog signaling depresses self-renewal of pancreatic cancer stem cells and reverses chemoresistance** Int J Oncol, 41 (2012), pp. 1707-1714.

224. K. P. Olive, M. A. Jacobetz, C. J. Davidson, A. Gopinathan, D. McIntyre, D. Honess, et al **Inhibition of Hedgehog signaling enhances delivery of chemotherapy in a mouse model of pancreatic cancer** Science, 324 (2009), pp. 1457-1461.

225. E. De Smaele, E. Ferretti, A. Gulino **Vismodegib, a small-molecule inhibitor of the hedgehog pathway for the treatment of advanced cancers** Curr Opin Investig Drugs, 11 (2010), pp. 707-718.

226. Tanase CP, Neagu AI, Necula LG, Mambet C, Enciu AM, Calenic B, et al. Cancer stem cells: involvement in pancreatic cancer pathogenesis and perspectives on cancer therapeutics. World J Gastroenterol 2014;20:10790-801.

227. Wellner U, Schubert J FAU - Burk,Ulrike C., Burk UC FAU - Schmalhofer,Otto, Schmalhofer O FAU - Zhu,Feng, Zhu F FAU - Sonntag,Annika, Sonntag A FAU - Waldvogel,Bettina, et al. The EMT-activator ZEB1 promotes tumorigenicity by repressing stemness-inhibiting microRNAs. Nat Cell Biol 2009;11(12):1187-95.

228. Y. Li, T. G. VandenBoom 2nd, D. Kong, Z. Wang, S. Ali, P. A. Philip, et al **Up-regulation of miR-200 and let-7 by natural agents leads to the reversal of epithelial-to-mesenchymal transition in gemcitabine-resistant pancreatic cancer cells** Cancer Res, 69 (2009), pp. 6704-6712.

229. S. Singh, D. Chitkara, V. Kumar, S. W. Behrman, R. I. Mahato **miRNA profiling in pancreatic cancer and restoration of chemosensitivity** Cancer Lett, 334 (2013), pp. 211-220.

230. S. M. Johnson, H. Grosshans, J. Shingara, M. Byrom, R. Jarvis, A. Cheng, et al **RAS is regulated by the let-7 microRNA family** Cell, 120 (2005), pp. 635-647.

231. P. Trang, P. P. Medina, J. F. Wiggins, L. Ruffino, K. Kelnar, M. Omotola, et al **Regression of murine lung tumors by the let-7 microRNA** Oncogene, 29 (2010), pp. 1580-1587.

232. K. Patel, A. Kollory, A. Takashima, S. Sarkar, D. V. Faller, S. K. Ghosh **MicroRNA let-7 downregulates STAT3 phosphorylation in pancreatic cancer cells by increasing SOCS3 expression** Cancer Lett, 347 (2014), pp. 54-64.

233. T. M. Sun, J. Z. Du, Y. D. Yao, C. Q. Mao, S. Dou, S. Y. Huang, et al **Simultaneous delivery of siRNA and paclitaxel via a "two-in-one" micelleplex promotes synergistic tumor suppression** ACS Nano, 5 (2011), pp. 1483-1494.

234. Tsouris V, Joo MK, Kim SH, Kwon IC, Won YY. Nano carriers that enable co-delivery of chemotherapy and RNAi agents for treatment of drug-resistant cancers. Biotechnol Adv 2014;32:1037-50.

235. M. Creixell, N. A. Peppas **Co-delivery of siRNA and therapeutic agents using nanocarriers to overcome cancer resistance** Nano Today, 7 (2012), pp. 367-379.

236. F. Li, M. Danquah, R. I. Mahato **Synthesis and characterization of amphiphilic lipopolymers for micellar drug delivery** Biomacromolecules, 11 (2010), pp. 2610-2620.

237. V. Kumar, V. Mundra, R. I. Mahato **Nanomedicines of Hedgehog inhibitor and PPAR-gamma agonist for treating liver fibrosis** Pharm Res, 31 (2014), pp. 1158-1169.

238. Z. Sezgin, N. Yuksel, T. Baykara **Preparation and characterization of polymeric micelles for solubilization of poorly soluble anticancer drugs** Eur J Pharm Biopharm, 64 (2006), pp. 261-268.

239. I. Vorechovsky, K. P. Benediktsson, R. Toftgard **The patched/hedgehog/smoothened signalling pathway in human breast cancer: no evidence for H133Y SHH, PTCH and SMO mutations** Eur J Cancer, 35 (1999), pp. 711-713.

240. S. Thiyagarajan, N. Bhatia, S. Reagan-Shaw, D. Cozma, A. Thomas-Tikhonenko, N. Ahmad, et al **Role of GLI2 transcription factor in growth and tumorigenicity of prostate cells** Cancer Res, 67 (2007), pp. 10642-10646.

241. T. Mazumdar, J. DeVecchio, T. Shi, J. Jones, A. Agyeman, J. A. Houghton **Hedgehog signaling drives cellular survival in human colon carcinoma cells** Cancer Res, 71 (2011), pp. 1092-1102.

242. A. Ruiz i Altaba, B. Stecca, P. Sanchez **Hedgehog--Gli signaling in brain tumors: stem cells and paradevelopmental programs in cancer** Cancer Lett, 204 (2004), pp. 145-157.

243. A. E. Proctor, L. A. Thompson, C. L. O'Bryant **Vismodegib: an inhibitor of the Hedgehog signaling pathway in the treatment of basal cell carcinoma** Ann Pharmacother, 48 (2014), pp. 99-106.

244. M. Huang, S. N. Tang, G. Upadhyay, J. L. Marsh, C. P. Jackman, S. Shankar, et al **Embelin suppresses growth of human pancreatic cancer xenografts, and pancreatic cancer cells isolated from KrasG12D mice by inhibiting Akt and Sonic hedgehog pathways** PLoS One, 9 (2) (2014), pp. e92161.

245. Z. Wang, Y. Li, D. Kong, S. Banerjee, A. Ahmad, A. S. Azmi, et al **Acquisition of epithelial-mesenchymal transition phenotype of gemcitabine-resistant pancreatic cancer cells is linked with activation of the notch signaling pathway** Cancer Res, 69 (2009), pp. 2400-2407.

246. A. Ahmad, M. Y. Maitah, K. R. Ginnebaugh, Y. Li, B. Bao, S. M. Gadgeel, et al **Inhibition of Hedgehog signaling sensitizes NSCLC cells to standard therapies through modulation of EMT-regulating miRNAs** J Hematol Oncol, 6 (2013), pp. 77-8722-6-77.

247. J. Torrisani, B. Bournet, M. C. du Rieu, M. Bouisson, A. Souque, J. Escourrou, et al **let-7 MicroRNA transfer in pancreatic cancer-derived cells inhibits in vitro cell proliferation but fails to alter tumor progression** Hum Gene Ther, 20 (2009), pp. 831-844.

248. S. Salmaso, P. Caliceti **Stealth properties to improve therapeutic efficacy of drug nanocarriers** J Drug Deliv, 2013 (2013), pp. 374252.

249. S. Fukushima, K. Miyata, N. Nishiyama, N. Kanayama, Y. Yamasaki, K. Kataoka **PEGylated polyplex micelles from triblock catiomers with spatially ordered layering of condensed pDNA and buffering units for enhanced intracellular gene delivery** J Am Chem Soc, 127 (2005), pp. 2810-2811.

250. H. J. Kim, K. Miyata, T. Nomoto, M. Zheng, A. Kim, X. Liu, et al **siRNA delivery from triblock copolymer micelles with spatially-ordered compartments of PEG shell, siRNA-loaded intermediate layer, and hydrophobic core** Biomaterials, 35 (2014), pp. 4548-4556.

251. J. Lei, J. Ma, Q. Ma, X. Li, H. Liu, Q. Xu, et al **Hedgehog signaling regulates hypoxia induced epithelial to mesenchymal transition and invasion in pancreatic cancer cells via a ligand-independent manner** Mol Cancer, 12 (2013), pp. 66-4598-12-66.

252. J. P. Morton, M. E. Mongeau, D. S. Klimstra, J. P. Morris, Y. C. Lee, Y. Kawaguchi, et al **Sonic hedgehog acts at multiple stages during pancreatic tumorigenesis** Proc Natl Acad Sci U S A, 104 (2007), pp. 5103-5108.

253. E. J. Kim, V. Sahai, E. V. Abel, K. A. Griffith, J. K. Greenson, N. Takebe, et al **Pilot Clinical Trial of Hedgehog Pathway Inhibitor GDC-0449 (Vismodegib) in Combination with Gemcitabine in Patients with Metastatic Pancreatic Adenocarcinoma** Clin Cancer Res, (2014), .

254. J. J. Lee, R. M. Perera, H. Wang, D. C. Wu, X. S. Liu, S. Han, et al **Stromal response to Hedgehog signaling restrains pancreatic cancer progression** Proc Natl Acad Sci U S A, 111 (2014), pp. E3091-100.

255. A. D. Rhim, P. E. Oberstein, D. H. Thomas, E. T. Mirek, C. F. Palermo, S. A. Sastra, et al **Stromal elements act to restrain, rather than support, pancreatic ductal adenocarcinoma** Cancer Cell, 25 (2014), pp. 735-747.

256. Mathew E, Zhang Y, Alexander MH, Kane TK, Song JY, Allen BL, et al **Dosage-Dependent Regulation of Pancreatic Cancer Growth and Angiogenesis by Hedgehog Signaling** Cell Reports, 9 (2014), pp. 1-11.

257. Ana De Jesus-Acosta, Peter J. O'Dwyer, Ramesh K. Ramanathan, Daniel D. Von Hoff, Anirban Maitra, Zeshaan Rasheed, Lei Zheng, N. V. Rajeshkumar, Dung T. Le, Antje Hoering, Vanessa Bolejack, Yabuuchi, Shinichi, Daniel A. Laheru. **A phase II study of vismodegib, a hedgehog (Hh) pathway inhibitor, combined with gemcitabine and nab-paclitaxel (nab-P) in patients (pts) with untreated metastatic pancreatic ductal adenocarcinoma (PDA)**. 2014.

258. I. Caro, J. A. Low **The role of the hedgehog signaling pathway in the development of basal cell carcinoma and opportunities for treatment** Clin Cancer Res, 16 (2010), pp. 3335-3339.

259. W. Wei, H. B. He, W. Y. Zhang, H. X. Zhang, J. B. Bai, H. Z. Liu, et al **miR-29 targets Akt3 to reduce proliferation and facilitate differentiation of myoblasts in skeletal muscle development** Cell Death Dis, 4 (2013), pp. e668.

260. M. P. Perez de Obanos, M. J. Lopez Zabalza, J. Prieto, M. T. Herraiz, M. J. Iraburu **Leucine stimulates procollagen alpha1(I) translation on hepatic stellate cells through ERK and PI3K/Akt/mTOR activation** J Cell Physiol, 209 (2006), pp. 580-586.

261. S. Reif, A. Lang, J. N. Lindquist, Y. Yata, E. Gabele, A. Scanga, et al **The role of focal adhesion kinase-phosphatidylinositol 3-kinase-akt signaling in hepatic stellate cell proliferation and type I collagen expression** J Biol Chem, 278 (2003), pp. 8083-8090.

262. W. Qin, A. C. Chung, X. R. Huang, X. M. Meng, D. S. Hui, C. M. Yu, et al **TGF-beta/Smad3 signaling promotes renal fibrosis by inhibiting miR-29** J Am Soc Nephrol, 22 (2011), pp. 1462-1474.

263. C. Roderburg, G. W. Urban, K. Bettermann, M. Vucur, H. Zimmermann, S. Schmidt, et al **Micro-RNA profiling reveals a role for miR-29 in human and murine liver fibrosis** Hepatology, 53 (2011), pp. 209-218.

264. J. K. Dyson, G. M. Hirschfield, D. H. Adams, U. Beuers, D. A. Mann, K. D. Lindor, et al **Novel therapeutic targets in primary biliary cirrhosis** Nat Rev Gastroenterol Hepatol, 12 (2015), pp. 147-158.

265. C. Y. Perrot, D. Javelaud, A. Mauviel **Overlapping activities of TGF-beta and Hedgehog signaling in cancer: therapeutic targets for cancer treatment** Pharmacol Ther, 137 (2013), pp. 183-199.

266. C. G. Tag, S. Sauer-Lehnen, S. Weiskirchen, E. Borkham-Kamphorst, R. H. Tolba, F. Tacke, et al **Bile duct ligation in mice: induction of inflammatory liver injury and fibrosis by obstructive cholestasis** J Vis Exp, (96). doi (2015), pp. 10.3791/52438.

267. B. L. Woolbright, K. Dorko, D. J. Antoine, J. I. Clarke, P. Gholami, F. Li, et al **Bile acid-induced necrosis in primary human hepatocytes and in patients with obstructive cholestasis** Toxicol Appl Pharmacol, 283 (2015), pp. 168-177.

268. M. S. Lee, J. E. Lee, E. Byun, N. W. Kim, K. Lee, H. Lee, et al **Target-specific delivery of siRNA by stabilized calcium phosphate nanoparticles using dopa-hyaluronic acid conjugate** J Control Release, 192 (2014), pp. 122-130.

269. J. Lu, S. C. Owen, M. S. Shoichet **Stability of Self-Assembled Polymeric Micelles in Serum** Macromolecules, 44 (2011), pp. 6002-6008.

270. X. Zhao, Z. Poon, A. C. Engler, D. K. Bonner, P. T. Hammond **Enhanced stability of polymeric micelles based on postfunctionalized poly(ethylene glycol)-b-poly(gamma-propargyl L-glutamate): the substituent effect** Biomacromolecules, 13 (2012), pp. 1315-1322.

271. K. Cheng, Z. Ye, R. V. Guntaka, R. I. Mahato **Biodistribution and hepatic uptake of triplex-forming oligonucleotides against type alpha1(I) collagen gene promoter in normal and fibrotic rats** Mol Pharm, 2 (2005), pp. 206-217.

272. S. C. Semple, A. Akinc, J. Chen, A. P. Sandhu, B. L. Mui, C. K. Cho, et al **Rational design of cationic lipids for siRNA delivery** Nat Biotechnol, 28 (2010), pp. 172-176.

273. R. A. Graham, B. L. Lum, S. Cheeti, J. Y. Jin, K. Jorga, D. D. Von Hoff, et al **Pharmacokinetics of hedgehog pathway inhibitor vismodegib (GDC-0449) in patients with**

locally advanced or metastatic solid tumors: the role of alpha-1-acid glycoprotein binding Clin Cancer Res, 17 (2011), pp. 2512-2520.

274. R. M. Hill, S. Kuijper, J. C. Lindsey, K. Petrie, E. C. Schwalbe, K. Barker, et al **Combined MYC and P53 defects emerge at medulloblastoma relapse and define rapidly progressive, therapeutically targetable disease** Cancer Cell, 27 (2015), pp. 72-84.

275. C. G. Lee, Y. W. Kim, E. H. Kim, Z. Meng, W. Huang, S. J. Hwang, et al **Farnesoid X receptor protects hepatocytes from injury by repressing miR-199a-3p, which increases levels of LKB1** Gastroenterology, 142 (2012), pp. 1206-1217.e7.

276. Y. Murakami, H. Toyoda, M. Tanaka, M. Kuroda, Y. Harada, F. Matsuda, et al **The progression of liver fibrosis is related with overexpression of the miR-199 and 200 families** PLoS One, 6 (2011), pp. e16081.

277. J. Hu, C. Chen, Q. Liu, B. Liu, C. Song, S. Zhu, et al **The role of the miR-31/FlH1 pathway in TGF-beta-induced liver fibrosis** Clin Sci (Lond), 129 (2015), pp. 305-317.

278. F. Yu, Y. Guo, B. Chen, P. Dong, J. Zheng **MicroRNA-17-5p activates hepatic stellate cells through targeting of Smad7** Lab Invest, (2015), pp. [Epub ahead of print].

279. R. Dong, Y. Zheng, G. Chen, R. Zhao, Z. Zhou, S. Zheng **miR-222 overexpression may contribute to liver fibrosis in biliary atresia by targeting PPP2R2A** J Pediatr Gastroenterol Nutr, 60 (2015), pp. 84-90.

280. M. M. Tiao, F. S. Wang, L. T. Huang, J. H. Chuang, H. C. Kuo, Y. L. Yang, et al **MicroRNA-29a protects against acute liver injury in a mouse model of obstructive jaundice via inhibition of the extrinsic apoptosis pathway** Apoptosis, 19 (2014), pp. 30-41.

281. H. Zhang, Z. Feng, R. Huang, Z. Xia, G. Xiang, J. Zhang **MicroRNA-449 suppresses proliferation of hepatoma cell lines through blockade lipid metabolic pathway related to SIRT1** Int J Oncol, 45 (2014), pp. 2143-2152.

282. H. He, A. Mennone, J. L. Boyer, S. Y. Cai **Combination of retinoic acid and ursodeoxycholic acid attenuates liver injury in bile duct-ligated rats and human hepatic cells** Hepatology, 53 (2011), pp. 548-557.

283. J. Wang, E. S. Chu, H. Y. Chen, K. Man, M. Y. Go, X. R. Huang, et al **microRNA-29b prevents liver fibrosis by attenuating hepatic stellate cell activation and inducing apoptosis through targeting PI3K/AKT pathway** Oncotarget, 6 (2015), pp. 7325-7338.

284. H. Yoshiji, S. Kuriyama, R. Noguchi, Y. Ikenaka, J. Yoshii, K. Yanase, et al **Amelioration of liver fibrogenesis by dual inhibition of PDGF and TGF-beta with a combination of imatinib mesylate and ACE inhibitor in rats** Int J Mol Med, 17 (2006), pp. 899-904.

285. S. Ni, Y. Li, S. Huang, W. Luo, C. Li, X. Li **Perindopril and losartan attenuate intrahepatic Toll-like receptor 4 protein expression in rats with bile duct ligation-induced hepatic fibrosis** Nan Fang Yi Ke Da Xue Xue Bao, 32 (2012), pp. 211-214.

286. A. Omenetti, S. Choi, G. Michelotti, A. M. Diehl **Hedgehog signaling in the liver** J Hepatol, 54 (2011), pp. 366-373.

287. G. M. Philips, I. S. Chan, M. Swiderska, V. T. Schroder, C. Guy, G. F. Karaca, et al **Hedgehog signaling antagonist promotes regression of both liver fibrosis and hepatocellular carcinoma in a murine model of primary liver cancer** PLoS One, 6 (2011), pp. e23943.

288. S. Sassen, E. A. Miska, C. Caldas **MicroRNA: implications for cancer** Virchows Arch, 452 (2008), pp. 1-10.

289. C. Zhang **MicroRNomics: a newly emerging approach for disease biology** Physiol Genomics, 33 (2008), pp. 139-147.

290. T. Nishiguchi, T. Imanishi, T. Akasaka **MicroRNAs and cardiovascular diseases** Biomed Res Int, 2015 (2015), pp. 682857.

291. T. Ogawa, M. Iizuka, Y. Sekiya, K. Yoshizato, K. Ikeda, N. Kawada **Suppression of type I collagen production by microRNA-29b in cultured human stellate cells** Biochem Biophys Res Commun, 391 (2010), pp. 316-321.

292. S. Dennler, J. Andre, I. Alexaki, A. Li, T. Magnaldo, P. ten Dijke, et al **Induction of sonic hedgehog mediators by transforming growth factor-beta: Smad3-dependent activation of Gli2 and Gli1 expression in vitro and in vivo** Cancer Res, 67 (2007), pp. 6981-6986.

293. Y. Jung, K. D. Brown, R. P. Witek, A. Omenetti, L. Yang, M. Vandongen, et al **Accumulation of hedgehog-responsive progenitors parallels alcoholic liver disease severity in mice and humans** Gastroenterology, 134 (2008), pp. 1532-1543.

294. C. L. Daige, J. F. Wiggins, L. Priddy, T. Nelligan-Davis, J. Zhao, D. Brown **Systemic delivery of a miR34a mimic as a potential therapeutic for liver cancer** Mol Cancer Ther, 13 (2014), pp. 2352-2360.

295. N. Mishra, N. P. Yadav, V. K. Rai, P. Sinha, K. S. Yadav, S. Jain, et al **Efficient hepatic delivery of drugs: novel strategies and their significance** Biomed Res Int, 2013 (2013), pp. 382184.

296. S. Zhang, J. Wu, H. Wang, T. Wang, L. Jin, D. Shu, et al **Liposomal oxymatrine in hepatic fibrosis treatment: formulation, in vitro and in vivo assessment** AAPS PharmSciTech, 15 (2014), pp. 620-629.

297. M. Hennenberg, J. Trebicka, Z. Kohistani, C. Stark, H. D. Nischalke, B. Kramer, et al **Hepatic and HSC-specific sorafenib effects in rats with established secondary biliary cirrhosis** Lab Invest, 91 (2011), pp. 241-251.

298. Y. Zhang, M. Ghazwani, J. Li, M. Sun, D. B. Stolz, F. He, et al **MiR-29b inhibits collagen maturation in hepatic stellate cells through down-regulating the expression of HSP47 and lysyl oxidase** Biochem Biophys Res Commun, 446 (2014), pp. 940-944.

299. M. Monaghan, S. Browne, K. Schenke-Layland, A. Pandit **A collagen-based scaffold delivering exogenous microrna-29B to modulate extracellular matrix remodeling** Mol Ther, 22 (2014), pp. 786-796.

300. E. F. Moshai, L. Wemeau-Stervinou, N. Cigna, S. Brayer, J. M. Somme, B. Crestani, et al **Targeting the hedgehog-glioma-associated oncogene homolog pathway inhibits bleomycin-induced lung fibrosis in mice** Am J Respir Cell Mol Biol, 51 (2014), pp. 11-25.

301. E. Roeb, E. Purucker, B. Breuer, H. Nguyen, P. C. Heinrich, S. Rose-John, et al **TIMP expression in toxic and cholestatic liver injury in rat** J Hepatol, 27 (1997), pp. 535-544.

302. N. Kawelke, M. Vasel, C. Sens, A. Au, S. Dooley, I. A. Nakchbandi **Fibronectin protects from excessive liver fibrosis by modulating the availability of and responsiveness of stellate cells to active TGF-beta** PLoS One, 6 (2011), pp. e28181.

303. S. Matsui, T. Takahashi, Y. Oyanagi, S. Takahashi, S. Boku, K. Takahashi, et al **Expression, localization and alternative splicing pattern of fibronectin messenger RNA in fibrotic human liver and hepatocellular carcinoma** J Hepatol, 27 (1997), pp. 843-853.

304. J. L. Mott, S. Kurita, S. C. Cazanave, S. F. Bronk, N. W. Werneburg, M. E. Fernandez-Zapico **Transcriptional suppression of mir-29b-1/mir-29a promoter by c-Myc, hedgehog, and NF-kappaB** J Cell Biochem, 110 (2010), pp. 1155-1164.

305. R. Yan, X. Peng, X. Yuan, D. Huang, J. Chen, Q. Lu, et al **Suppression of growth and migration by blocking the Hedgehog signaling pathway in gastric cancer cells** Cell Oncol (Dordr), 36 (2013), pp. 421-435.

306. S. Wang, Y. Lee, J. Kim, J. Hyun, K. Lee, Y. Kim, et al **Potential role of Hedgehog pathway in liver response to radiation** PLoS One, 8 (2013), pp. e74141.

307. J. P. Iredale, R. C. Benyon, J. Pickering, M. McCullen, M. Northrop, S. Pawley, et al **Mechanisms of spontaneous resolution of rat liver fibrosis. Hepatic stellate cell apoptosis and reduced hepatic expression of metalloproteinase inhibitors** J Clin Invest, 102 (1998), pp. 538-549.

308. M. K. Son, Y. L. Ryu, K. H. Jung, H. Lee, H. S. Lee, H. H. Yan, et al **HS-173, a novel PI3K inhibitor, attenuates the activation of hepatic stellate cells in liver fibrosis** Sci Rep, 3 (2013), pp. 3470.

309. M. Kwiecinski, N. Elfimova, A. Noetel, U. Tox, H. M. Steffen, U. Hacker, et al **Expression of platelet-derived growth factor-C and insulin-like growth factor I in hepatic stellate cells is inhibited by miR-29** Lab Invest, 92 (2012), pp. 978-987.